國立交通大學

材料科學與工程學系

博士論文

分子束磊晶低溫成長 III-V 族稀磁半導體之結構與性質

Structures and properties of III-V diluted magnetic semiconductors grown by low temperature molecular beam epitaxy

研究生：李薇妮

指導教授：郭正次博士

中華民國九十五年一月

分子束磊晶低溫成長 III-V 族稀磁半導體之結構與性質

Structures and properties of III-V diluted magnetic semiconductors grown by low temperature molecular beam epitaxy

研究生：李薇妮 Student : Wei-Ni Lee

指導教授：郭正次博士 Advisor: Dr. Cheng-Tzu Kuo

國立交通大學

材料科學與工程學系

博士論文

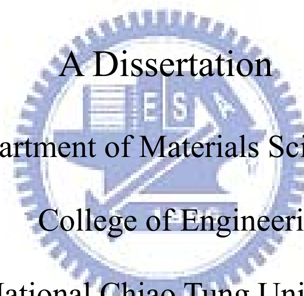

A Dissertation

Submitted to Department of Materials Science and Engineering,

College of Engineering

National Chiao Tung University

In Partial Fulfillment of the Requirements

For the Degree of

Doctor of Philosophy

in

Materials Science and Engineering

January 2006

Hsinchu, Taiwan, Republic of China

中華民國九十五年一月

分子束磊晶低溫成長 III-V 族稀磁半導體之結構與性質

研究生：李薇妮　　　　　　　　　　　　　指導教授：郭正次博士

國立交通大學材料科學與工程學系

摘　　要

III-V 族半導體廣為應用在光電及快速元件。然而，同時具有半導體傳導特性與磁性之奈米薄膜，因具有降低元件膜層間自旋電子散射之特性，而成為可應用在自旋電子元件的重要關鍵技術之一。在傳統的半導體材料中加入少量磁性元素，形成所謂稀磁半導體(DMS)，例如將 Mn 原子加入傳統的 III-V 族半導體，即屬於此類應用而新發展的材料。本實驗成功的在 GaAs 與 InP 基材上，生長系列稀磁半導體多層膜，並研究其結構與性質。不同於傳統磊晶的生長方法，利用分子束磊晶低溫(＜300℃)成長，降低沉積時原子間互相擴散而形成介穩態，較傳統方法可加入較高含量的磁性原子以增加其磁性。利用 TEM、DXRD、EPMA 與 SQUID 研究其結構與性質，實驗結果略分為三類：

1、LT-GaAs磊晶層中過量砷析出行為的研究，發現不同方向的GaAs基板之磊晶層中過量砷濃度在GaAs(311)B＞ (311)A＞ (001)。可能因晶面配位數因子與鍵結位置的差異而形成。比較表面空懸雙鍵與單鍵的鍵結位置，後者配位數因子較高。此外另設計一LT-GaAs 包含 6 層區域(i-n_1-i, i-n_2-i, i-n_3-i, i-p_1-i, i-p_2-i, 與i-p_3-i多層膜) 結構，調變Si與Be的摻雜濃度(10^{16}～10^{18} ㎝$^{-3}$)，發現一有趣結果，當摻雜Si濃度≦10^{17}㎝$^{-3}$，As析出在n層形成空乏區，此現象在文獻中從未被報導。此現象可由i-n上、下二界面的德拜長度重疊區超越n層膜厚度之關係解釋。

2、有關生長摻雜 7 ％ Mn，後退火處理和DMS厚度對的LT-(Ga, Mn)As稀磁半導體，(LT-(Ga, Mn)As / LT-GaAs / GaAs)三層結構磁性之研究。結果顯示：DMS的居里溫度(T_c)隨著膜厚度下降與退火處理，而大幅的上升，並且在GaAs(001)方向的基材具最高T_c。退火處理基本上是將晶格內多出的插入型Mn_I原子移出，因而減少其類施者型缺陷，使電洞載子濃度提高而增加T_c 。換句話說，當膜厚度下降，Mn擴散的路徑縮短，在退火時更有效地將插入型Mn_I原子移出，並使T_c增加。不同GaAs基材方向之效應，基本上是影響多餘As原子之析出行為。因為過量的砷反置缺陷在GaAs(311)A晶面基板上，比在(001)面基板上多，所以會中和較多電洞載子，使電洞濃度下降，所以T_c的下降在

GaAs(311)A面較多。

3、有關在InP基板上變化緩衝層晶格常數效應對摻雜Mn的LT-(In, Al, Mn)As DMS之影響研究。緩衝層晶格變化包括：與基板晶格常數幾乎吻合的單層膜晶格，以及3層膜梯度結構的晶格。磁性量測結果顯示，DMS皆顯示順磁行為，但當Mn的成分≧6%，LT-(In, Al, Mn)As DMS由順磁態變為鐵磁態。利用梯度緩衝層調變晶格常數，Mn濃度可提高到18％，且沒有第二相產生。當Mn濃度由11％增加到18％，T_c從25K變為40K。

Structures and properties of III-V diluted magnetic semiconductors grown by low temperature molecular beam epitaxy

Student: Wei-Ni Lee　　　　　　　　　　　　Advisor: Dr. Cheng-Tzu Kuo

Department of Materials Science and Engineering,
National Chiao Tung University

ABSTRACT

The III-V compound semiconductors have been widely used for high-speed electronic devices as well as for optoelectronic devices. However, new magnetic semiconducting nanosized film materials to minimize the scattering of electron spins between layers in the devices have been one of the key issues in spintronic device applications. The semiconductor with lower concentration of magnetic material (also called "diluted magnetic semiconductor (DMS)") is one of the new developing materials for such applications, which can be formed by incorporating magnetic atoms, e.g. Mn, into conventional III-V semiconductors. In this work, series of processes for fabricating DMS multilayer materials based on GaAs and InP semiconductors were successfully developed to examine their structures and properties. The processes include using the low temperature-molecular beam epitaxial (LT-MBE) (＜300℃) techniques to minimize the mutual diffusion between elements during the deposition period, so the metastable phases can be obtained with a relative higher concentration of magnetic material than the conventional method to improve their magnetic properties. The structures and propertied were characterized by TEM, DXRD (double crystal XRD), EPMA and SQUID. The experimental results can be roughly divided into three categories:

(1) On examining excess arsenic precipitation behaviors in LT-GaAs deposits, the results indicate that the excess arsenic content (As_{ex}) is depending on crystallographic orientation of the GaAs substrate, i.e., As_{ex} on (311)B > (311)A > (001);　this may be due to a combination effect of the accommodation factors of the crystallographic plane and bonding site difference.

By comparing the double- and single-dangling-bond sites, the latter sites preferentially possess a greater accommodation factor. Furthermore, the results of annealing experiments of the LT-GaAs structure containing six active regions (i-n_1-i, i-n_2-i, i-n_3-i, i-p_1-i, i-p_2-i, and i-p_3-i multilayers) find an interesting result: the excess arsenic depletion zone or distribution in i-n-i structures after annealing is depending on the doping concentration. For Si-doped concentration ≦ 10^{17} cm^{-3}, the arsenic depletion zone in n-layer can be formed in the present cases, which had not reported in the literature. This can be explained by the overlapping the n-layer thickness with the Debye length of the substrate at both sides of i-n interfaces.

(2) As to effects of 7 % Mn addition, post annealing and DMS layer thickness of Mn-doped LT-GaAs on their magnetic properties in three-layers structure (LT-(Ga, Mn)As /LT-GaAs/GaAs), the results show that the Curie temperature (T_c) of DMS can be greatly increased by a decrease in thickness and via annealing treatment, and indicates the greatest T_c for (001) GaAs substrate orientation. Annealing treatment is essentially to remove excess Mn_I from the interstitial sites in the lattice to decrease the donor-like defects, which may cause an increase in hole concentration and T_c. In other words, the diffusion path of Mn for the thinner DMS thickness is much shorter, which may result in a more effective removal of excess Mn_I from the lattice and a greater increase in T_c after annealing. Effect of substrate orientation is basically to affect the excess arsenic precipitation behavior. Therefore, a greater excess arsenic antisite defects in (311)A substrate orientation than in (001) orientation may neutralize more holes in the lattice to decrease T_c more in (311)A orientation.

(3) On (001) InP substrate, effects of the lattice constant variations of buffer layers on Mn doping of LT-(In, Al, Mn)As DMS materials were examined. The buffer layers of LT-(In, Al)As include nearly matched one-layer and the graded three-layers lattice structures. The results show that the LT-(In, Al, Mn)As DMS materials are paramagnetic, and become

ferromagnetic for Mn % ≧ 6 %. By using the graded buffer structures, the Mn concentration of DMS can reach 18 % without 2nd phase precipitation. The T_c of the DMS changes from 25K to 40K, when Mn concentration varies from 11 to 18 %.

誌　　謝

首先，要向我的指導教授 郭正次博士，致上 最高的謝意。感謝他在這些年間，給我極大的鼓勵與包容，並耐心指導我撰寫論文。使我能順利完成博士學位，並學習到追求知識的積極態度與研究的方法。

另外要感謝的是清華大學 黃金花博士。他在研究經費上的全力支持，並協助我討論實驗結果，與寫作技巧。還要感謝清華大學材料中心的長官與同事，使我在這個大家庭之中，受到大家的支持與鼓勵，才能順利的工作與學習。

特別要感謝我的口試委員們:

成功大學機械研究所李驊登教授、逢甲大學材料研究所何主亮教授中央大學機械研究所林景琦教授、清華大學材料研究所黃金花教授、交通大學奈米科技研究所許鉦宗教授、清華大學材料研究所游萃蓉教授、交通大學材料研究所潘扶民教授與交通大學材料研究所郭正次教授，在百忙之中抽控前來，並提出寶貴的建議。

感謝國科會貴儀中心蔡淑月小姐、陳怡蕙小姐、賴樹琴先生在實驗上的協助。還要感謝郭行建博士與陳遠富博士在實驗上的大力協助與討論，及劉恩惠博士，何金華小姐的幫助使我能克服困境，繼續往前。感謝分子束磊晶實驗室的夥伴 林文祥、楊武璋、方偉權、黃柏瑋及交通大學郭正次教授材料製程實驗室優秀的學弟、學妹們幫忙。

感謝我的父母、兄姐給我的支持與鼓勵。還有丈夫 賴蔚海與子女，陪我分享生活與學習上的一切苦與樂。

謝謝所有支持我的朋友！願將此成果與大家分享，並祝福大家！

List of symbols

a: Lattice constant

α: The angle between the molecular beam and the normal to the substrate

[As_{ex}]: Concentration of excess arsenic

[As_{Ga}]$_x$: Concentration of arsenic atoms which replace the Ga atom sites, where x can be p, i or n to represent the p-type, undoped or n-type doping, respectively.

BEP: Beam equivalent pressure

BF: Bright field image

2DEG: Two-dimensional electron gas

DF: Dark field image

DMS: Diluted magnetic semiconductor

DXRD: Double-crystal X-ray diffraction

ε_0: Permittivity of vacuum

ε: Permittivity of materials

fcc: Face-centered cubic

GaAs: Gallium arsenide

(Ga, Mn)As: Mn-doped GaAs

HEMT: High electron mobility transistor

(h, k, l)A: (h, k, l) GaAs wafer, where the single- and double-dangling-bond sites are As and Ga sites, respectively. (Ref. to Fig. 4.4)

(h, k, l)B: (h, k, l) GaAs wafer, where the single- and double-dangling-bond sites are Ga and As sites, respectively. (Ref. to Fig. 4.4)

HT-GaAs: High temperature growth GaAs

(In, Al, Mn)As: Mn-doped InAlAs

i-n-i: 3-layers structure (undoped/Si-doped/undoped GaAs layers)

i-p-i: 3-layers structure (undoped/Be-doped/undoped GaAs layers)

J**:** Beam flux of an ideal Knudsen cell

J_x**:** Beam flux of x source material

k**:** Boltzmann constant (= $8.617\times10^{-5}eVK^{-1}$)

λ_D**:** Debye wavelength

LT-GaAs: Low temperature growth GaAs

LT-MBE: Low temperature molecular-beam epitaxy techniques

M: Molecular weight

MBE: Molecular-beam epitaxy

Milli-Q: A trademark of ultrapure water purification system

Mn_I**:** Interstitial Mn atoms

N_A**:** Carrier concentration of acceptor

N_D**:** Carrier concentration of donor

n_x**:** Ionization efficiency of the x source materials

P**:** Pressure

q**:** Electron charge

RHEED: Reflection high-energy electron diffraction

RTA: Rapid thermal annealing

(Si, Be)GaAs: Si- and/or Be-doped GaAs

SQUID: Superconducting quantum interference device magnetometry

T_c**:** Curie temperature

T_S**:** Substrate temperature

TEM: Transmission electron microscopy

UHV: Ultra-high vacuum

Contents

Chinese abstract i

English abstract iii

Acknowledgment vi

List of symbols vii

Contents ix

Table headings xi

Figure captions xii

CHAPTER 1 INTRODUCTION 1

CHAPTER 2 TECHNICAL BACKGROUND 6

2.1 Structures, properties and applications of GaAs and InP 6

2.2 III-V diluted magnetic semiconductors (DMS) 9

2.3 LT-MBE 13

CHAPTER 3 EXPERIMENTAL METHODS 15

3.1 Flow chart of the experiments 15

3.2 MBE growth system 17

3.3 Raw materials and specimens pretreatments 19

3.4 MBE system calibration 22

3.5 Growth of LT-GaAs and LT-(Si,Be)GaAs on GaAs wafers 25

3.6 Growth and post annealing of LT-(Ga, Mn)As DMS on GaAs wafers 31

3.7 Growth of LT-(In, Al, Mn)As DMS and LT-(In, Al)As buffers on InP wafers 34

3.8 Structure analysis methods 37

3.9 Properties measurements 44

CHAPTER 4 RESULTS AND DISCUSSION 45

4.1 Effect of substrate orientation on arsenic precipitation in low-temperature-grown GaAs

45

4.2 Effects of doping type and concentration on precipitation of arsenic clusters in low-temperature-grown GaAs 56

4.3 Effects of thickness and post-annealing on the magnetic properties of $Ga_{0.93}Mn_{0.07}As$ 63

4.4 Effects of substrates orientation on the magnetic properties of $Ga_{0.93}Mn_{0.07}As$ 71

4.5 Property of $(In_{0.52}Al_{0.48})_{1-x}Mn_xAs$ / $In_{0.52}Al_{0.48}As$ / InP layer structure 78

4.6 Property of $(In_{1-y}Al_y)_{1-x}Mn_xAs$ / $(In_{1-y}Al_y)As$ / InP layer structure 85

CHAPTER 5 CONCLUSIONS 92

CHAPTER 6 FURTURE WORK 95

REFERENCES 96

Vita 109

List of my publications 110

Table headings

Table 3.1 Sample designations and their growing conditions of the LT-GaAs and LT-(Si, Be)GaAs epi-layers structures 26

Table 3.2 Sample designations and their growing conditions of the $Ga_{0.93}Mn_{0.07}As$ epi-layers structures 32

Table 3.3 Sample designations and their growing conditions of the $(In_{1-y}Al_{y})_{1-x}Mn_{x}As$ / $(In_{1-y}Al_{y})As$ / InP epi-layers structures 35

Figure Captions

Figure 1.1 Concept of spintronics 2

Figure 2.1 Schematic unit cell of zinc-blende structure 6

Figure 2.2(a) Schematic diagram of HEMT, (b) schematic diagram of 2DEG at the heterojunctions 8

Figure 2.3 Schematic diagram of carrier-induced ferromagnetism 9

Figure 2.4 Schematic diagram of a spin valve, a material can function as either (a) a conductor or (b) an insulator for electrons 11

Figure 3.1 Flow chart of the experiments 16

Figure 3.2 Schematic diagram of MBE growth chamber 18

Figure 3.3 The streak pattern of surface reconstructure by RHEED 21

Figure 3.4 (a) X-ray diffraction (XRD) measurements show that the (004) reflection of (Ga,Mn)As has the zinc-blende structure and the lattice constant *a* of (Ga,Mn)As increases with the increase of cell temperature (b) A relation of lattice constants of (Ga, Mn)As versus Mn content. 24

Figure 3.5 Schematic structures of alternately undoped and [Si] = $3\times10^{18}cm^{-3}$-doped LT-GaAs superlattice samples 27

Figure 3.6 Schematic illustration of the LT-GaAs structure containing six active regions (i-n_1-i, i-n_2-i, i-n_3-i, i-p_1-i, i-p_2-i, and i-p_3-i multilayers). The "*i*" denotes 35 nm thick undoped GaAs layer, "n_1", "n_2", and "n_3" ("p_1", "p_2", and "p_3") denote the Si-doped (Be-doped) GaAs layers with doping concentration of 10^{16}, 10^{17}, and $10^{18}cm^{-3}$, respectively. A 10 nm AlAs layer separated each active region. 30

Figure 3.7 Schematic diagram of the LT-(Ga, Mn)As structure 33

Figure 3.8 RHEED intensity oscillation of the reflected beam during MBE growth of GaAs 38

Figure 3.9 Cross-sectional samples preparation for transmission electron microscopy 40

Figure 3.10 Schematic diagram to show TEM method to determine the number density of arsenic clusters 41

Figure 3.11 Schematic illustration of DXRD technique 43

Figure 4.1(a) Cross-sectional TEM bright-field images of Sample H1 (The annealed LT-GaAs on GaAs(001) substrate) 48

Figure 4.1(b) Cross-sectional TEM bright-field images of Sample H2 (The annealed LT-GaAs on GaAs(311)A substrate) 49

Figure 4.1(c) Cross-sectional TEM bright-field images of Sample H3 (The annealed LT-GaAs on GaAs(311)B substrate) 50

Figure 4.2(a) Plan-view TEM images of Sample H1 (The annealed LT-GaAs on GaAs(001) substrate) 51

Figure 4.2(b) Plan-view TEM images of Sample H2 (The annealed LT-GaAs on GaAs(311)A substrate) 52

Figure 4.2(c) Plan-view TEM images of Sample H3 (The annealed LT-GaAs on GaAs(311)B substrate) 53

Figure 4.3 DXRD rocking curves of as-grown LT-GaAs of Samples H4, H5, and H6: (004) reflection for sample grown on (001), (311) reflections for samples grown on (311)B and (311)A substrates 54

Figure 4.4 Schematic illustration of ideal atomic structures at (311)A and (311)B surfaces 55

Figure 4.5(a) TEM bright field images of Sample B1 showing arsenic precipitates in different active regions after annealing at 600°C 58

Figure 4.5(b) TEM bright field images of Sample B2 showing arsenic precipitates in different active regions after annealing at 700°C 59

Figure 4.5(c) TEM bright field images of Sample B3 showing arsenic precipitates in different active regions after annealing at 800°C 60

Figure 4.6 DXRD rocking curves of GaAs (004) for 1-μm-thick undoped (Sample B6), [Si] = 10^{18} cm^{-3} doped (Sample B4), and [Be] = 10^{18} cm^{-3} doped (Sample B5) LT-GaAs samples 61

Figure 4.7 Arsenic cluster number density in each *i-x-i* region after annealing at 700°C (Sample B2) and 800°C (Sample B3), where $x = n_i$ or p_i 62

Figure 4.8 M-H curves of (Ga, Mn)As DMS (Sample C1) measured with in-plane magnetic field applied along [110] or $[\bar{1}10]$ directions at 10K 65

Figure 4.9 M-T curves of as-grown and post-annealed (Ga, Mn)As DMS (Samples C1, C2 and C3) measured under 1 Oe in-plane magnetic field 66

Figure 4.10 Curie temperature values (T_C) vs. thickness of as-grown and post-annealed (Ga, Mn)As DMS (Samples C1, C2 and C3) 67

Figure 4.11 The DXRD rocking curves of as-grown and post-annealed (Ga, Mn)As DMS (Sample C3) 68

Figure 4.12(a) M-H curves of as-grown (Ga, Mn)As DMS (Sample C1) measured with in-plane magnetic field applied along [110], $[\bar{1}10]$, [100], [010] directions,

respectively, at 10K 69

Figure 4.12(b) M-H curves of post-annealed sample C1 measured with in-plane magnetic field applied along [110], $[\bar{1}10]$, [100], [010] directions, respectively, at 10K 70

Figure 4.13(a) M-T curves of as-grown and post-annealed (Ga, Mn)As DMS (Samples D1), with $Ga_{0.93}Mn_{0.07}As$ epi-layer on (001) oriented substrate, measured under 1 Oe in-plane magnetic field 73

Figure 4.13(b) M-T curves of as-grown and post-annealed (Ga, Mn)As DMS (Samples D2), with $Ga_{0.93}Mn_{0.07}As$ epi-layer on (311)A oriented substrate, measured under 1 Oe in-plane magnetic field 74

Figure 4.14(a) M-H curves of $Ga_{0.93}Mn_{0.07}As$ epi-layer on GaAs(001) oriented substrate (Sample D1), measured with in-plane magnetic field applied along [110], $[\bar{1}10]$] directions at 10K 75

Figure 4.14(b) M-H curves of $Ga_{0.93}Mn_{0.07}As$ epi-layer on GaAs(311)A oriented substrate (Sample D2), measured with in-plane magnetic field applied along $[01\bar{1}]$, $[\bar{2}33]$ directions at 10K 76

Figure 4.15 The DXRD rocking curves of as-grown and post-annealed (Ga, Mn)As DMS (Sample D3) 77

Figure 4.16 The interfacial micrographs between (In, Al, Mn)As and InAlAs (Sample E4): (a) bright field TEM image and (b) lattice image 80

Figure 4.17 The DXRD rocking curves of (004) for (In, Al, Mn)As on InP (Sample E2, E4, and E5) 81

Figure 4.18 The M-H curves for $(In_{0.52}Al_{0.48})_{0.95}Mn_{0.05}As$ epilayer on InP (Sample E2), measured with in-plane magnetic field at 5K. Closed circles stand for "net" magnetization after subtracting the magnetization of InP substrate and solid line is results of linear fit of the experimental data. Inset shows the applied field dependence of magnetization at 5K for $(In_{0.52}Al_{0.48})_{0.95}Mn_{0.05}As$ epilayer on InP (Sample E2) and "bare" InP substrate with same size 82

Figure 4.19. M-H curves of as-grown and post-annealed for $(In_{0.52}Al_{0.48})_{0.92}Mn_{0.08}As$ epilayer on InP (Sample E4) and $(In_{0.52}Al_{0.48})_{0.89}Mn_{0.11}As$ epilayer on InP (Sample E5) measured with in-plane magnetic field at 5K 83

Figure 4.20 M-T curves under 100 Oe in-plane applied magnetic field along with [100] direction for $(In_{0.52}Al_{0.48})_{0.92}Mn_{0.08}As$ epilayer on InP (Sample E4) and $(In_{0.52}Al_{0.48})_{0.89}Mn_{0.11}As$ epilayer on InP (Sample E5) 84

Figure 4.21 The DXRD rocking curves of $(In_{1-y}Al_y)_{1-x}Mn_xAs$ epilayer on InP substrate (Samples G1, G2, and G4) 88

Figure 4.22 (a) High-resolution lattice image of the $In_{0.52}Al_{0.48})_{0.89}Mn_{0.11}As/In_{0.52}Al_{0.48}As$ interface region (Sample G3) and (b) the selected area diffraction pattern of $(In_{0.52}Al_{0.48})_{0.89}Mn_{0.11}As$ layer along [110] zone axis 89

Figure 4.23 M-H curves for $(In_{1-y}Al_y)_{1-x}Mn_xAs$ on InP substrate (Sample G1, G2, G4, and G5) with in-plane magnetic field applied along the $[\bar{1}10]$ direction. The dash dot line is a linear fit of the *M-H* curve for Sample G1 90

Figure 4.24 M-T curves under 100 Oe in-plane applied magnetic field along with $[\bar{1}10]$ direction for $(In_{1-y}Al_y)_{1-x}Mn_xAs$ on InP substrate (Samples G2, G3, G4, and G5) 91

CHAPTER 1

INTRODUCTION

III-V compound semiconductors are widely used for high-speed electronic devices as well as for optoelectronic devices. However the device size is getting smaller, the quantum effect will emerge as the size of device reducing to nanometer range. Thus, new materials of device, e.g. combined with the advantage of charges and spin of electrons, have been speculating by scientists. Conventional semiconductor device relies on electrical charge, while another important property of the electron spin plays no role in information communication and processing. A new class of devices based on the electron spin, rather than on the electrical charge, may yield the next generation of microelectronics. To combine semiconductors with magnetic materials, getting the advantage of charges and spin of carriers will create new device configurations. For instance, spintronics microprocessor could combine storage, logic, and computation on a single chip.

From a materials science point of view, the search for new magnetic semiconductors as well as some spintronic materials is making the field of spintronics more practical. III-V diluted magnetic semiconductors (DMS) are formed by incorporating magnetic atoms such as Mn into conventional semiconductors. Usually GaAs was grown at 600°C and InP at 450°C by MBE. The second phase (NiAs-structure MnAs) will be formed when Mn content is too high, which will interrupt the conductivity of materials. The LT-MBE has been developed; increase the Mn concentrations and suppress the segregation of second phase, thus III-V DMS is produced [Munekata-89-1849; Ohno-96-363]. In this thesis, the growth and characterizations of low-temperature GaAs (LT-GaAs) by Molecular-Beam Epitaxy (MBE) and the application of the LT-MBE growth skill to the formation III-V diluted magnetic semiconductors (DMS) are discussed. Figure 1.1 shows schematic concept of spintronics. In semiconductor spin-electronics, spin properties as well as electronic and optical properties

are utilized at the same time.

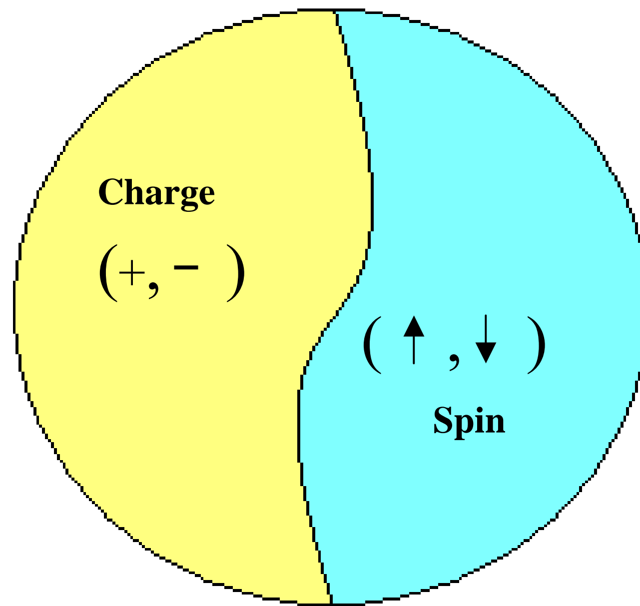

Figure 1.1 Concept of spintronics

For the application of magnetic semiconductors, a Curie point for ferromagnetic above room temperature is required. Zener model of ferromagnetism proposed by Dietl *et al.* [Dietl-00-1019] predicts that $T_C = Cxp^{1/3}$, where x is the mole fraction of substitutional Mn^{+2} ions, p is the concentration of hole and C is a constant specific to the host material. The growth substrate temperature (T_S) of LT-MBE is around 200~300°C. Either T_S or Mn content is too high the second-phase (NiAs-structure MnAs) formation at the growth front would take place. The RHEED patterns during growth provide the in-situ check of whether the two-dimensional growth is retained. The maximum x obtained so far is 0.08–0.1, and beyond this critical concentration formation of second phase takes place even at low growth temperatures. While ordinary GaAs is grown at 600°C, low temperature growth results in structural disorder, including a high density of donor-like arsenic antisite (As_{Ga}) and interstitial Mn defects (Mn_I), which compensate the hole concentration. The concentration of holes in the layer is only a fraction of the expected one, leading the degradation of magnetic and electrical properties [Yu-02-201303; Blinowski-03-121204]. Currently, the value of T_c of (Ga,Mn)As as high as 150-170K has been reported by several groups [Edmonds-02-4991; Ku-03-2302; Chiba-03-3020], including the work presented in this thesis.

The recent discovery of ferromagnetism in III-V DMSs [Munekata. 89-1849; Ohno. 96-363] opens up the possibilities of real practical spintronic devices because of the maturity of III-V semiconductor technology. The research for new magnetic semiconductors and other suitable spintronic materials is bringing the field of spintronics closer to the realm of practice. The LT-MBE is the first motivating factor to perform these studies. It is essential to understand the inevitably excess arsenic on the epi-layer during LT-growth and its application for LT-DMS growth. In this work, the experimental can be roughly divided into three subjects:

(1) Arsenic precipitation behaviors of LT-GaAs and LT-(Si,Be)GaAs on GaAs wafers

The LT-GaAs was grown on differently oriented GaAs substrates have been reported [Cheng-95-55; O'Hagan-97-2400], however none reported the control of arsenic precipitation upon

postgrowth annealing. Nevertheless, control of the density and distribution of arsenic precipitates is crucial for potential device applications. The aim of the study is to study effects of substrate orientation, doping type and concentrations on arsenic precipitation. The arsenic precipitation behavior was carefully characterized by transmission electron microscopy (TEM) and discussed.

(2) Structure and magnetic property of LT-(Ga, Mn)As DMS on GaAs wafers

(Ga, Mn)As growth on substrates with different (001) or (311)A orientations have an influence on the magnetic properties of this material. The extensive research activity in this field caused considerable progresses in understanding the physical phenomena leading to integrated ferromagnetism in III-V DMS. The aim of the study is to study structures and magnetic properties of the (Ga, Mn)As epitaxial films on GaAs substrates, focusing on effects of different orientation substrates, thickness and post-annealing on the magnetic properties of $Ga_{0.93}Mn_{0.07}As$, where high concentration Mn content exists.

(3) Magnetic property of the layer structures of LT-(In, Al, Mn)As DMS with LT-(In, Al)As buffers on InP wafers

It is well-known that most of III-V DMS are ternary and grown on GaAs substrates. Demonstrating the magnetic properties of new quaternary DMS, e.g. (In, Ga, Mn)As and (In, Al, Mn)As grown on InP substrates is significant for the study of spin transport effects in devices built on InP substrates. Moreover, such quaternary magnetic semiconductor has many potential advantages, for example, it is easy to adjust the bandgap energy, easy magnetization direction, and band structure by changing the indium content, which cannot be realized by ternary alloy magnetic semiconductors. Also, the quaternary $(In, Al)_{1-x}Mn_xAs$ DMS raises the possibility of fabricating complex heterostructures with engineered properties, combining magnetic layers having a large variety of electronic, optical, and spintronic properties in InP-based devices. But there are no reports about Mn doping in (In, Al)As and another important ternary semiconductor grown on InP substrates as well. The aim of the

project is to study structures and magnetic properties of the (In, Al, Mn)As epitaxial films on InP substrates, series of quaternary DMS, $(In_{0.52}Al_{0.48})_{1-x}Mn_xAs$ and $(In_{1-y}Al_y)_{1-x}Mn_xAs$ diluted magnetic semiconductors were grown on InP substrates are discussed.

CHAPTER 2

TECHNICAL BACKGROUND

2.1 Structures, properties and applications of GaAs and InP

III-V compound semiconductors such as GaAs, InP crystalline is cubic zinc-blende structure, which consists of two interpenetrating fcc sublattices. One sublattice is displaced by 1/4 of a lattice parameter in each direction from the other sublattice, so that each site of one sublattice is tetrahedrally coordinated with sites from the other sublattice. Figure 2.1 shows a unit cell of zinc-blende structure.

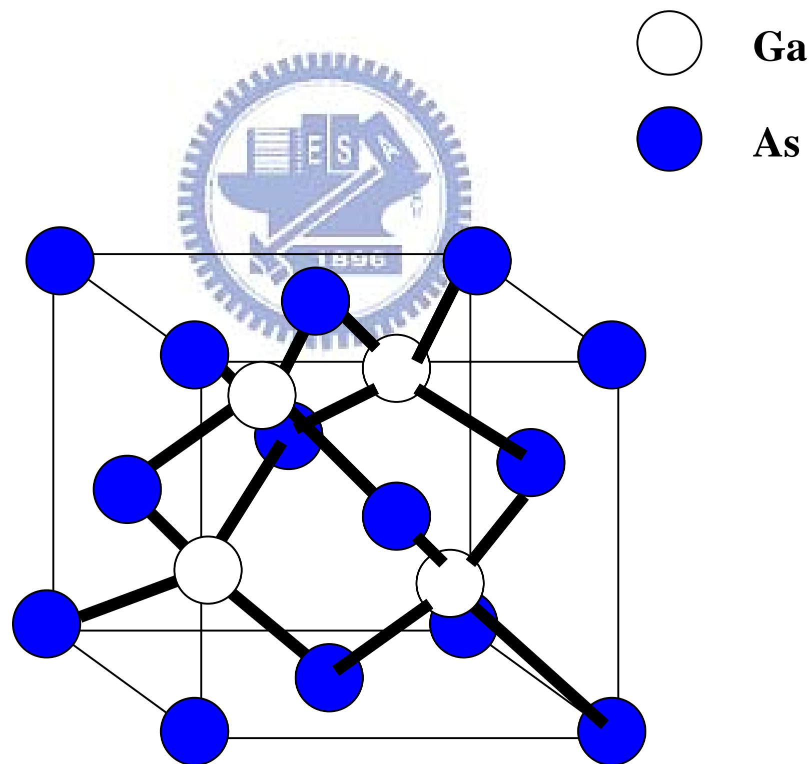

Figure 2.1 Schematic unit cell of zinc-blende structure

The benefit of GaAs over Si is its application to communications industry. GaAs is a kind of direct band gap material with the ability to emit light, which is useful for making lasers, light-emitting diodes, and microwave emitters used in cellular phones. Besides, it is attractive for high-speed devices since the electron saturation velocity in GaAs is 1.5 times that of Si. Scientists have been intrigued with the idea of fabricating artificial structures. The heteroepitaxial techniques allow one to grow heterostructures by changing the periodicity of the crystal during growth. The most widely used heterostructures are quantum wells, in which a single layer of one semiconductor is sandwiched between two layers of a large bandgap material. Such structures allow one to exploit special quantum effects that have become very useful in electronic and optoelectronic devices. The major application of GaAs at present is in the areas of microwave devices, high-speed digital integrated circuit, and as substrates for epitaxial layer growth to fabricate photonic and electronic devices. Figure 2.2(a) Shows schematic diagram of high electron mobility transistor (HEMT) with a junction between two materials with different band gaps e.g. GaAs and AlGaAs. The effect of this junction is to create a very thin layer where the Fermi level is above the conduction band, giving the channel very low resistance. This layer is called a two-dimensional electron gas(2DEG). A voltage applied to the gate alters the conductivity of this layer. Figure 2.2(b) Shows schematic diagram of 2DEG be formed at the heterojunctions.

For InP, the use is almost exclusively as substrates for growing lattice matched epitaxial film of alloy semiconductors such as $In_{0.53}Ga_{0.47}As$ and $In_{0.52}Al_{0.48}As$, the heterostructure epitaxy films can be formed on InP substrates. These ternary compounds semiconductor has many potential advantages, for example, it is easy to adjust the bandgap energy and band structure by changing the indium content. These compounds have been used in the light sources, detectors and wireless communication devices.

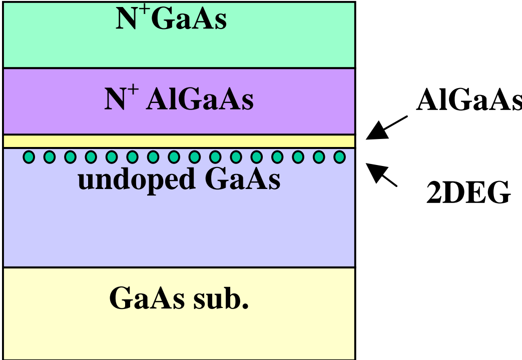

(a)

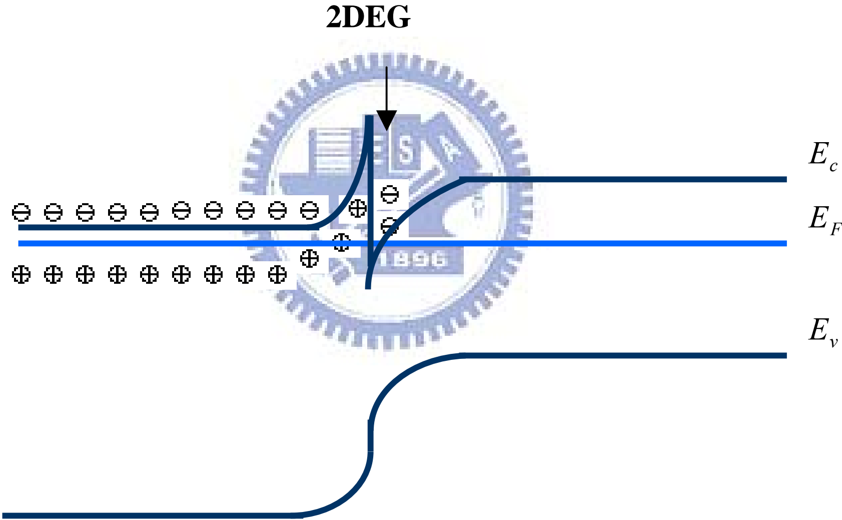

(b)

Figure 2.2(a) Schematic diagram of HEMT, (b) schematic diagram of 2DEG at the heterojunctions

2.2 III-V diluted magnetic semiconductors (DMS)

The III-V semiconductors such as GaAs have been in use in a wide variety of electronic equipments in the form of electronic and optoelectronic devices. Recently, III–V diluted magnetic semiconductors (DMSs), e.g. (In, Mn)As and (Ga, Mn)As have attracted intense attention due to their significance in basic physics and potential application to spintronics devices [Ohno. 92-2664; Hayashi. 97-4865]. Since the hole-mediated ferromagnetism [Dietl. 00-1019] in III–V semiconductors is sensitive to both electrical and less understood structural properties, the investigation of new diluted magnetic semiconductor is interesting and rewarding [Hayashi. 01-169139; Ohya. 03-139; Matsukura. 02-1].

The first successful growth of (In,Mn)As thin film on GaAs substrates was reported by Munekata et al. in 1989 [Munekata. 89-1849]. Subsequent discovery of the hole-induced ferromagnetism in p-type (Ga,Mn)As by Ohno et al. in 1996 [Ohno. 96-363]. The properties of (Ga,Mn)As films in relation to the growth parameters [Ohno. 98-363; Shen. 99-679]have been reported. Typical (Ga,Mn)As is realized by using solid source MBE where in Mn provides both localized spin and holes. Mn atoms couple to charge carriers in the host semiconductors via the exchange interaction, and the carriers behave like connectors, which get spin information from one Mn atom and deliver to the other Mn atoms. The spin of Mn atoms can be aligned in the same direction so that the (Ga, Mn)As compound exhibits ferromagnetic state. Figure 2.3 shows schematic diagram of carrier-induced ferromagnetism.

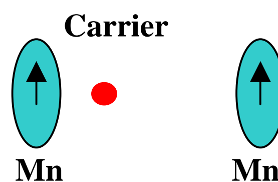

Figure 2.3 Schematic diagram of carrier-induced ferromagnetism

The lattice constants of LT-(Ga,Mn)As DMS were reported by a few investigators [Ohno. 96-363; Sadowski. 01-3271], which were determined by DXRD techniques. It was found that the lattice constant of LT-(Ga, Mn)As increases linearly with increasing Mn content. Basing on Vegard's law, the lattice constant (a) at room temperature for ($Ga_{1,}$ Mn)As DMS can be expressed by the following relations[Ohno. 96-363, Sadowski. 01-3271]

$$a = 0.566(1-x) + 0.598x \text{ (nm)} \quad (2\text{-}1)$$

and

$$a = 0.5654(1-x) + 0.5901x \text{ (nm)} \quad (2\text{-}2)$$

where x is fraction of Mn content, and the relation is a function of BEP and substrate temperature. Where BEP denotes beam equivalent pressure.

Usually, magnetic measurement of (Ga, Mn)As is carried out in a superconducting quantum interference device (SQUID) magnetometer. Ohno *et. al.* reported that the magnetization of easy axis of (Ga, Mn)As dependent on the strain of epilayers [Ohno. 96-405]. The direction of the magnetization of easy axis is in perpendicular to surface of (Ga,Mn)As with tensile strain on a thick lattice-relaxed ($In_{0.16}Ga_{0.84}$)As buffer layer, while for (Ga,Mn)As on a GaAs buffer layer with compressive strain, the direction of the magnetization of easy axis is in-plane.

Prinz *et al.* have reported a concept of spin valve [Prinz. 98-1660]. Figure 2.4 shows schematic diagrams of a spin valve. Two ferromagnetic layers were considered, a sandwiching non-magnetic conducting layer between them, which can function as either a conductor, or an insulator, for electrons. This means that the spin valve acts as a conductor for parallel of spin electrons, while it behaves as an insulator for anti-parallel spin electrons of two ferromagnetic layers. In Figure 2.4 (a), the device is expected as a conductor and the resistance is at its minimum, (b) the device is expected as an insulator. Thus, the resistance of this device strongly depends on the relative configurations of the ferromagnetic moments. This simple tri-layer system is commonly referred as a "spin valve". For practical usage, it is often constructed so that the magnetic moment of one ferromagnetic layer (the hard magnet) is very difficult to reverse at small magnetic field, while the other layer (the soft magnet) is very easy

to reverse.

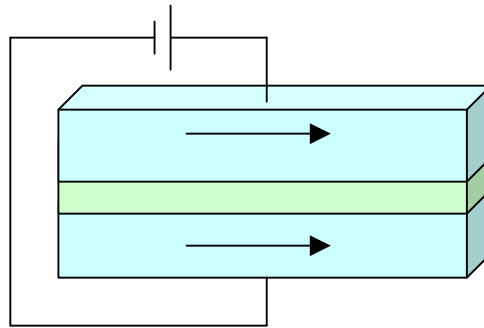

(a) Conductor

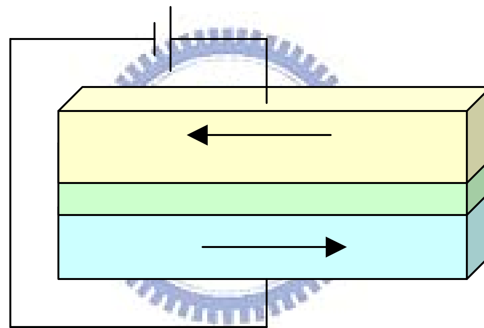

(b)Insulator

Figure 2.4 Schematic diagram of a spin valve, a material can function as either (a) a conductor or (b) an insulator for electrons

Both giant magnetoresistance (GMR) and tunneling magnetoresistance (TMR) are attracting much attention because of their potential applications in magnetic recording technology and memory devices. GMR effect is due to the spin-dependent scattering in metallic multilayers and TMR effect is due to the spin-dependent tunneling in ferromagnet/insulator/ferromagnet tunnel junctions. TMR effect, have been reported by Higo's group [Higo. 01-292]. The light-emitting spintronic devices using III-V heterostructures on GaAs substrate have been reported by Ohno's group [Ohno-99-709]. Their experimental results exhibiting the potential of ferromagnetic semiconductors based on III-V compound semiconductors system for exploring new physics and for developing new functionality toward future electronics. Other advantages of the new spintronic devices include increased data processing speed, decreased electric power consumption, and increased integration densities compared to semiconductor devices [Wolf. 03-703]. For instance, magnetic random access memory (MRAM) has the potential to higher data storage, faster data access and less power consumption than conventional memory devices. However, the T_c values to be expected by the mean-filed Zener model [Dietl-02-1019] as if of 5% Mn and 3.5×10^{20} cm^{-3} of holes are introduced into wide-gap semiconductors, the materials will be ferromagnetic at room temperature. As for $Ga_{1-x}Mn_xAs$ semiconductors, if the hole density of p is $3.5x10^{20}$ ㎝$^{-3}$, it will be possible to achieve a T_c beyond room temperature by increasing the Mn density to x =0.15. Figure 2.7 a Curie temperature was expected by the mean-filed Zener model [Dietl 00-1019].

Recently, T_c increases to 160–170 K [Edmonds-02-4991; Ku-03-2302]. Mathieu *et al.* Mathieu-03-184421] and Sørensen *et al.* [Sørensen-03-2287] studied the thickness dependence of magnetic properties for ultrathin $Ga_{1-x}Mn_xAs$ (≤ 25 nm) and have been reported. Very recently, several groups had focused on Mn doped (In, Ga)As and the Curie temperature of 100–130 K, similar to that of (Ga, Mn)As, had been reported in $(In, Ga)_{1-x}Mn_xAs$ with x ≥ 0.10 [Slupinski. 02-1592; Ohya. 03-2175].

2.3 LT-MBE

While ordinary GaAs is grown at 600°C, GaAs grown at a low temperature (LT-GaAs) has attracted much attention due to its unique electronic and optical properties [Look-90-3578; Nolte-93-1356]. When growing at 200 ~ 300°C, the GaAs layer contains quenched-in arsenic (~1%) in excess of the bulk equilibrium concentration [Kaminska-89-1881]. This excess arsenic thus results in an expansion of the lattice and a high concentration of antisite defects with a deep-level donor-like character [Liliental-Weber- 91- 2153]. The reduced recombination time of approximately 400 fs [Gupta-91-3276] makes LT-GaAs very suitable for integrated subpicosecond optoelectronic switches [Loukakos-01-2883; Yano-03-3966]. Moreover, upon post-growth annealing above 500°C, excess arsenic precipitates into clusters, accompanied by the relaxation of strain, and the resistance of LT-GaAs changes from a low-resistivity state to an excellent semi-insulating state [Warren-90-1331]. The arsenic precipitates have been identified as hexagonal arsenic [Melloch-90-1531].

This semi-insulating property offers the benefits of excellent device isolation in GaAs The optically inactive, and crystalline, and high-quality GaAs active layers can be grown on top of the buffer to improve output resistance and breakdown voltages was reported [Smith-88-77]. And a metal-semiconductor field-effect transistor (MESFET) utilizing surface layers of GaAs grown at a low temperature by MBE (LT-GaAs) under the gate electrode has been reported. The high trap density of LT-GaAs reduces the surface fields of the FET, suppresses gate leakage, and increases the gate-drain breakdown voltage without sacrificing current drive capability [Lin-90-561].

Two models compete to explain the behavior of annealed LT-GaAs. The first model proposed by Look [Look-90-3578] explains the semi-insulating property of annealed LT-GaAs as the compensation of carriers by the deep EL2-like donor levels. The second model proposed by Warren et al. is usually referred to as "buried Schottky model" [Warren-90-1331]. In this model,

the metallic arsenic precipitate forms a Schottky barriers at metallic/GaAs interface, depleting a portion of the surrounding apace. When the depletion regions are overlapped, the material will demonstrate the semi-insulating property.

Previous studies showed that arsenic precipitation in annealed LT materials can controlled by doping effects [Melloch-92-177; Liu-95-279; Missous-94-3396]. It has been found that arsenic precipitates preferentially form in Si-doped GaAs then intrinsic and least favorably in Be-doped GaAs for moderately doped GaAs. However, when the Si and Be doping concentrations reach certain levels (≥ 5 x 10^{18} cm^{-3}), an opposite precipitation behavior occurs [Huang-03-305; O'Hagan-96-8384] and arsenic precipitation at the *i*/*n* interface will be influenced by the Debye length λ_D.

$$\lambda_D = \left[\frac{\varepsilon \varepsilon_0 kT}{q^2 (N_D - N_A)} \right]^{1/2} . \qquad (2\text{-}3)$$

CHAPTER 3

EXPERIMENTAL METHODS

3.1 Flow chart of the experiments

In this experiment, GaAs and InP wafers were used as the substrates to deposit LT-GaAs, LT-(Ga, Mn)As and LT-(In, Al, Mn)As by MBE system. The wafers were thoroughly degreased using organic solvents and then baked to remove the adsorb vapor. The baked samples were then transfer to the MBE growth chamber and subjected to de-oxidation to remove the oxides from the surface, and then followed by MBE deposition. The grown samples were examined by TEM, DXRD, EMPA and SQUID. The detailed procedures are shown in Figure 3.1.

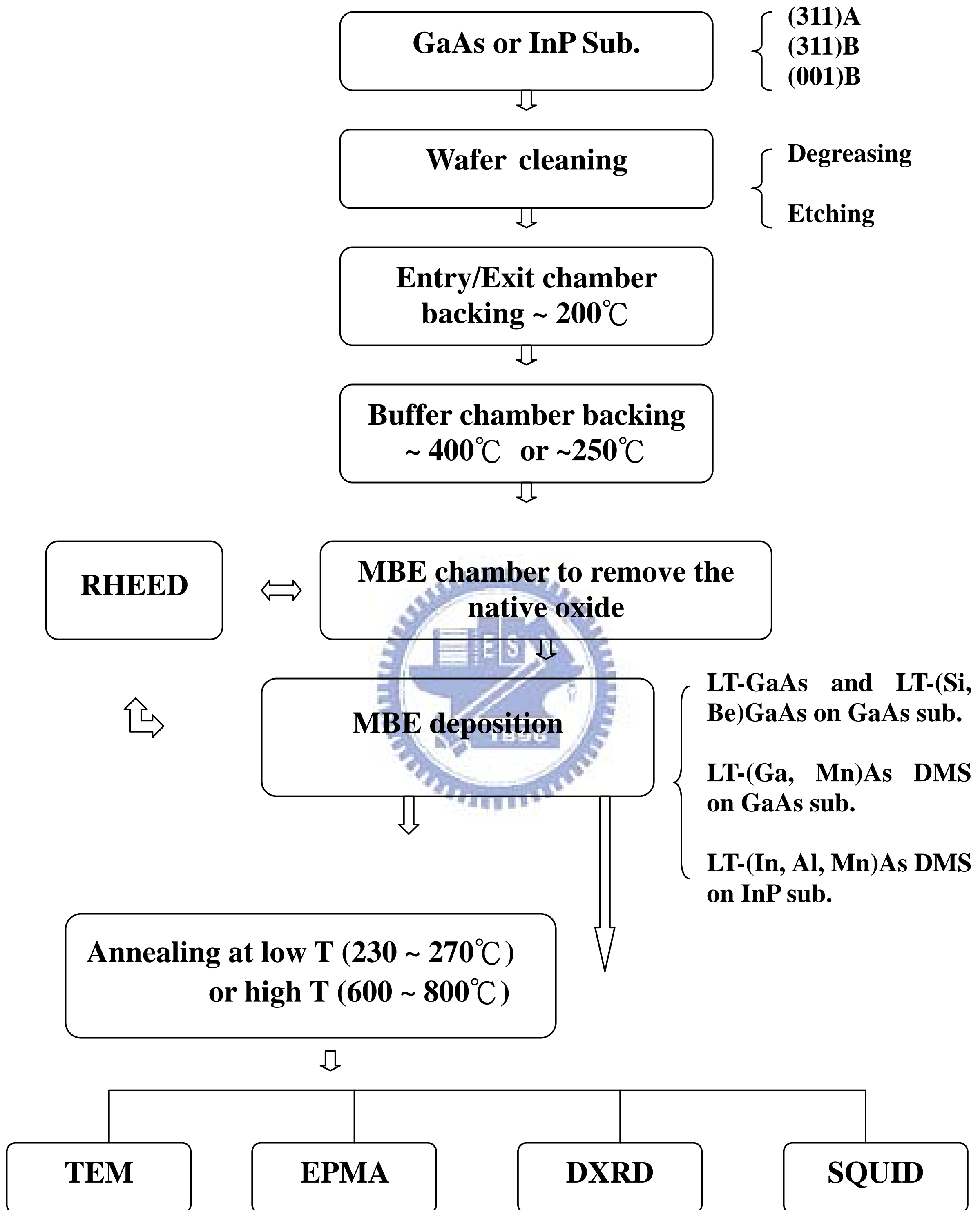

Figure 3.1 Flow chart of the experiments

3.2 MBE growth system

A MBE of Varian GEN-II ultra-high vacuum (UHV) system includes Entry/Exit chamber, buffer chamber, and growth chamber. ion pump, cryo-pump, titanium sublimation pump, dry pump, and sorption pumps are used to achieve UHV pressures in the chamber. Figure 3.2 shows a schematic diagram of MBE growth chamber system. The growth chamber includes 8 source cells (including two Ga sources, Al, In, Mn, Be, Si and arsenic sources), reflection high-energy electron diffraction (RHEED) analysis system, ionization gauges, quadruple mass spectrometer and rotating substrate holder. The working ranges of 5 different types of vacuum pumps in the systems are:

(1) Sorption pump: 760 ~ 10^{-4} torr

(2) Dry pump: 760 ~ 10^{-6} torr

(3) Ion pump: 10^{-3} ~ 10^{-11} torr

(4) Cryogenic pump: 10^{-3} ~ 10^{-10} torr

(5) Titanium sublimation pump: 10^{-4} ~ 10^{-11} torr

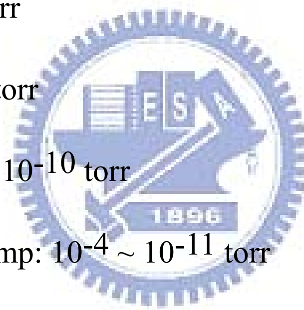

The growth chamber is equipped with 8 source cells configured in circle array, and the central axes of these cells cross at the substrate holder. The beam flux monitor is an ion gauge located 180° from the substrate. By rotating this ion gauge to the growth position, it is possible to measure the change in pressure caused by molecular beams striking the gauge. The molecular and atomic beams can be switched on and off by shutters in front of the cells, which are actuated by computer control. The Eurtherm controller governs the temperature of each substrate heater and all sources heated with a temperature accuracy of typically ±0.1℃.

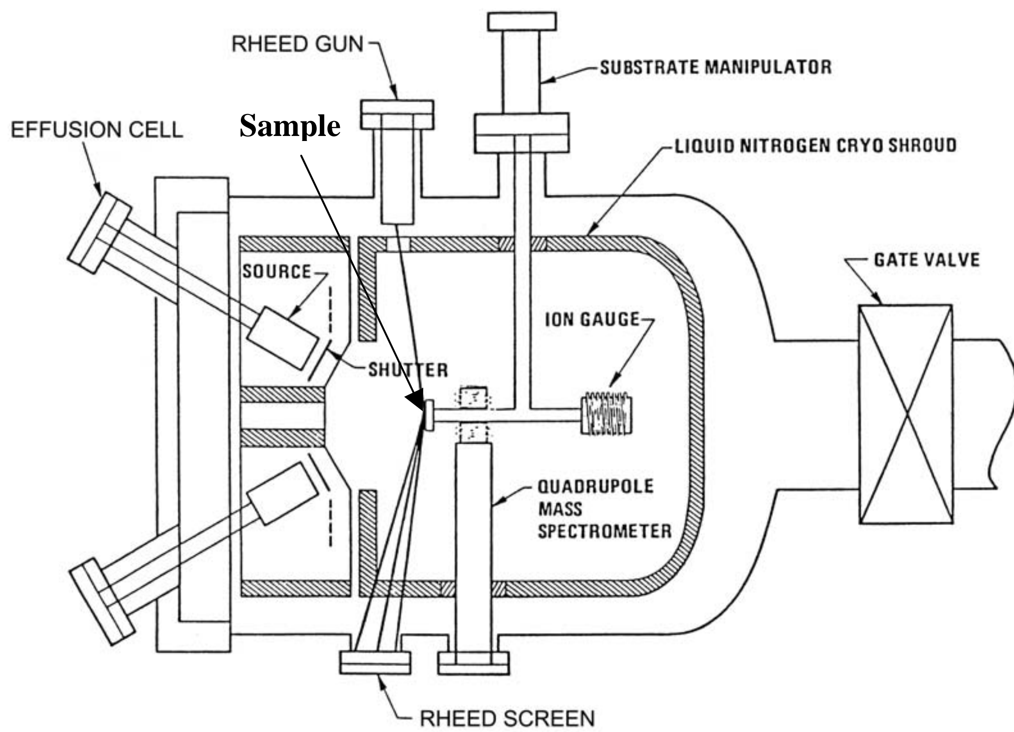

Figure 3.2 Schematic diagram of MBE growth chamber system (From the Manual of Varian GEN-II, 1987)

3.3 Raw materials and wafer pretreatments

The raws materials used in this experiment include 7 different source materials for MBE deposition, two substrate materials (GaAs and InP) and some organic solvents and etching solutions. The specifications of the raw materials are shown in the following tables.

Source	Purity	Manufacturer
Gallium	8N	Wafer Technology
Arsenic	7N	United Mineral & Chemical corp
Manganese	7N	Wafer Technology
Aluminium	6N	UMAT
Indium	7N	RASA Industries
Silicon	7N	Wafer Technology
Beryllium	5N	Wafer Technology

Chemical solution		Manufacturer
Acetone	CMOS	J. T. Baker
Methanol	CMOS	J. T. Baker
Hydrogen peroxide	31%	Merck
Sulfuric Acid	98%	Merck
Hydrochloric Acid	30%	Merck
Ammonium Hydroxide	10%	Merck
Bromine	15%	Merck

Substrate	Manufacturer
GaAs(001)	American Xtal Technology
GaAs(311)A	American Xtal Technology
GaAs(311)B	American Xtal Technology
InP(001)	Sumitomo

Wafer pretreatment includes wafers cleaning, baking and deoxidization. The GaAs and InP wafers were used in this study. The cleaved wafers were first chemically cleaned and blown dry with nitrogen gas. Mount the wafers on Mo blocks for sample handling. Load and bake them in entry/exit chamber at 200℃ for 2 hour to desorb the water vapor, and followed by baking in buffer chamber at 400℃ for 30 min for GaAs wafers (or at 250℃ for InP wafers) for further outguessing the chemical organic solvent. The samples are then transferred to growth chamber and subjected to de-oxidation to remove the oxides from the surface. The de-oxidation process was monitored *in situ* with reflection high-energy electron diffraction (RHEED) system. When the surface protective oxide layer was removed, the surface reconstruction RHEED pattern changed to streak, as shown in Figure 3.3. The epi-layers structure was then grown.

The cleaning procedures for GaAs and InP substrates are different. The detailed procedures are described as below:

For GaAs wafers cleaning procedures:

(1) Degreasing steps: Sequence with hot acetone, methanol, and rinsed in deionized water.

(2) Etching steps: H_2SO_4 : H_2O_2 : H_2O (5:1:1) for 10 minutes.

(3) After etching, the wafer is flooded with deionized water to stop the etchant, rinsed in deionized water, and blown dry with nitrogen gas.

For InP wafers cleaning procedures:

(1) Degreasing steps: Sequence with hot acetone, methanol, and rinsed in deionized water.

(2) Etching steps: Bromine-methanol (0.2 ~ 0.5%) for 10 minutes.

(3) After etching, the wafer is flooded with methanol to stop the etchant, rinsed in methanol and deionized water, and blown dry with nitroger gas.

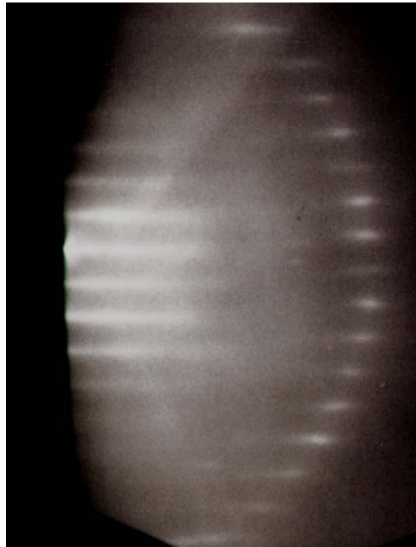
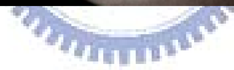

Figure 3.3 The streak pattern of surface reconstructure by RHEED system

3.4 MBE system calibration

The system calibration for growth rate and doping concentration is essential to MBE precise deposition. One way to calibrate the growth rate is to use the BEP gauge. The BEP is proportional to the flux at the sample surface and hence the growth rate. This measurement is dependent on factors such as the geometry of the system and ionization efficiency of the material being measured. One way to calibrate the growth rate is to use the BEP gauge. The BEP is proportional to the flux at the sample surface and hence the growth rate. This measurement is dependent on factors such as the geometry of the system and ionization efficiency of the material being measured.

For calibration of growth rates (In, Al, Mn, Ga)

The furnace for growth are set to the intended operating temperatures, and allowed to equilbrate for about 20 minutes. It is easier to change the Group III fluxes rather than the Group V fluxes. For a given system, the relative flux ratios from two cells may be calculated from the beam equivalent pressures (BEP) values according to:

$$\frac{J_1}{J_2} = \frac{BEP_1}{BEP_2}\frac{n_2}{n_1}\left(\frac{T_1 M_2}{T_2 M_1}\right)^{1/2} \tag{3-1}$$

Where J_x: Beam flux, T: cell temperature (K), M: molecular weight and n: ionization efficiency.

The growth rates were measured by RHEED oscillation at given furnace and substrate temperatures. During growth of a high quality surface oscillations in intensity of the integral streaks can be observed, which can in very simple terms be described by layer-by-layer growth, where a complete layer gives the brightest streaks, while a half layer somewhat disturbs the surface periodicity causing the RHEED intensity to decrease. The frequency of the oscillations, correspond to the growth rate, while during layer-by-layer growth, the surface

periodically changes its morphology because of the nucleation and coalescence of islands in the growing layers.

For calibration of doping concentration (Si, Be)

Substiuting the dopent atoms of Si for Ga sites will form an n-type GaAs. And substiuting the dopent atoms of Be for Ga sites will form a p-type GaAs. The doping concentrations of as-grown samples measured by a C-V electrochemical system or a Hall set-up.

For calibration of Mn concentrations

A relation of lattice constants versus Mn cell temperature was shown in Fig. 3.4(a) X-ray diffraction (XRD) measurements show that the (004) reflection of (Ga,Mn)As has the zinc-blende structure and the lattice constant *a* of (Ga,Mn)As increases with the increase of cell temperature (b) A relation of lattice constants of (Ga, Mn)As versus Mn content. Mn contents were determined by electron microprobe analysis (EMPA).

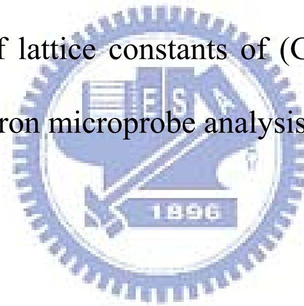
1896

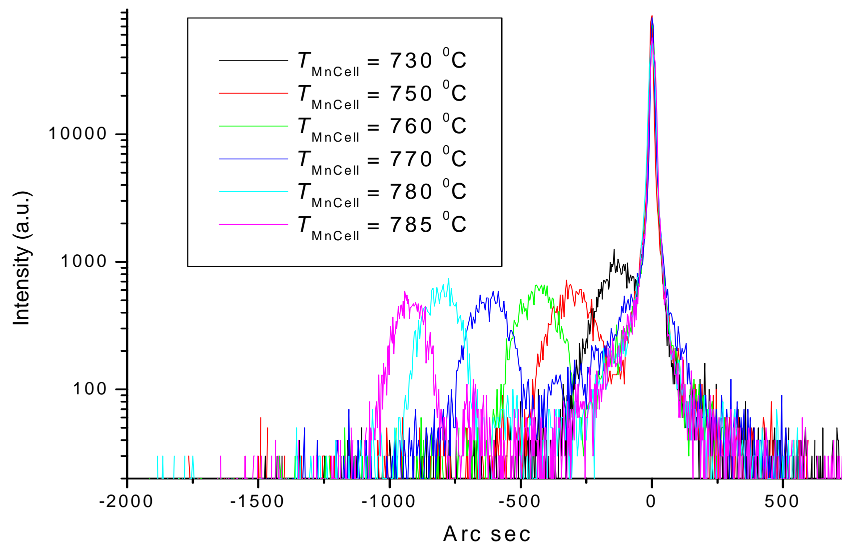

(a)

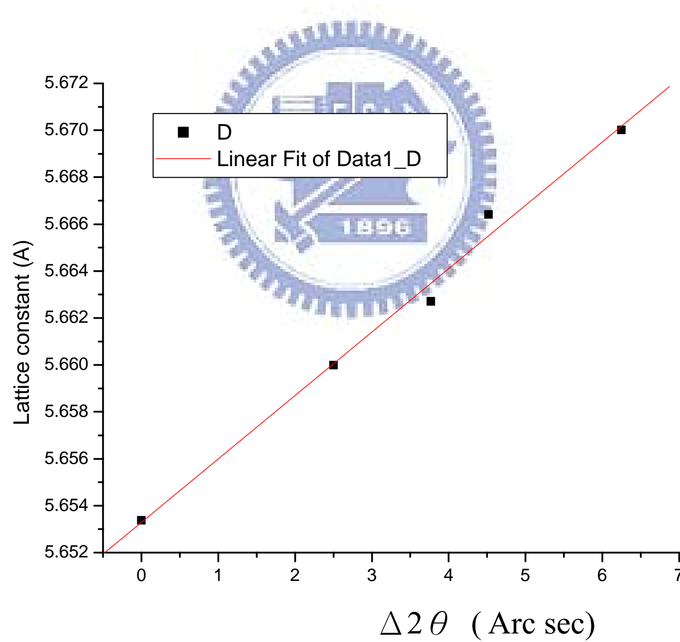

(b)

Figure 3.4 The surface reconstruction (a) Double crystal X-ray diffraction (DXRD) measurements show that the (004) reflection of (Ga,Mn)As has the zinc-blende structure and the lattice constant *a* of (Ga,Mn)As increases with the increase of Mn cell temperature (b) A relation of lattice constants of (Ga, Mn)As versus Mn content.

3.5 Growth of LT-GaAs and LT-(Si,Be)GaAs on GaAs wafers

This experiment includes two parts, (1) the effects of substrate orientation and (2) the effects of doping type and concentrations on arsenic precipitation. The growth procedures for the 1st part are as follow: The sample designations and their growing conditions for different structures are shown in Table 3.1 and Figure. 3.5. The epi-layers of LT-GaAs were grown on (001), (311)A, and (311)B GaAs substrates, denoted as H1, H2 and H3. Growth rates of 0.8 μm/h for GaAs and 0.2 μm/h for AlAs and and V/III beam equivalent pressure ratio of 15 were used. The LT-GaAs structure consists of a 5-period "superlattice" of alternately undoped and [Si] = 3×10^{18} cm^{-3}-doped GaAs layers. The three (001), (311)A, and (311)B GaAs substrates were mounted on the same Mo block to ensure identical growth conditions. Following native oxide desorption, a 300 nm undoped GaAs buffer layer was first grown at 580°C to smooth the surface, followed by a 15 nm AlAs mark layer at the same temperature. Growth was then interrupted and the substrate temperature was ramped down to 250°C. The 5 periods of 33 nm undoped and 33 nm Si-doped GaAs "superlattices", a 15 nm AlAs diffusion barrier, and a 50 nm GaAs cap layer were subsequently grown. The AlAs layer was grown as a marker for later transmission electron microscope observations. Post-growth annealing was carried out by a rapid thermal annealing system at 800°C in forming gas for 30 s. To further characterize the concentration of excess arsenic incorporated into the LT-GaAs layers, three samples with 1000 nm undoped LT-GaAs were also grown under the same growth conditions as aforementioned on the (001), (311)A, and (311)B-oriented substrates, denoted as H4, H5 and H6.

Table 3.1

Sample designations and their growing conditions of the LT-GaAs and LT-(Si, Be)GaAs epi-layers structures

※

Sample No.	Substrate	BEP (V/III)△ ratio	Epi-layer structure* (Thickness, nm)	Post-annealing (℃)
H1	GaAs(001)	15	as Fig.3.4	800
H2	GaAs(311)A	15	as Fig.3.4	800
H3	GaAs(311)B	15	as Fig.3.4	800
H4	GaAs(001)	15	LT-GaAs (1000)	x
H5	GaAs(311)A	15	LT-GaAs (1000)	x
H6	GaAs(311)B	15	LT-GaAs (1000)	x
B1	GaAs(001)	25	as Fig.3.5	600
B2	GaAs(001)	25	as Fig.3.5	700
B3	GaAs(001)	25	as Fig.3.5	800
B4	GaAs(001)	25	LT-Si-doped GaAs (1000)	x
B5	GaAs(001)	25	LT-Be-doped GaAs (1000)	x
B6	GaAs(001)	25	Undoped LT-GaAs (1000)	x

*Growth rates of GaAs = 0.8 μm/h; AlAs = 0.2 μm/h

Substrate temperature = 250℃

△For samples H1~H6: BEP of Ga = 7×10^{-7} torr, BEP of As = 1.05×10^{-5} torr

For samples B1~B6: BEP of Ga = 7×10^{-7} torr, BEP of As = 1.75×10^{-5} torr

Layer	Thickness
LT GaAs Cap layer	**50 nm**
LT AlAs Mark layer	**15 nm**
LT GaAs: Si-doped	**33 nm**
LT GaAs	**33 nm**
HT AlAs Mark layer	**15 nm**
HT GaAs Buffer	**300 nm**
GaAs Substrate	

A ‘‘superlattice’’ with five-periods of alternately undoped and Si-doped GaAs layers

Figure 3.5 the surface reconstruction Schematic structures of alternately undoped and [Si] = $3\times10^{18}cm^{-3}$-doped LT-GaAs superlattice samples

The growth procedures for 2nd part on the effects of doping type and concentrations on arsenic precipitation are shown in Table 3.1 and Figure 3.6. Previous studies showed that arsenic precipitation in annealed LT materials be controlled by doping effects, It has been found that arsenic precipitates preferentially form in Si-doped GaAs than intrinsic and less favorably in Be-doped GaAs for moderately doped GaAs. However, when the Si and Be doping concentrations reach certain levels ($\geq 5 \times 10^{18}$ cm^{-3}), an opposite precipitation behavior occurs [Huang-03-305]. Both the inter-diffusion of arsenic related defects and doping effects during annealing among the LT layers make this a more complicated system for understanding the arsenic precipitation behavior in lightly doped LT-GaAs. Thereby, the aim of the project is to study effects of doping type and concentration on arsenic precipitation.

The designed structure consists of three *i-n-i* and three *i-p-i* active regions, with doping levels ranging from 10^{16} to 10^{18} cm^{-3}, in which each active region is separated with a 10 nm AlAs marker layer. Owing to the high activation energy but small diffusion constant for Al and Ga inter-diffusion, the thin AlAs layer acts as an inter-diffusion barrier between adjacent active regions, and the effects of doping type and concentration on arsenic precipitation behaviors can be clearly recognized. The growth rates of 0.8 μm/h for GaAs and 0.2 μm/h for AlAs and the V/III beam equivalent pressure ratio of 25 were used. Following native oxide desorption, a 100 nm GaAs buffer layer was first grown at 580°C to smooth the surface, followed by a 10 nm AlAs diffusion barrier at the same temperature. Growth was then interrupted by closing the Al effusion furnace shutter, the substrate temperature was ramped down to 250 °C and the As shutter was closed when the substrate temperature was below 400 °C to maintain a clear 2x4 surface reconstruction, as observed by reflection high-energy electron diffraction (RHEED). It took about 15 minutes to stabilize the substrate temperature. Subsequently, the low-temperature active layers and a 35 nm GaAs cap layer were grown. The LT-GaAs sample was consisted of six active regions, i.e., three regions of undoped/Be-doped/undoped (*i-p-i*) multilayers and another three regions of

undoped/Si-doped/undoped (*i-n-i*) multilayers. Each *i-n-i* or *i-p-i* region was separated by a thin AlAs layer, which acted as both a diffusion barrier and a marker layer. The thickness of each doped or undoped GaAs layer was 35 nm. The doping levels in the p_1, p_2 and p_3 layers (and n_1, n_2, and n_3 layers) were 2×10^{16}, 2×10^{17}, and 2×10^{18}cm^{-3}, respectively.

The as-grown the sample was cleaved into three pieces and the post-annealing was carried out in a rapid thermal annealing (RTA) system at 600, 700 and 800°C for 30 s, respectively, denoted as B1, B2 and B3. To further characterize the concentration of excess As incorporated into the LT-GaAs layers, three 1 μm thick LT GaAs samples of [Si] = 10^{18} cm^{-3} doped, [Be] = 10^{18} cm^{-3} doped and undoped were also grown under the same growth conditions as aforementioned, denoted as B4, B5 and B6.

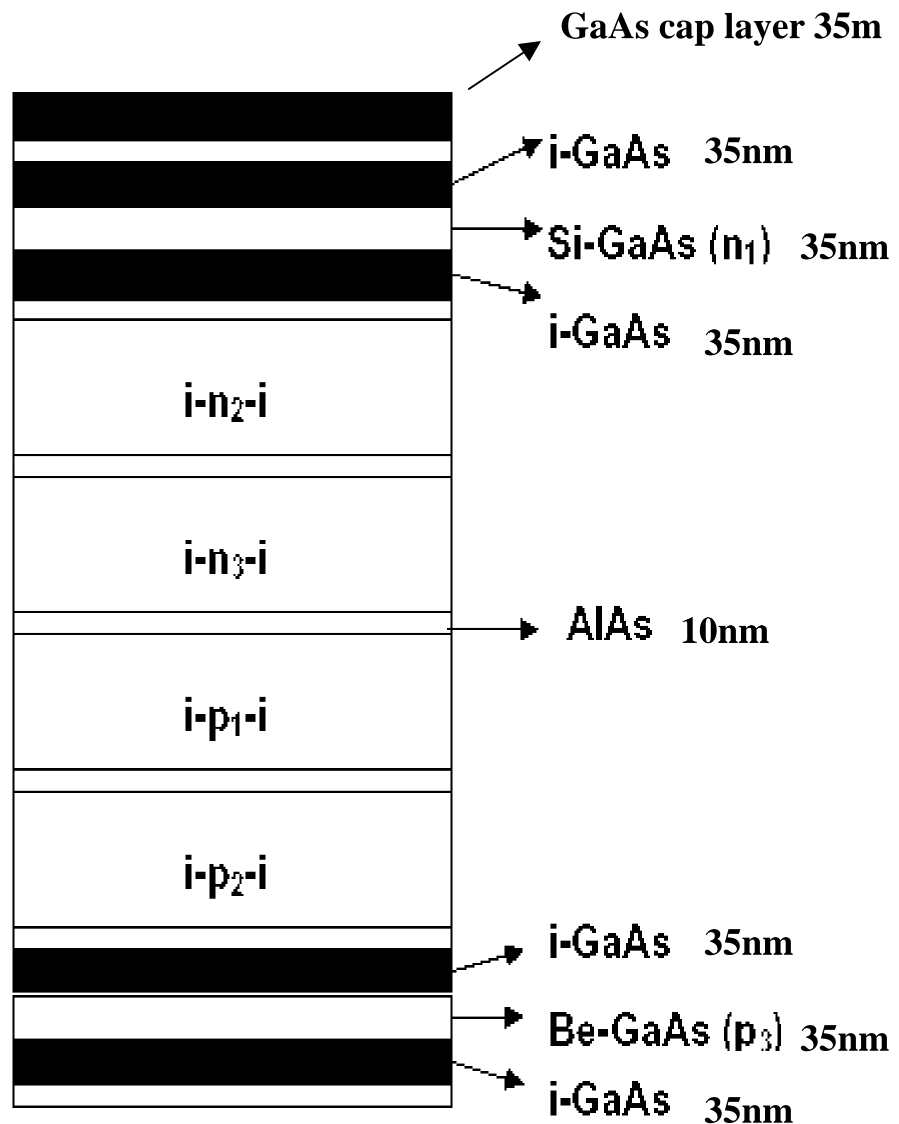

Figure 3.6 Schematic diagram of the LT-GaAs structure containing six active regions (i-n_1-i, i-n_2-i, i-n_3-i, i-p_1-i, i-p_2-i, and i-p_3-i multilayers). The "*i*" denotes 35 nm thick undoped GaAs layer, "n_1", "n_2", and "n_3" ("p_1", "p_2", and "p_3") denote the Si-doped (Be-doped) GaAs layers with doping concentration of 10^{16}, 10^{17}, and 10^{18}cm^{-3}, respectively. Each active region were separated by a 10 nm AlAs layer

3.6 Growth and post annealing of LT- (Ga, Mn)As DMS on GaAs wafers

This experiment includes two parts, (1) the effects of thickness and post-annealing and (2) the effects of substrates orientation on the magnetic properties of $Ga_{0.93}Mn_{0.07}As$. The growth procedures for the 1st part are as follows: The sample designations and their growing conditions for different structures are shown in Table 3.2 and Figure. 3.7. The Samples of (Ga, Mn)As DMS on GaAs wafers were grown on GaAs (001) substrates. A growth rate of 0.5 μm/h and a V/III beam equivalent pressure ratio of 15 were used. Following native oxide desorption, a 250 nm thick GaAs buffer layer was first grown at 560°C to smoothen the surface. Then the substrate temperature was lowered to 250°C, and subsequently 250 nm LT-GaAs buffer layer was grown. Finally, a series of 25 nm, 100 nm and 1000 nm of $Ga_{0.93}Mn_{0.07}As$ epi-layers were grown, respectively, denoted as C1, C2 and C3. Post-growth annealing of samples are carried out at 250℃ for 1.5 hrs in air.

The growth procedures for the 2nd part of the effects of substrates orientation on the magnetic properties of $Ga_{0.93}Mn_{0.07}As$ are as follows: The sample designations and their growing conditions for different structures are shown in Table 3.2 and Figure. 3.7. The samples of LT-(Ga, Mn)As DMS on GaAs wafers were grown on GaAs (001) and (311)A substrates, denoted as D1 and D2. The (001) and (311)A GaAs substrates were mounted on the same Mo block to ensure identical growth conditions. Growth rates of 0.5 μm/h for GaAs and a V/III beam equivalent pressure ratio of 15 were used. Following native oxide desorption, a 250 nm thick GaAs buffer layer was first grown at 580 °C to smoothen the surface. Growth was then interrupted and the substrate temperature was lowered to 250 °C, followed by the growth of 250 nm LT-GaAs buffer layer and 25nm of $Ga_{0.93}Mn_{0.07}As$ epilayers. Post-growth annealing was carried out by a thermal annealing system at 250℃ in air for 1.5hrs. To further characterize the concentration of excess arsenic incorporated into the $Ga_{0.93}Mn_{0.07}As$ epilayers, one sample with 250 nm LT-GaAs buffer layer and 1000 nm of

$Ga_{0.93}Mn_{0.07}As$ was subsequently grown on the (001) oriented substrates under the same growth condition as aforementioned, denoted as D3.

Table 3.2 Sample designations and their growing conditions of the $Ga_{0.93}Mn_{0.07}As$ epi-layers structures

Sample No.	Substrate	Epi-layer structure* (Thickness, nm)
C1	GaAs(001)	as Fig. 3.6 (25)
C2	GaAs(001)	as Fig. 3.6 (100)
C3	GaAs(001)	as Fig. 3.6 (1000)
D1	GaAs(001)	as Fig. 3.6 (25)
D2	GaAs(311)A	as Fig. 3.6 (25)
D3	GaAs(001)	as Fig. 3.6 (1000)

* Growth rate of GaAs = 0.5 μm/h,

Growth substrate temperature = 250℃

HT-GaAs buffer layer: Thickness = 250 nm, Temperature = 580℃

LT-GaAs buffer layer: Thickness = 250 nm, Temperature = 250℃

BEP of Ga = 4.5×10^{-7} torr, BEP of As = 6.75×10^{-6} torr

i.e. BEP (V/III) ratio =15,

LT-$Ga_{0.93}Mn_{0.07}As$ (250℃) 25 ~ 1000 nm
LT-GaAs 250 nm (250℃)
HT-GaAs 250 nm (580℃)
GaAs Substrate

Figure 3.7 Schematic diagram of the LT-(Ga, Mn)As structure

3.7 Growth of LT-(In, Al, Mn)As DMS and LT-(In, Al)As buffers on InP wafers

This experiment includes two parts, (1) $(In_{0.52}Al_{0.48})_{1-x}Mn_xAs$ DMS and (2) $(In_{1-y}Al_y)_{1-x}Mn_xAs$ DMS. The growth procedures for the 1st part are as follows: The sample designations and their growing conditions for different structures are shown in Table 3.3. A series of $(In_{0.52}Al_{0.48})_{1-x}Mn_xAs$ / $In_{0.52}Al_{0.48}As$ / InP layer structures were grown on (001) semi-insulating InP substrates. The Samples are denoted as E1, E2, E3, E4 and E5. A growth rate of 0.3 μm/hr and a V/III beam equivalent pressure ratio of 20 were used. Following native oxide desorption, a 100 nm $In_{0.52}Al_{0.48}As$ buffer layer was first grown at 460 °C to smoothen the surface. Then, the substrate temperature was lowered to 220-230°C. Subsequently, the 100-nm-thick $(In_{0.52}Al_{0.48})_{1-x}Mn_xAs$ ($0 < x \leq 0.11$) active epilayer was grown.

The as-grown samples were cleaved into a number of pieces for various characterizations. The cleaved samples were examined by double-crystalline x-ray diffraction (DXRD) and transmission electron microscopy (TEM). The cross-sectional samples parallel to (110) plane were prepared by mechanical thinning and followed by Ar-ion milling for TEM observation. Mn concentrations were determined by electron microprobe analysis (EMPA). Magnetic measurements were carried out in a superconducting quantum interference device (SQUID) magnetometer.

Table 3.3

Sample designations and their growing conditions of the $(In_{1-y}Al_y)_{1-x}Mn_xAs$ / $(In_{1-y}Al_y)As$ / InP epi-layers structures

Sample No.△	Buffer layer structure (Thickness, nm)	Epi-layer structure* (Thickness, nm)
E1	$In_{0.52}Al_{0.48}As$ (100)	$(In_{0.52}Al_{0.48})_{0.97}Mn_{0.03}As$ (100)
E2	$In_{0.52}Al_{0.48}As$ (100)	$(In_{0.52}Al_{0.48})_{0.95}Mn_{0.05}As$ (100)
E3	$In_{0.52}Al_{0.48}As$ (100)	$(In_{0.52}Al_{0.48})_{0.94}Mn_{0.06}As$ (100)
E4	$In_{0.52}Al_{0.48}As$ (100)	$(In_{0.52}Al_{0.48})_{0.92}Mn_{0.08}As$ (100)
E5	$In_{0.52}Al_{0.48}As$ (100)	$(In_{0.52}Al_{0.48})_{0.89}Mn_{0.11}As$ (100)
G1	$In_{0.52}Al_{0.48}As$ (100)	$(In_{0.52}Al_{0.48})_{0.95}Mn_{0.05}As$ (100)
G2	$In_{0.52}Al_{0.48}As$ (100)	$(In_{0.52}Al_{0.48})_{0.92}Mn_{0.08}As$ (100)
G3	$In_{0.52}Al_{0.48}As$ (100)	$(In_{0.52}Al_{0.48})_{0.89}Mn_{0.11}As$ (100)
G4	$In_{0.61}Al_{0.39}As$ (50) $In_{1-y}Al_yAs$; $0.39 < y < 0.45$ (75) $In_{0.55}Al_{0.45}As$ (75)	$(In_{0.61}Al_{0.39})_{0.85}Mn_{0.15}As$ (100)
G5	$In_{0.63}Al_{0.37}As$ (50) $In_{1-y}Al_yAs$; $0.37 < y < 0.45$ (75) $In_{0.55}Al_{0.45}As$ (75)	$(In_{0.63}Al_{0.37})_{0.82}Mn_{0.18}As$ (50)

* Growth rate = 0.3 μm/h

△For Samples E1~E5 and G1~G3: BEP of Al = 3.0×10^{-8} torr,

BEP of In = 1.2×10^{-7} torr BEP of As = 3.0×10^{-6} torr

For Samples G4: BEP of Al = $2.4 \sim 3.0 \times 10^{-8}$ torr, BEP of In = 1.2×10^{-7} torr

BEP of As = 3.0×10^{-6} torr

For Samples G5: BEP of Al = $2.1 \sim 3.0 \times 10^{-8}$ torr, BEP of In = 1.2×10^{-7} torr

BEP of As = 3.0×10^{-6} torr

Substrates: InP

The growth procedures for the 2nd part are as follows: The sample designations and their growing conditions for different structures are shown in Table 3.3. A series of $(In_{1-y}Al_y)_{1-x}Mn_xAs$ / $(In_{1-y}Al_y)As$ / InP layer structures were grown on (001) semi-insulating InP substrates. The Samples are denoted as G1, G2, G3, G4 and G5. The samples of a growth rate of 0.3 μm/hr and a V/III beam equivalent pressure ratio of 20. Following native oxide desorption, a 100-nm $In_{0.52}Al_{0.48}As$ or a graded 3-layer $In_{1-y}Al_yAs$ buffer structure of 200 nm thick was grown at 460 °C. Growth was then interrupted and the substrate temperature was lowered to 200-230 °C. Finally, a 50 or 100 nm $(In_{1-y}Al_y)_{1-x}Mn_xAs$ epilayer of interest was grown. Since the $(In_{1-y}Al_y)_{1-x}Mn_xAs$ epilayers have larger lattice constants than the InP substrate, here we have employed different (In, Al)As buffer layer structures, in order to avoid the misfit-induced dislocation and to obtain a smooth starting surface for the growth of $(In_{1-y}Al_y)_{1-x}Mn_xAs$ epilayers. The surface reconstruction of the samples during growth was monitored *in situ* with the reflection high-energy electron diffraction (RHEED). Basically, a (2x4) RHEED pattern was observed during the growth of high-temperature (In, Al)As buffer layers, while it changed to (1x1) or (1x2) during and after the growth of (In, Al, Mn)As layer, implying a two-dimensional growth mode. Had the Mn flux or the substrate temperature been too high, a complicated RHEED pattern would have appeared, implying the formation of a second phase on the sample surface [Park-05-396].

The as-grown samples were cleaved into pieces for various characterizations. The Mn concentrations were determined by a calibration curve based on the electron microprobe analysis (EMPA). The samples were examined by double-crystal x-ray diffraction (DXRD) and transmission electron microscopy JEOL JEM-2010 (TEM). Cross-sectional samples parallel to (110) plane were prepared conventionally by mechanical thinning and Ar-ion milling for TEM observation. Magnetic properties were measured by a Quantum Design MPMS2 superconducting quantum interference device (SQUID) magnetometer.

3.8 Structure analysis methods

(1) Reflection high-energy Electron Diffraction (RHEED)

The surface reconstruction of the samples during growth was monitored *in situ* with the reflection high-energy electron diffraction (RHEED) system. RHEED system employs an electron beam impinging on a sample at a grazing angle (typically about 1~2°) electron beam incidence is under Bragg diffraction condition of the surface. The diffracted beams can observe on a phosphorus screen. RHEED is a very powerful method for surface studies due to the fact that the electron beam penetrates only about 2 or 3 monolayers deep into the lattice, the reciprocal lattice will consists of lattice rods in the direction normal to the surface. When only elastic scattering events are considered, the diffraction condition can be cast into the geometrical construction of the Ewald sphere in reciprocal space. The Ewald sphere is much larger than the reciprocal rods of GaAs. This phenomenon produces an almost planar cut through the first few Brillouin zones of the reciprocal lattice. If a phosphorus screen is placed in a distance from the samples, diffraction spots on the screen to become streaks. Which is satisfied the Bragg condition of 2-D growth. An application of RHEED in MBE is to calibrate the growth rate. Figure 3.8 shows RHEED intensity oscillation of the reflected beam during MBE growth of GaAs; the period of oscillation corresponds precisely to a monolayer, $a_o/2$ for GaAs. The period of the RHEED intensity oscillations is explicitly related to the growth rate and as such is of practical value in determining the beam fluxes and in controlling the layer thickness accuracy to one monolayer.

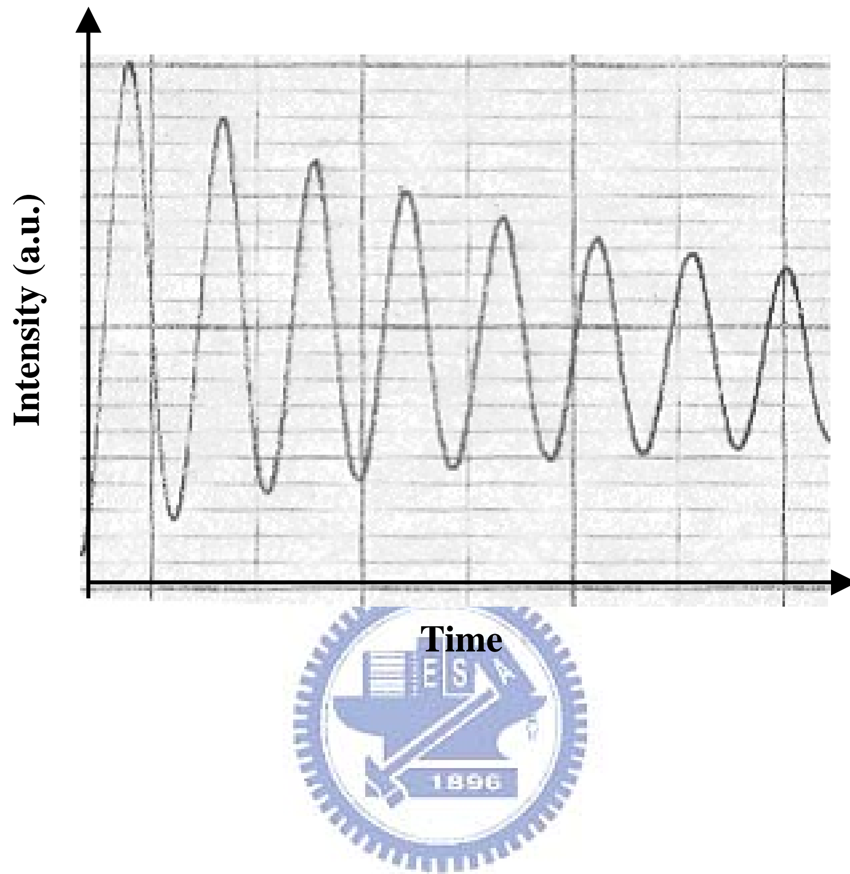

1896

Figure 3.8 RHEED intensity oscillation of the reflected beam during MBE growth of GaAs

(2) Transmission Electron Microscopy (TEM)

The morphology and crystallographic information of samples were characterized by transmission electron microscope (TEM). Transmission electron microscope uses a beam of high-energy electrons to project a magnified image of a sample onto a fluorescent screen. The size, number density and arrangement of the arsenic precipitation in the annealed LT-GaAs samples were examined using a JEOL JEM-2010 electron microscope. Cross-sectional samples for transmission electron microscopy observations were prepared with mechanical thinning and Ar-ion milling. Schematic illustration cross-sectional samples preparation procedures are shown in Figure 3.9(a)-(d). Figure 3.10 shows the number density of arsenic clusters for each sample is determined by assuming that the penetration thickness of electron beam of TEM is 100 nm.

$$Density = \frac{average\ \ number\ \ of\ \ clusters}{volume}$$

The crystalline structures of (Ga, Mn)As and (In, Al, Mn)As epilayers were examined by transmission electron microscopy (TEM). Cross-sectional samples parallel to the (110) plane were prepared for TEM observation.

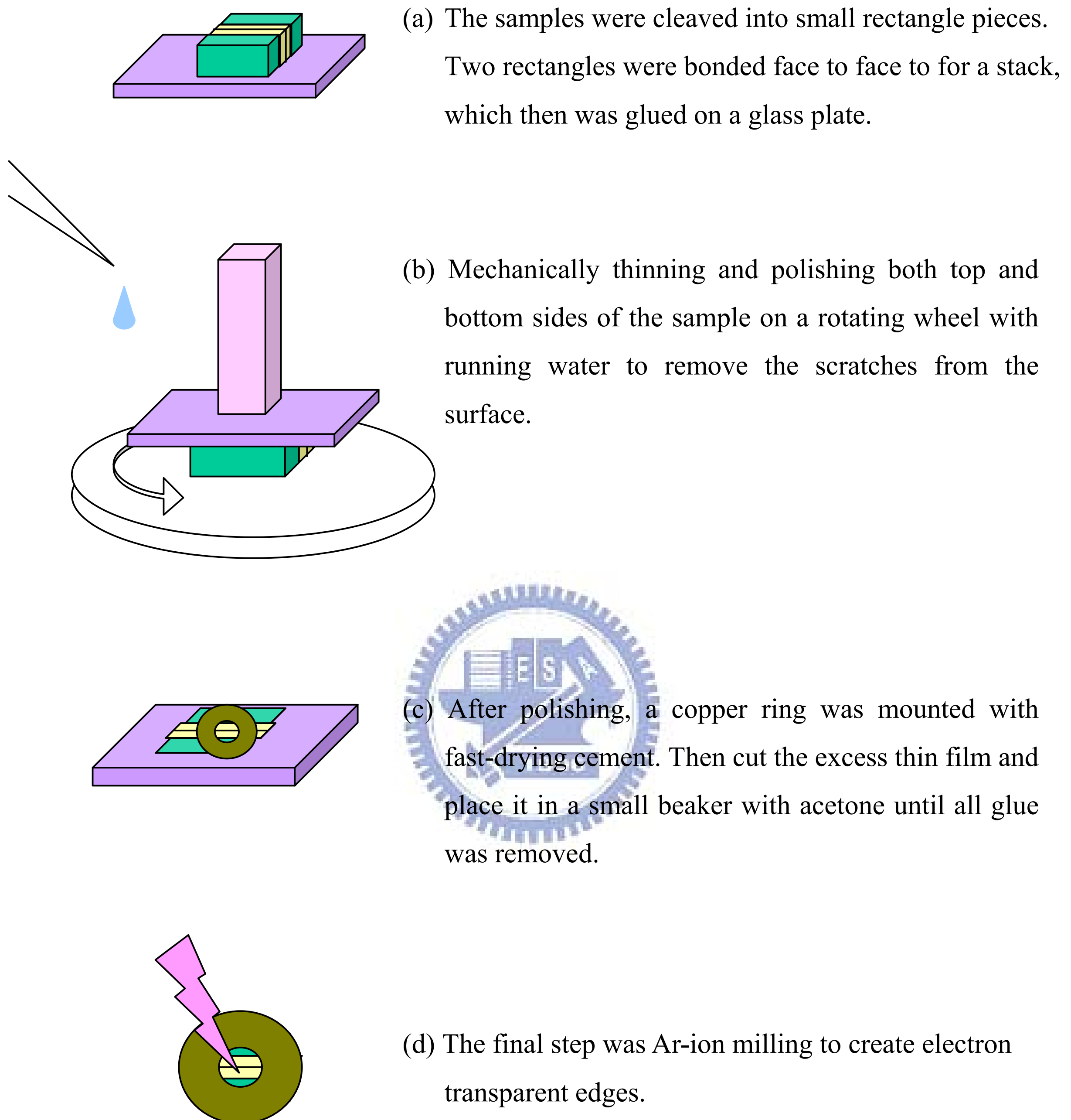

Figure 3.9 Cross-sectional samples preparation for transmission electron microscopy

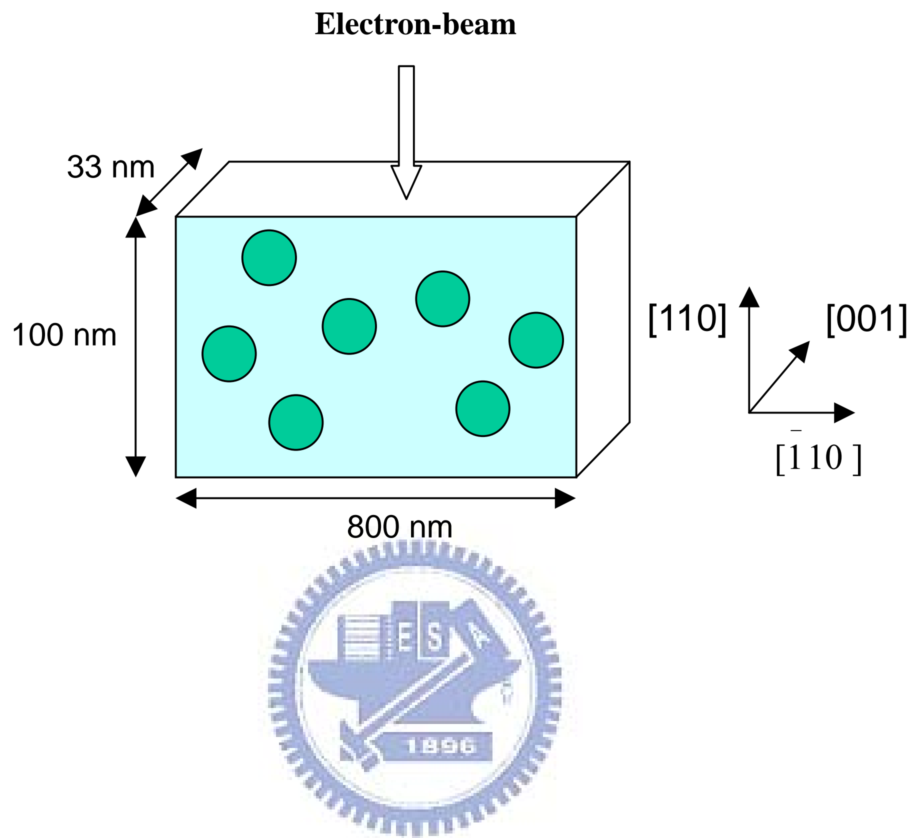

Figure 3.10 Schematic diagram to show TEM method to determine the number density of arsenic clusters

(3) Double-crystal X-ray Diffraction (DXRD)

Information from substrate and epi-layer peaks includes lattice mismatch, composition, thickness and strain. The double-crystal diffractometer (DXRD) is a powerful characterization tool for epitaxial crystal growth. Samples can be easily mounted quickly and non-destructive evaluation of their materials parameters. Figure 3.11 schematically illustrates the top view of DXRD instrument, where the reference crystal is aligned to sit on the Cu $K_{\alpha 1}$ line and the wavelength dispersion is eliminated by the reference crystal. And specimen crystals are provided with two rotation axes driven by stepper motors. The signals of rocking curves of samples are collected by the detector.

The $Ga_{1-x}Mn_xAs$ lattice constant is larger than that of GaAs, the corresponding perpendicular lattice mismatches, $(\Delta a / a)_\perp$ can be measured by DXRD. The (004) reflection of $Ga_{1-x}Mn_xAs$ epitaxial layers grown on (001) oriented GaAs substrates, the Bragg spacing is given by $a_\perp/4$ where $a_\perp$ is the lattice parameter in the [001] direction. The mismatch of the epitaxial layer is given by

$$(\frac{\Delta a}{a})_\perp = \frac{a_\perp - a_s}{a_s} = -\frac{\Delta\theta}{\tan\theta_B} \tag{3-2}$$

Here a_s is the lattice parameter of the substrate, θ_B is the Bragg angle corresponding to a_s and $\Delta\theta$ is the measured angular separation between the Bragg peaks. The presence of two well-defined peaks indicates the existence of a single-crystal layer containing excess arsenic other than bulk GaAs in antisite and interstitial positions. The lattice expansion of the LT GaAs epilayer is directly proportional to excess arsenic content in the layer by double-crystal X-ray diffraction [Lavrent'eva-02-118]. Double-crystal X-ray diffraction (DXRD) rocking curves were examined using a Philip DCD-3 double-crystal diffractometer.

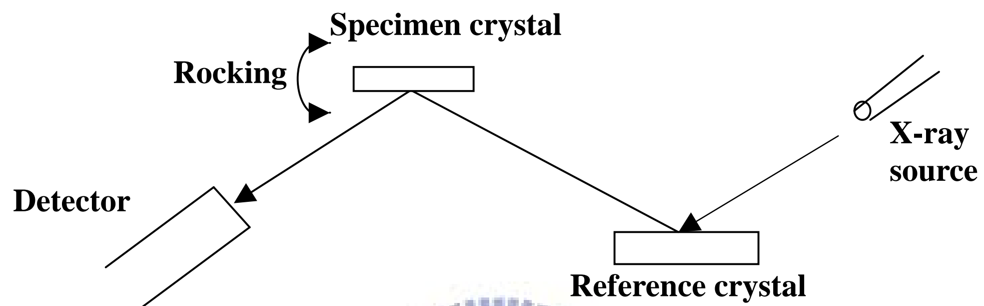

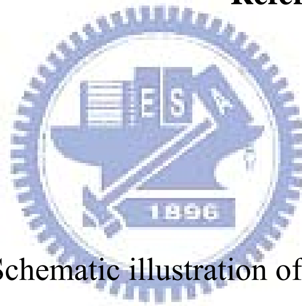

Figure 3.11 Schematic illustration of DXRD technique

3.9 Properties measurements

Superconducting Quantum Interference Device magnetometry (SQUID)

A Superconducting Quantum Interference Device (SQUID) uses the properties of electron-pair wave coherence and Josephson Junctions to detect very small magnetic fields. The MPMS5 system comprises of two main sections: the dewar, probe and SQUID assembly, and the electronic control system. The probe contains a high precision temperature control system, allowing measurements between 2 - 400K and superconducting electromagnet, giving a field of up to 5.5 Tesla.

The dewar consists of an inner liquid helium reservoir and outer liquid nitrogen jacket, to reduce excessive liquid helium boil off. The liquid helium is used for both maintaining the electromagnet in a superconducting state and for cooling the sample space. Samples are mounted within a plastic straw and connected to one end of a sample rod, which is inserted into the dewar/probe. The other end is attached to a stepper motor, which is used to position the sample within the center of the SQUID pickup coils. These measurements have a sensitivity of 5×10^{-8} E.M.U. To measure the magnetic properties of (Ga, Mn)As epi-layers, the sample is cooled down to 10K under an external field of 1000 Oe applied along the measurement axis. Then field is removed, and projection of the remnant magnetization along the measurement axis is recorded as a function of temperature.

CHAPTER 4

RESULTS AND DISCUSSION

4.1 Effect of substrate orientation on arsenic precipitation in low-temperature-grown GaAs

Arsenic precipitation in "superlattice" structures of alternately undoped and [Si] = 3 × 10^{18} cm^{-3} doped GaAs grown at 250 °C on (100), (311)A, and (311)B GaA substrates has been studied. The cross-sectional bright-field TEM images of Samples H1, H2 and H3 are shown in Figs. 4.1(a), (b), and (c). For reference, plan-view TEM images of arsenic precipitations are shown in Figs. 4.2(a), (b), and (c). It is found that upon annealing at 800℃, the precipitates are totally confined in Si-doped regions, forming into two-dimensional arrays located approximately at the center of each Si-doped layer. The precipitates in each LT "superlattice" structure also differ in density and size. Arsenic precipitates in Sample H3 (on GaAs(311)B substrate) are slightly denser and larger than those in Sample H2 (on GaAs(311)A substrate, and both are remarkably denser and larger than those in Sample H1(on GaAs(001) substrate. This can be explained by the varying excess arsenic incorporations in LT-GaAs grown on differently oriented substrates. The brighter zones observed near the top and bottom of each image are the AlAs layers, which thus provide good markers for the periodic structure. It can be seen that most of the spherical-like arsenic clusters are confined in Si-doped regions. The preferential precipitation can be explained by the so-called strain-driven vacancy-assisted diffusion mechanism [Chang-98-587, Hsieh-96-1790]. This is because Si-doped GaAs contains more Ga vacancies than intrinsic GaAs; moreover, in the former, arsenic antisites will diffuse to vacancy-rich regions to form arsenic precipitates. Owing to the high-temperature annealing, the arsenic clusters further form into two-dimensional arrays located approximately at the center of each Si-doped region. Furthermore, The average diameter and density of arsenic clusters are approximately 13.9, 16.0, and 17.5 nm, and 6.44,

7.20, and 7.58 $\times10^{15}$ cm^{-3} for Samples H1, H2, and H3, respectively. The number density of arsenic clusters in each sample is determined by assuming that the penetration thickness of electron beam of TEM is 100 nm.

The DXRD patterns of as-grown control Samples H4, H5 and H6 were recorded in the vicinity of the GaAs (004) reflection for the (001) substrate and (311) reflections for (311)A and (311)B substrates, and the resulting rocking curves are shown in Fig. 4.3 Clearly, two peaks due to the Bragg reflections from the LT-GaAs epilayer and the GaAs substrate are present in all control samples. The peak separations of 72, 144, and 162 arcsec, and the corresponding perpendicular lattice mismatches $(\Delta a/a)_\perp$ of 0.05, 0.138, and 0.155% were observed for control LT-GaAs Samples H4, H5, and H6, respectively. This DXRD result agrees generally with what O'Hagan and Missous have observed. [O'Hagan-97-2400, Missous-97-197] The lattice expansion should be attributed mainly +to growth conditions such as the growth temperature T_g and the ratio of As to Ga fluxes, J_{As}/J_{Ga}.

The presence of two well-defined peaks indicates the existence of a single-crystal layer containing excess arsenic other than bulk GaAs in antisite and interstitial positions. The lattice expansion of the LT GaAs epilayer is directly proportional to excess arsenic content in the layer by double-crystal X-ray diffraction [Lavrent'eva-02-118]. A linear correlation exists between the lattice mismatch $(\Delta a/a)_\perp$ and the concentration of excess arsenic $[As_{ex}]$. This correlation dependence can be used to estimate the total concentration of excess arsenic from the DXRD data. Therefore, the $[As_{ex}]$ values of the LT-GaAs layers grown on (100), (311)A, and (311)B substrates were estimated approximately to be 1.0, 2.7, and 3.1 $\times10^{20}$ cm^{-3}, respectively.

As summarized $[As_{ex}]$ and $(\Delta a/a)_\perp$ values are dependent on J_{As}/J_{Ga} and growth temperature. In this study, the (001) and (311) substrates were mounted side by side on the same Mo block and thereby subjected to identical J_{As}/J_{Ga} ratios and growth temperatures. Therefore, the difference in $(\Delta a/a)_\perp$ values in the present (311) control samples should be not

related to the J_{As}/J_{Ga} ratio and growth temperature but to the surface bonding configuration. [Wang-02-2965; Wang-85-826]. On a (311)A surface, the single-dangling-bond sites are arsenic sites and the double-dangling-bond sites are Ga sites. The (311)B surface, on the contrary, has an opposite bonding arrangement, as shown in Fig. 4.4 Such bond configurations would cause the incorporation of excess arsenic in Ga sites to form As_{Ga} defects more easily on the (311)B than on the (311)A surfaces. Our DXRD result is consistent with this analysis that the LT-GaAs grown on the (311)B surface has a larger lattice expansion than that grown on the (311)A surface.

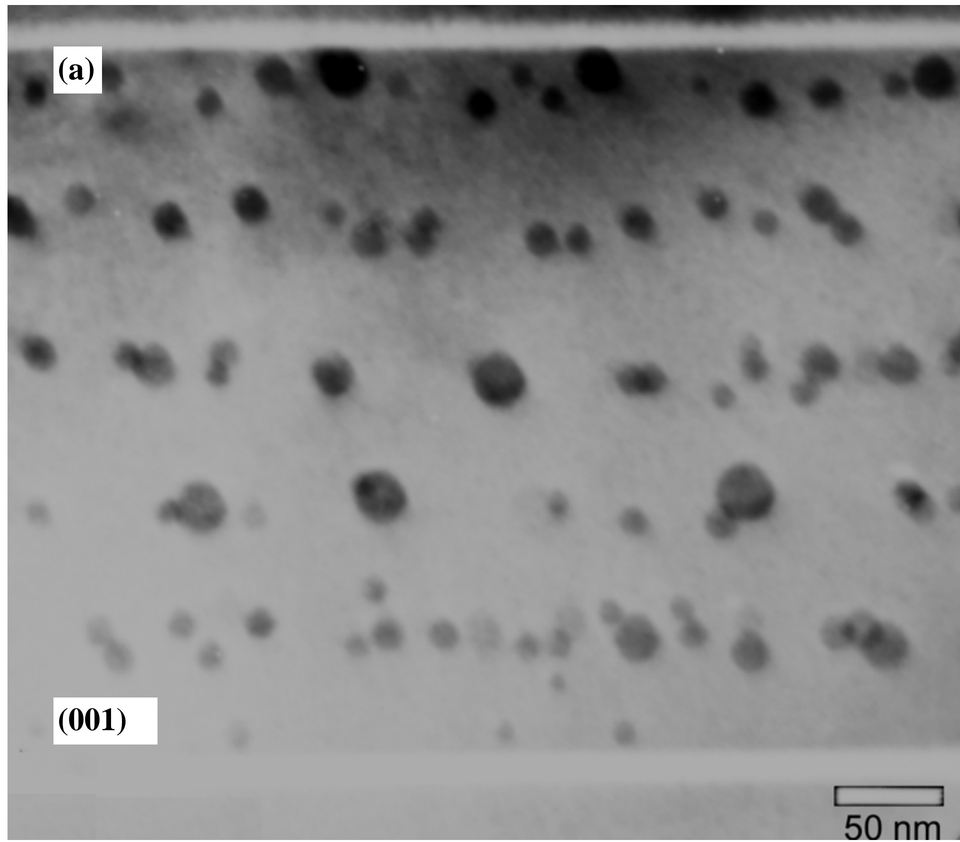

Figure 4.1(a) Cross-sectional TEM bright-field images of Sample H1 (The annealed LT-GaAs on GaAs(001) substrate)

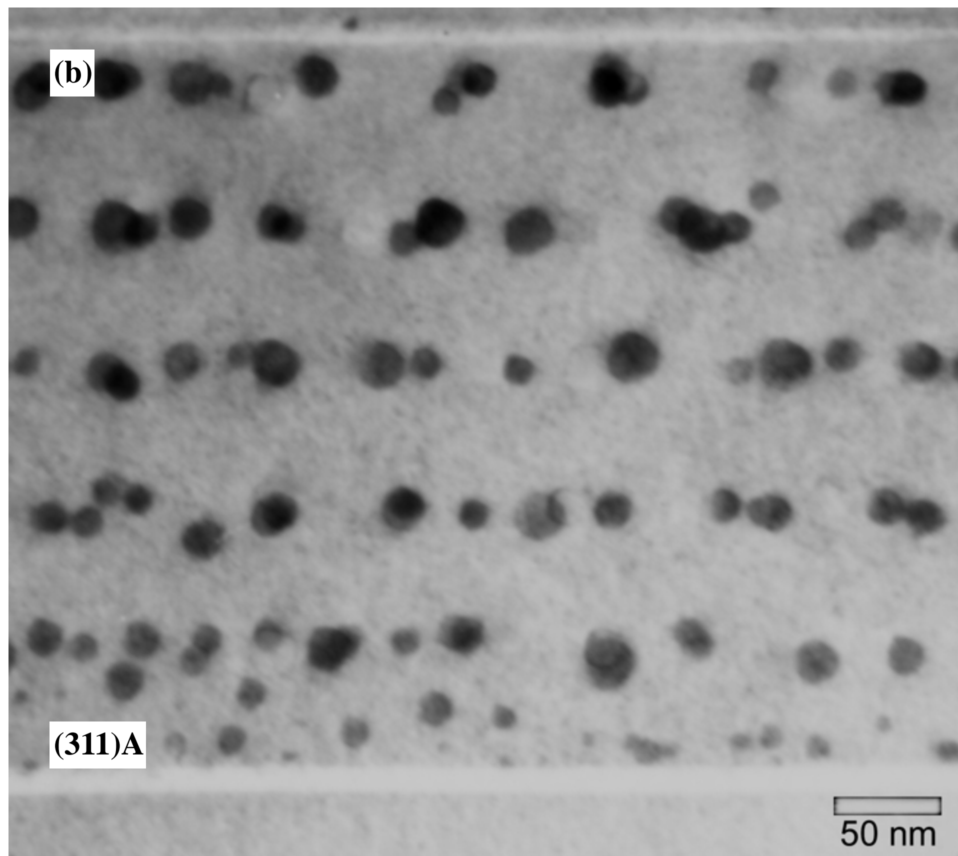

Figure 4.1(b) Cross-sectional TEM bright-field images of Sample H2 (The annealed LT-GaAs on GaAs(311)A substrate)

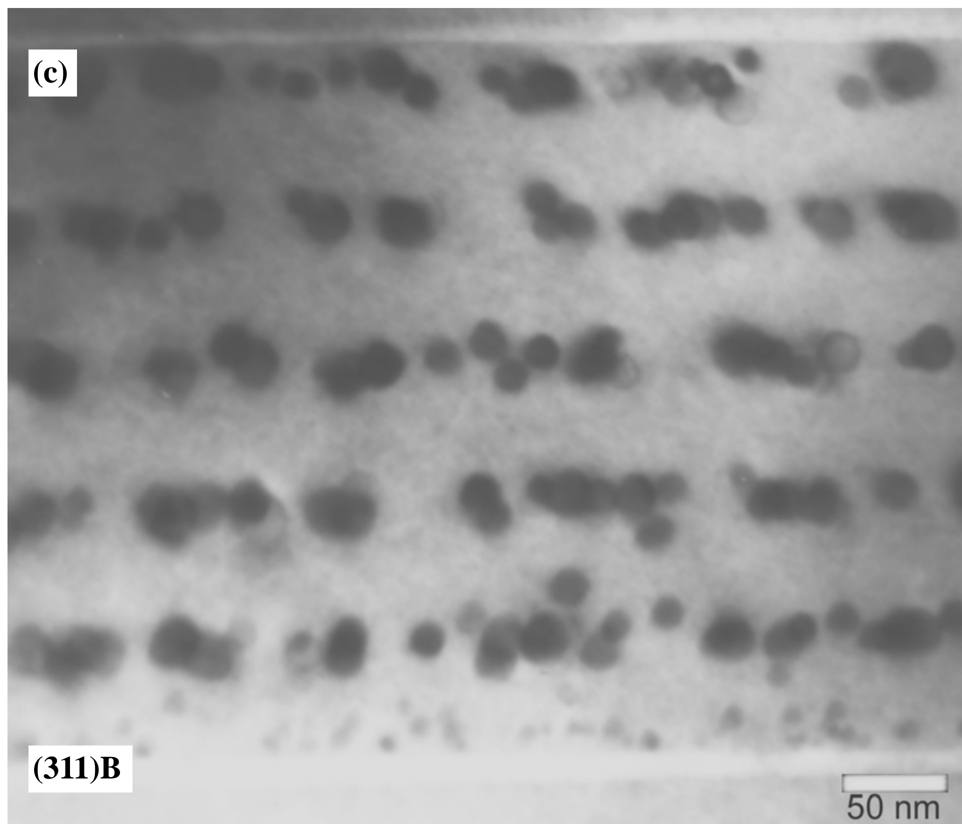

Figure 4.1(c) Cross-sectional TEM bright-field images of Sample H3 (The annealed LT-GaAs on GaAs(311)B substrate)

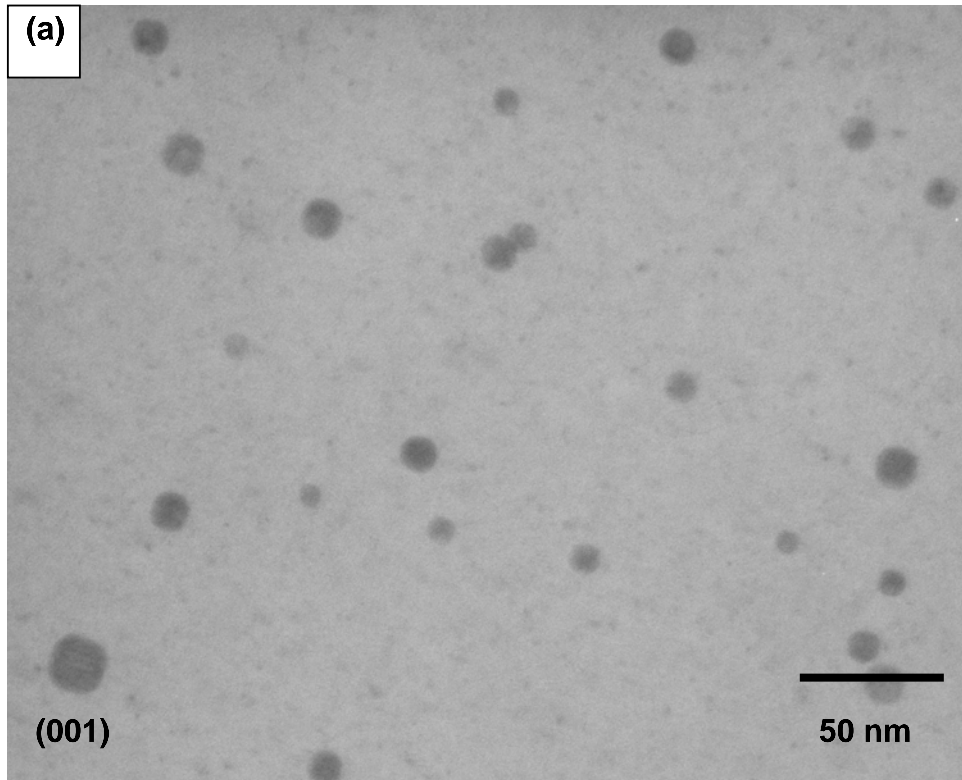

Figure 4.2(a) Plan-view TEM images of Sample H1 (The annealed LT-GaAs on GaAs(001) substrate)

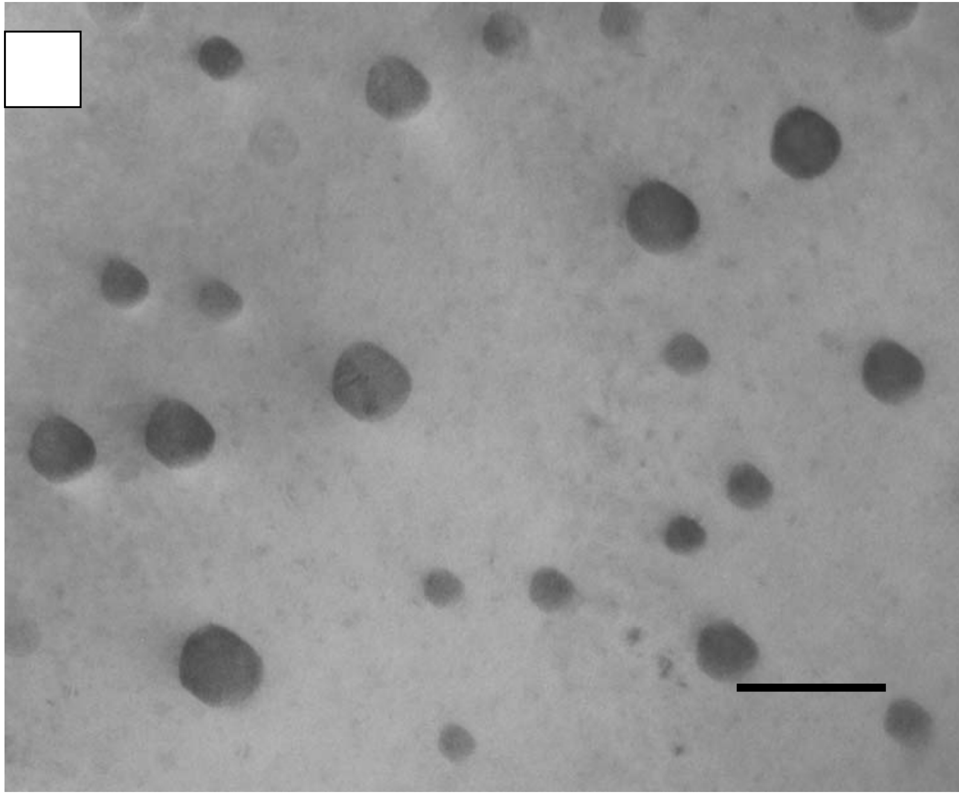

Figure 4.2(b) Plan-view TEM images of Sample H2 (The annealed LT-GaAs on GaAs(311)A substrate)

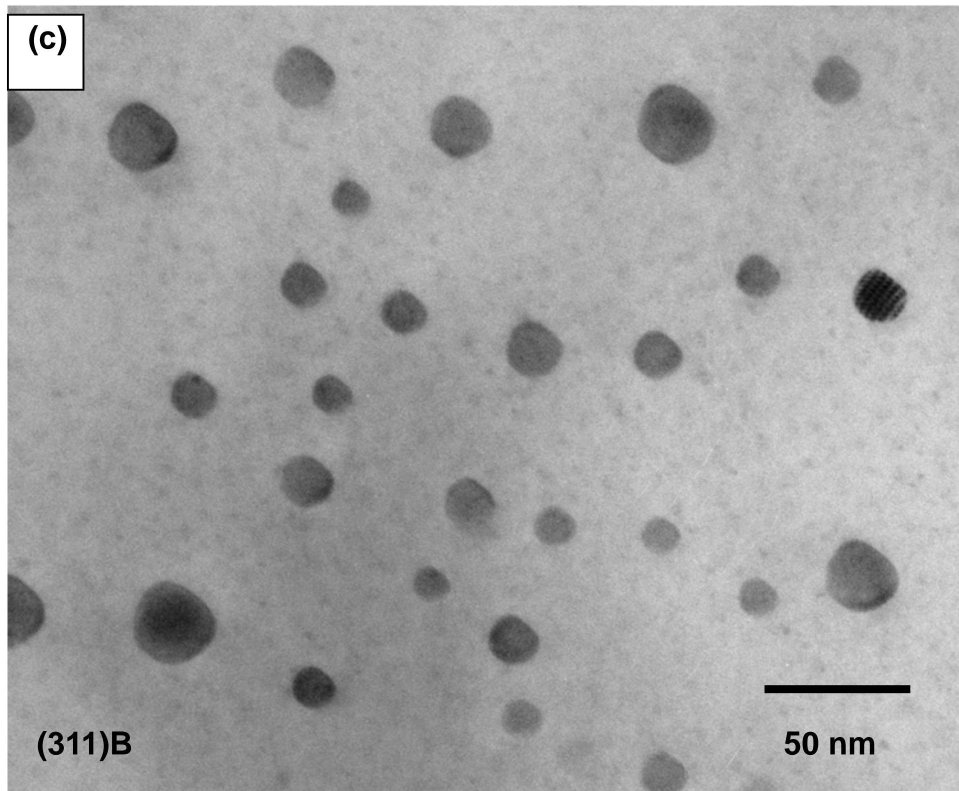

Figure 4.2(c) Plan-view TEM images of Sample H3 (The annealed LT-GaAs on GaAs(311)B substrate)

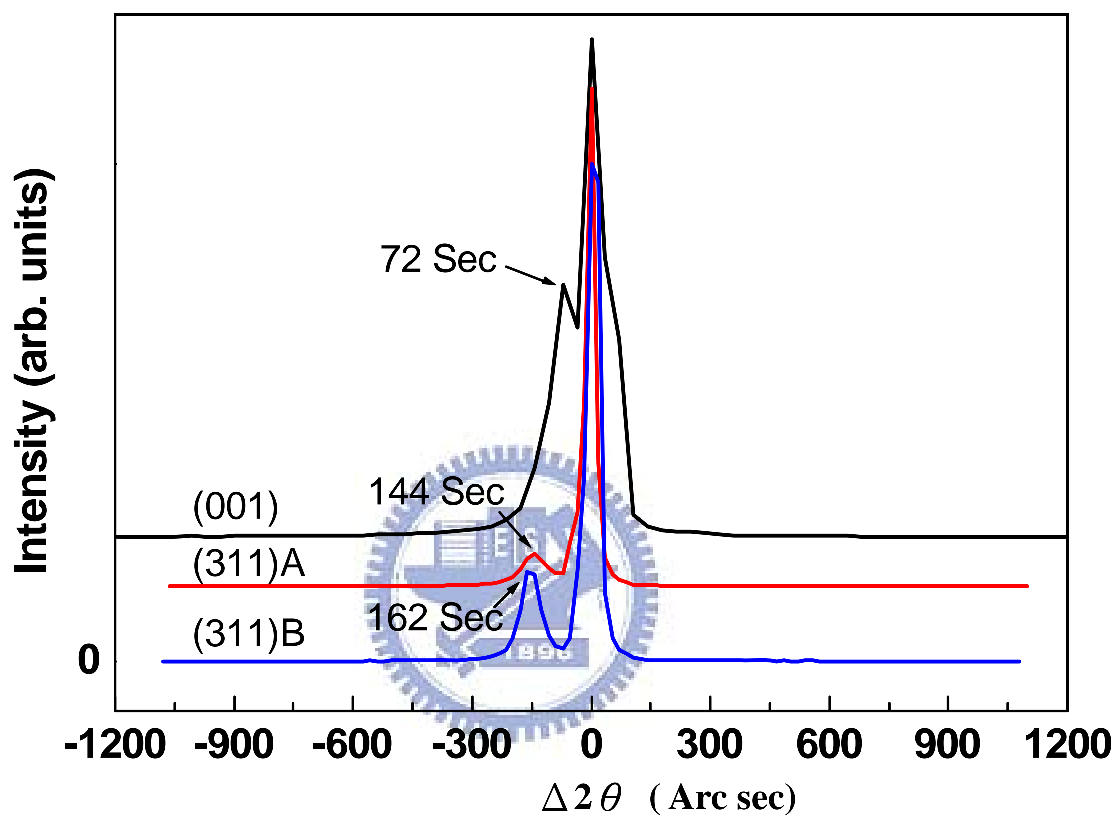

Figure 4.3 DXRD rocking curves of as-grown LT-GaAs of Samples H4, H5, and H6: (004) reflection for sample grown on (001), (311) reflections for samples grown on (311)B and (311)A substrates

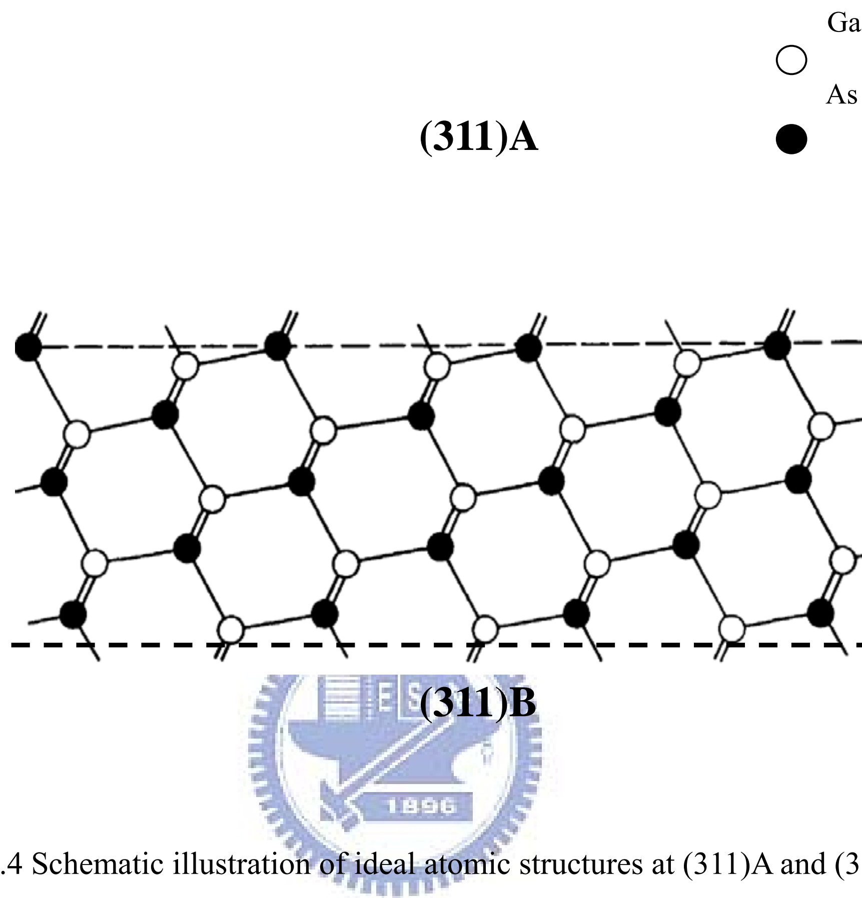

Figure 4.4 Schematic illustration of ideal atomic structures at (311)A and (311)B surfaces

4.2 Effects of doping type and concentration on precipitation of arsenic clusters in low-temperature-grown GaAs

In this study, the effects of doping type and concentration on arsenic precipitation in low-temperature-grown GaAs upon postgrowth annealing at 600, 700 and 800°C were investigated. Figures 4.5(a), (b), and (c) show the bright-field TEM images of Samples B1, B2 and B3 after 30 s anneals at 600, 700, and 800°C, respectively. The bright stripes seen in each picture are the AlAs layers. It is noted that AlAs layers provide good markers among the (*i*-*n*-*i*) or (*i*-*p*-*i*) regions. Arsenic precipitation depletion was observed in all Be-doped layers for all annealing temperatures; moreover, the arsenic clusters accumulate toward the undoped layers. The DXRD rocking curves of GaAs (004) reflection for the three control Samples B4, B5 and B6 are shown in Fig. 4.6 Clearly, peak separations of 108 and 72 arc sec, caused by excess arsenic incorporated in LT GaAs, were observed in Be-doped and undoped LT-GaAs epilayers, respectively; however, no obvious peak separation was observed in the Si-doped LT GaAs. This suggests that the Be doping enhanced the incorporation of excess arsenic into the lattice of LT GaAs while the Si doping suppressed this effect. According to a previous report [Liu. 95-279], the concentration of arsenic antisites, [As_{Ga}], is directly proportional to the lattice expansion of the LT-GaAs epilayer. Therefore, we can conclude that $[As_{Ga}]_{p3} > [As_{Ga}]_{i} > [As_{Ga}]_{n3}$, where $[As_{Ga}]_{x}$ denotes the arsenic antisite concentration in the *x*-doped control sample. Moreover, during postgrowth annealing, the reduction of strain caused by the As_{Ga} defects is also a driving force for precipitation. For the i-p_3-i region, the As_{Ga} defects diffused from the p_3 to *i* layers, and for the i-n_3-i region from *i* to n_3 layer, which is opposite to the V_{Ga} defects. Our experimental result about i-n_3-i region and all *i*-*p*-*i* regions is therefore consistent with the vacancy-assisted arsenic antisite diffusion mechanism [Melloch-92-3509; Chang-992442; Chang-98-587]. Interestingly, a "dual" arsenic precipitation phenomenon were observed in Si-doped regions: arsenic precipitates accumulate toward the center of the [Si] = 2 x

10^{18}cm^{-3} doped layer for all annealed temperatures; however, arsenic precipitates are depleted away the other two lightly Si-doped regions (n = 2 x 10^{16} and 2 x 10^{17} cm^{-3}) toward the undoped regions. The latter depletion behavior contrasts with the earlier observation. [Chang-99-2442]. In their work, the i-n_1-i-n_2-i-n_3-i multiplayer structure did not consist of any isolation layer to prevent the inter-diffusion of defects and doping effect from n_1 to n_2 or n_3. As a result, arsenic precipitation behaviors were disturbed and the correlation of doping concentration to arsenic precipitation could not be clearly identified.

In order to understand the "dual" arsenic precipitation phenomenon in Si-doped GaAs layers indicates that other effects must be considered in addition to the vacancy-assisted arsenic antisite diffusion mechanism. The Debye length can influence the arsenic precipitation at the i/n interface, and the depletion of the "*n*" regions to a depth of up to a few Debye lengths would occur at each *i*/*n* interface [O'Hagan-96-8384]. Moreover, the Debye lengths at the current annealing temperatures in our structure are estimated to be around 560, 180, and 50 Å for n_1, n_2 and n_3 layers, respectively. Therefore, the total depletion depth should be ~1120, ~360 and ~100 Å for n_1, n_2 and n_3 layers, respectively, due to the double *n*/*i* interfaces in each active region. Therefore, since each Si-doped layer is 350 Å thick, it is likely that complete depletion occurred in the n_1 and n_2 layers but an incomplete depletion in the n_3 layer, the latter was also noted as an "arsenic accumulation" layer.

Figure 4.7 shows the average number density of arsenic clusters in each *i*-*x*-*i* region after annealing at 700 and 800 °C, respectively. The volume is determined by assuming that the penetration thickness of electron beam of TEM is 100 nm. The analysis reveals that the cluster densities of the *i*-*p*-*i* regions are higher than those of the *i*-*n*-*i* regions under the same doping concentration and annealing condition, which is consistent with the DXRD results. The analysis reveals that the cluster densities of the *i*-*p*-*i* regions are higher than those of the *i*-*n*-*i* regions under the same doping concentration and annealing condition, which is consistent with the DXRD results.

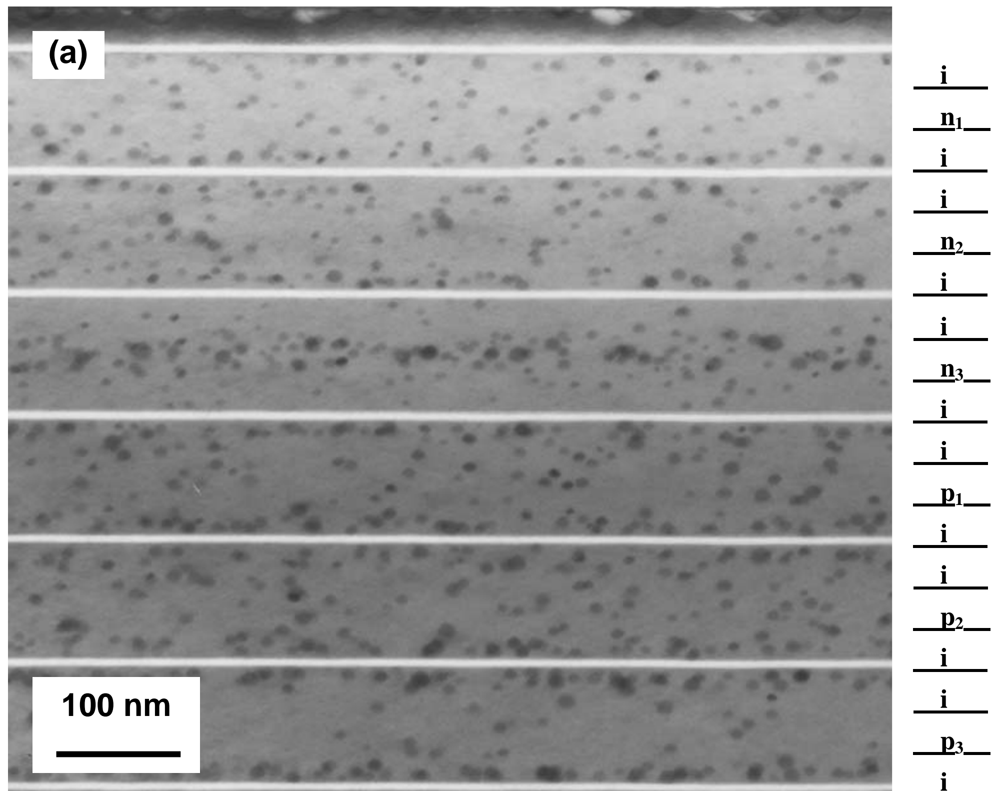

Figure 4.5(a) TEM bright field images of Sample B1 showing arsenic precipitates in different active regions after annealing at 600°C

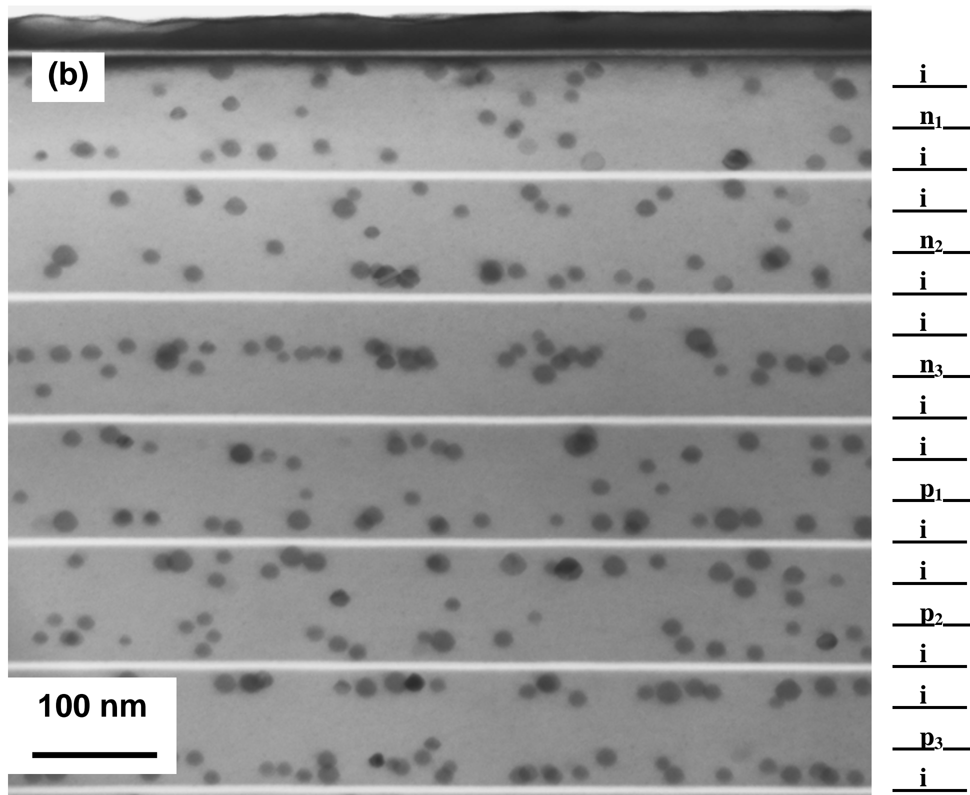

Figure 4.5(b) TEM bright field images of Sample B2 showing arsenic precipitates in different active regions after annealing at 700°C

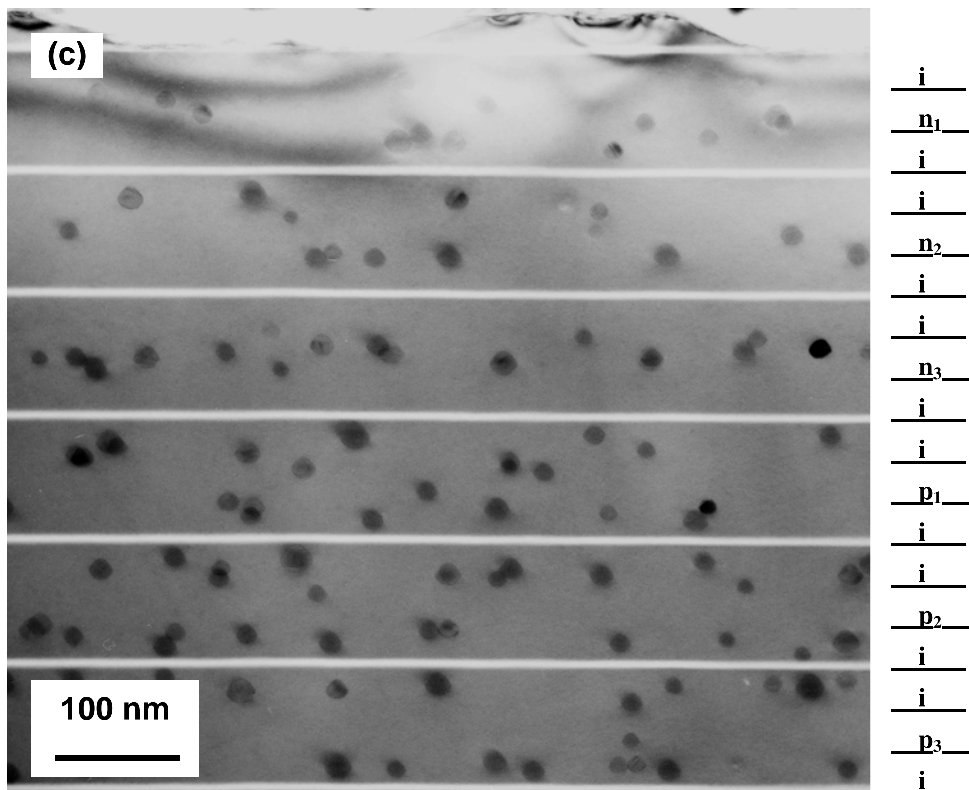

Figure 4.5(c) TEM bright field images of Sample B3 showing arsenic precipitates in different active regions after annealing at 800°C

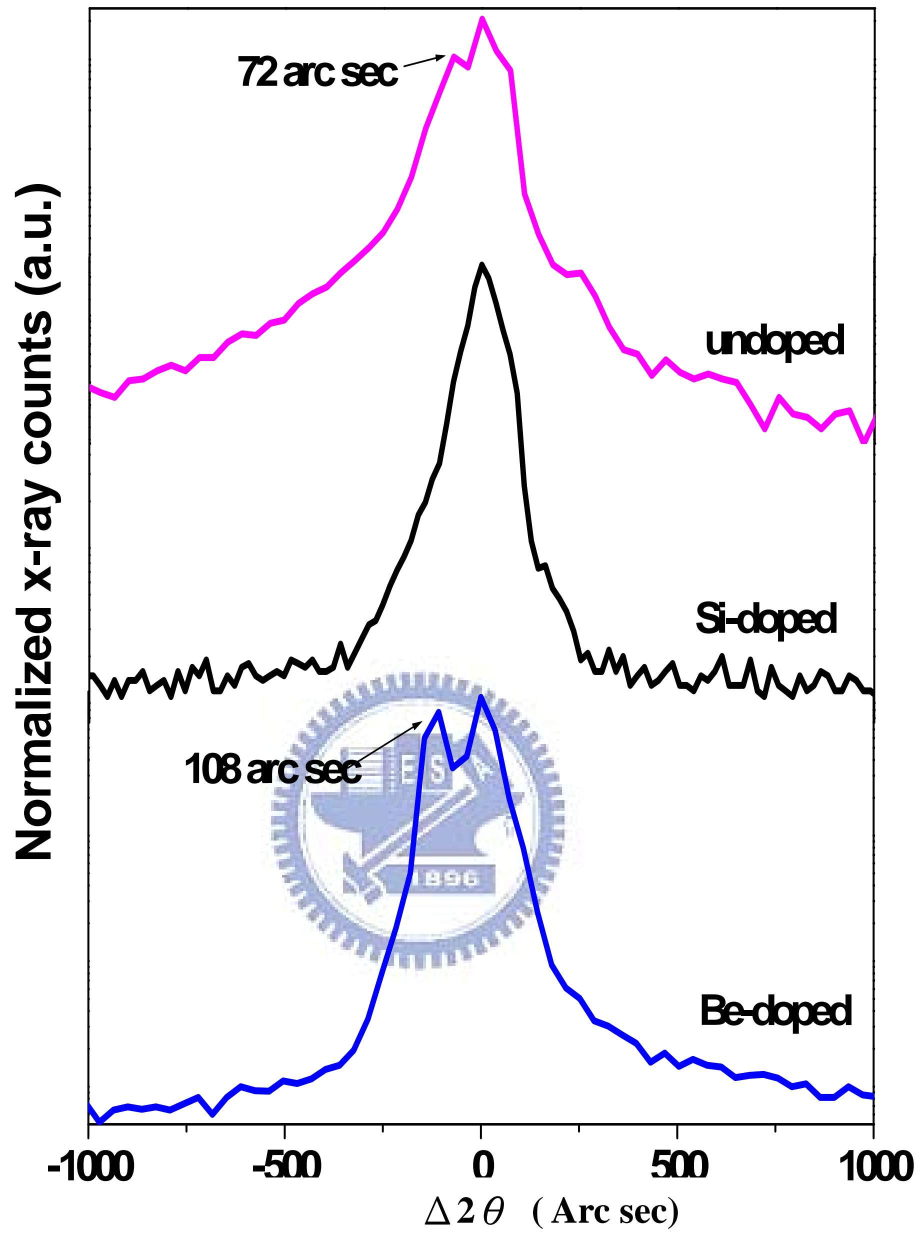

Figure 4.6 DXRD rocking curves of GaAs (004) for 1-μm-thick undoped (Sample B6), [Si] = 10^{18} cm^{-3} doped (Sample B4), and [Be] = 10^{18} cm^{-3} doped (Sample B5) LT-GaAs samples

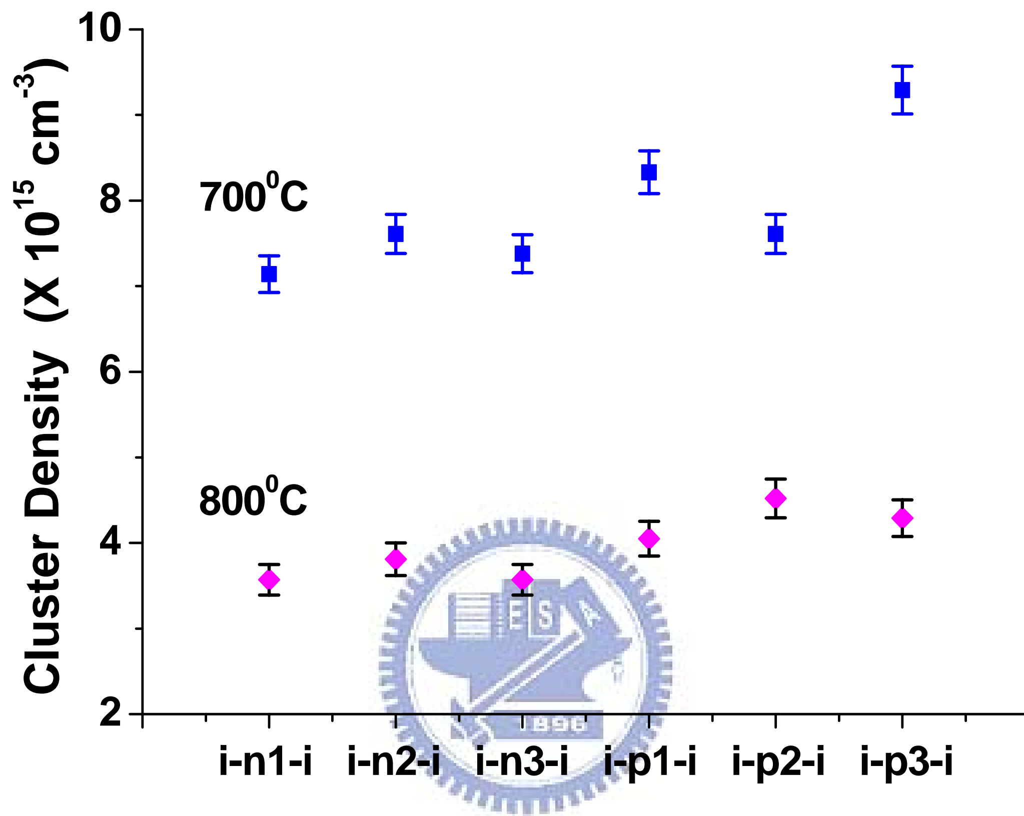

Figure 4.7 Arsenic cluster number density in each *i*-*x*-*i* region after annealing at 700°C (Sample B2) and 800°C (Sample B3), where $x = n_i$ or p_i

4.3 Effects of thickness and post-annealing on the magnetic properties of $Ga_{0.93}Mn_{0.07}As$

In the study focusing on the effects of thickness and post-annealing on the magnetic properties of $Ga_{0.93}Mn_{0.07}As$, where high concentration Mn content exists. The M-H curve of post-annealed Sample C1 is shown in Fig. 4.8, which indicates a typical ferromagnetic hysteresis behavior and easy axis near [110] direction. All samples show a ferromagnetic state at 10 K as confirmed by the M-H curves. Figure 4.9 shows the M-T curves of as grown and post-annealed Samples C1, C2 and C3, which were measured in a small magnetic field (H = 1 Oe) applied in-plane direction. The Curie temperature (T_c) of post-annealed Samples C1, C2 and C3 are 160, 135 and 70 K, respectively, which are 80, 40 and 10 K higher than that of the as-grown samples. It is noted that the T_c of the annealed Sample C1 is considerably higher (160 K) than that of the Sample C3 (70 K). It is apparent that the T_c, depends on the thickness of $Ga_{0.93}Mn_{0.07}As$ epi-layers, and the T_c value increases as the thickness decreases. Figure 4.10 shows the T_c values of the as-grown and post-annealed Samples C1, C2 and C3.

The low-temperature growth of (Ga,Mn)As inevitably leads to numerous point defects in (Ga,Mn)As, presumably As_{Ga}, and Mn_I both resulting in heavy compensation in (Ga,Mn)As due to the donor nature of those defects. This compensation prevents Mn atoms from acting as acceptors. Therefore, the Mn_I defects and their diffusion during growth and annealing play a key role in determining the magnetic properties of (Ga, Mn)As epilayers. During growth, the Mn_I atoms tend to diffuse to the surface of the (Ga, Mn)As epilayer, resulting in an increase in the effective hole concentration in the bulk and thus enhancing the exchange interaction and T_c. This diffusion process would be continued and accelerated during post-growth annealing at a temperature near or slightly higher than the growth temperature.

Figure 4.11 shows the DXRD rocking curves of (004) as-grown and post-annealed Sample C3, where three distinct peaks are for GaAs substrate, LT-GaAs buffer layer and

$Ga_{0.93}Mn_{0.07}As$ epi-layer, respectively. The rocking curves of Sample C3 layers clearly reveal an expansion of the lattice constant along the growth direction, indicating that samples are tetragonal and coherently strained to the GaAs substrate. When growing at a temperature of about 230℃, LT-GaAs buffer layer and LT-(Ga, Mn)As epi-layers are non-stoichiometric containing As_{Ga}, Mn_{Ga} and Mn_I defects, resulting in an expansion of the lattice. The $Ga_{0.93}Mn_{0.07}As$ epi-layers peaks are 696 and 636 arcsec for post-annealed and as-grown Sample C3. Annealing decreases the lattice expansion of $Ga_{0.93}Mn_{0.07}As$ epi-layers by about 60 arcsec. But the peak separation of LT-GaAs buffer layers for post-annealed and as-grown Sample C3 shows no obvious difference. It reveals that annealing effect removes not the As_{Ga} defects, but the Mn_I defects. A large proportion of donor-like Mn_I defects of $Ga_{0.93}Mn_{0.07}As$ epi-layers are removed by annealing. This results in the strengthening of the hole-mediated interaction between substitutions Mn of Sample C1. Sample C3 of $Ga_{0.93}Mn_{0.07}As$ epi-layer was 1000 nm thick and its corresponding out-diffusion is insufficient in comparison with those of thin Samples C1 and C2.

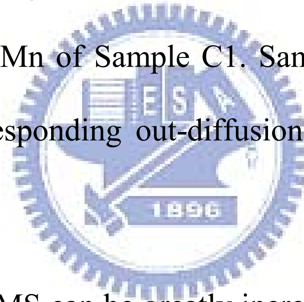

The Curie temperature of DMS can be greatly increased by a decrease in thickness, and via annealing treatment Annealing treatment is essentially to remove excess Mn_I from the interstitial sites in the lattice to decrease the donor-like defects, which may cause an increase in hole concentration and T_c. In other words, the diffusion path of Mn atoms for the thinner DMS thickness is much shorter, which may result in a more effective removal of excess Mn_I from the lattice and a greater increase in T_c.

The magnetic field dependence of magnetization (M-H) curves was measured along [110], [$\bar{1}$10], [100] and [010] axis, respectively. M-H curves of as-grown and annealed Sample C1 are shown in Fig. 4.12 (a) and (b). The easy axis of as-grown and annealed Sample C1 can be rotated from [100] direction to [010] direction by low-temperature annealing and the coercivity is from 50 G decrease to 18 G.

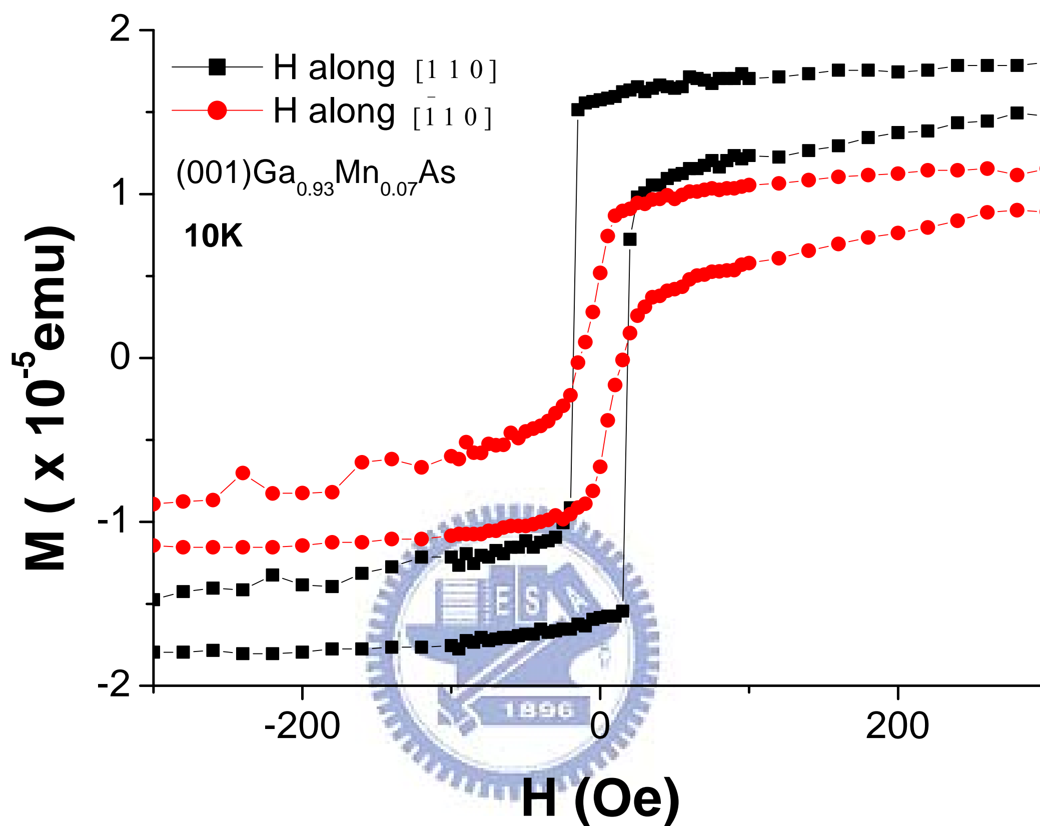

Figure 4.8 M-H curves of (Ga, Mn)As DMS (Sample C1) measured with in-plane magnetic field applied along [110] or [$\bar{1}$10] directions at 10K

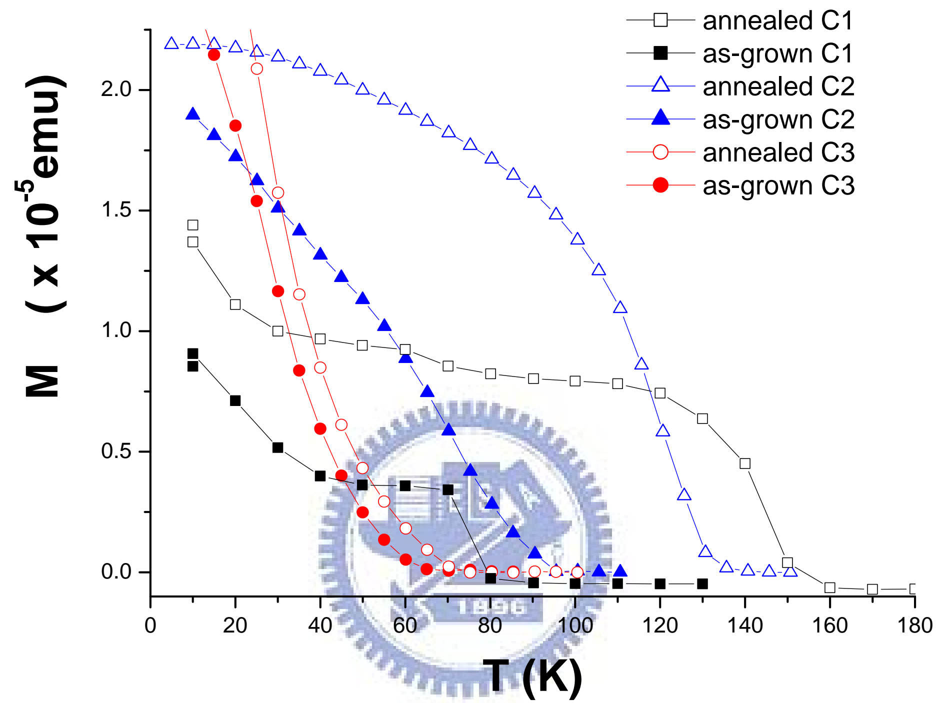

Figure 4.9 M-T curves of as-grown and post-annealed (Ga, Mn)As DMS (Samples C1, C2 and C3) measured under 1 Oe in-plane magnetic field

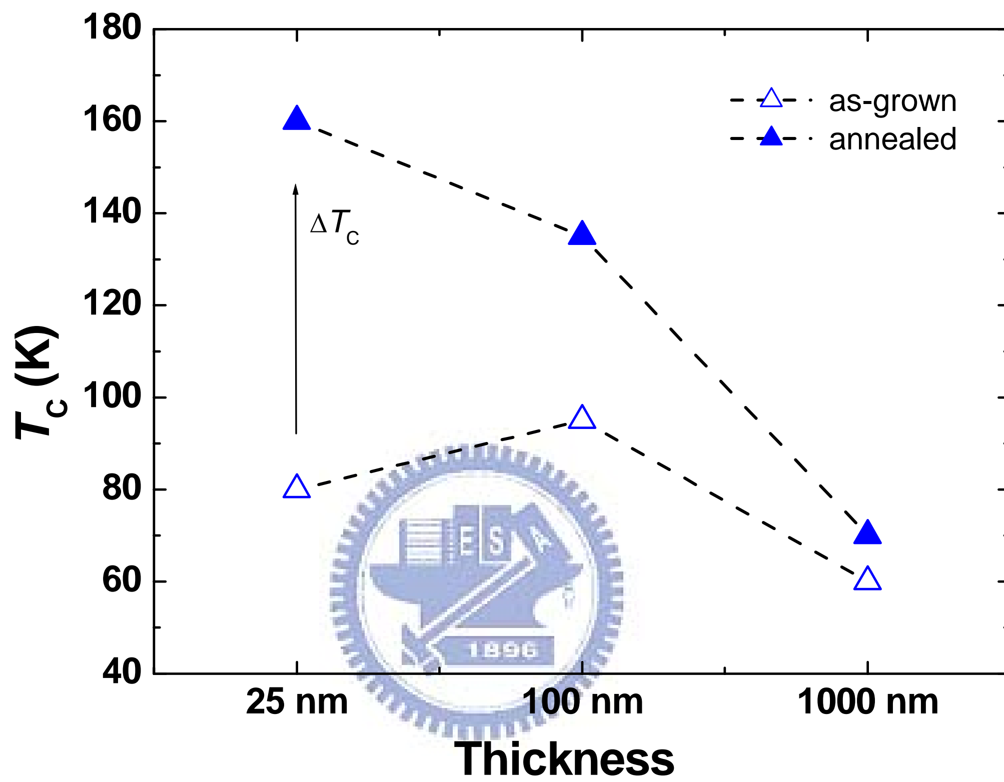

Figure 4.10 Curie temperature values (T_C) vs. thickness of as-grown and post-annealed (Ga, Mn)As DMS (Samples C1, C2 and C3)

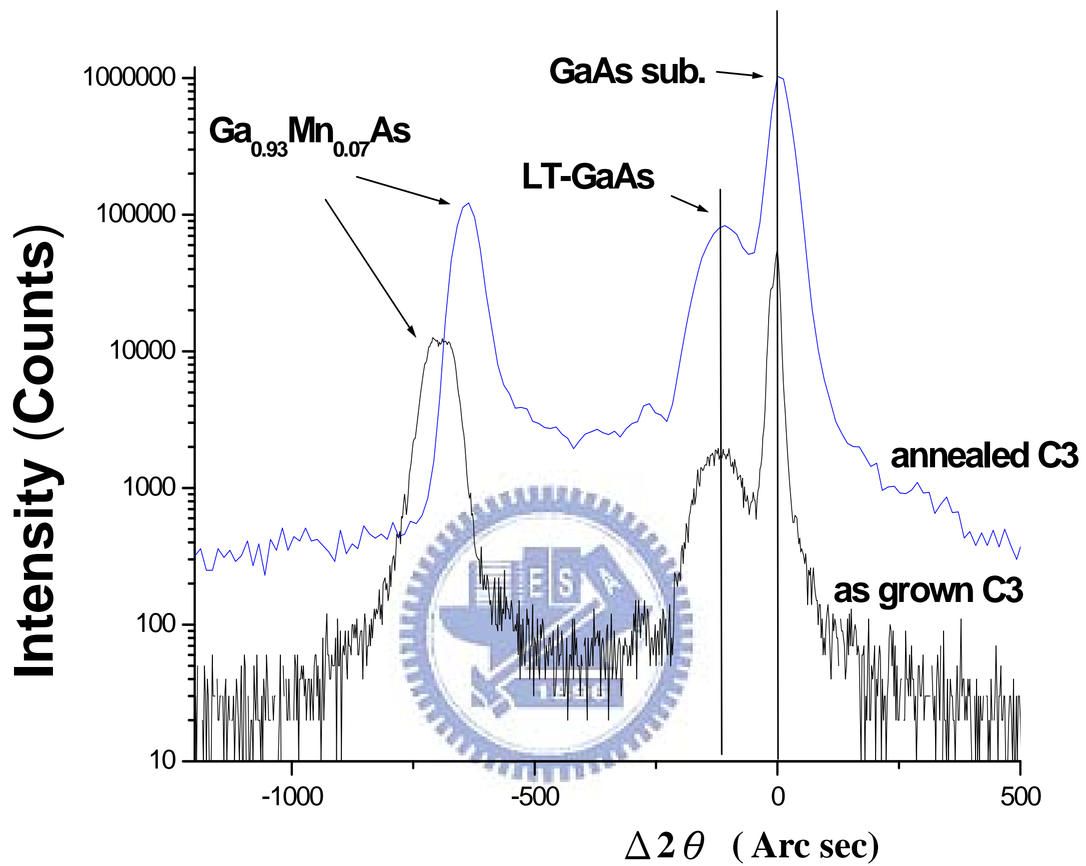

Figure 4.11 The DXRD rocking curves of as-grown and post-annealed (Ga, Mn)As DMS (Sample C3)

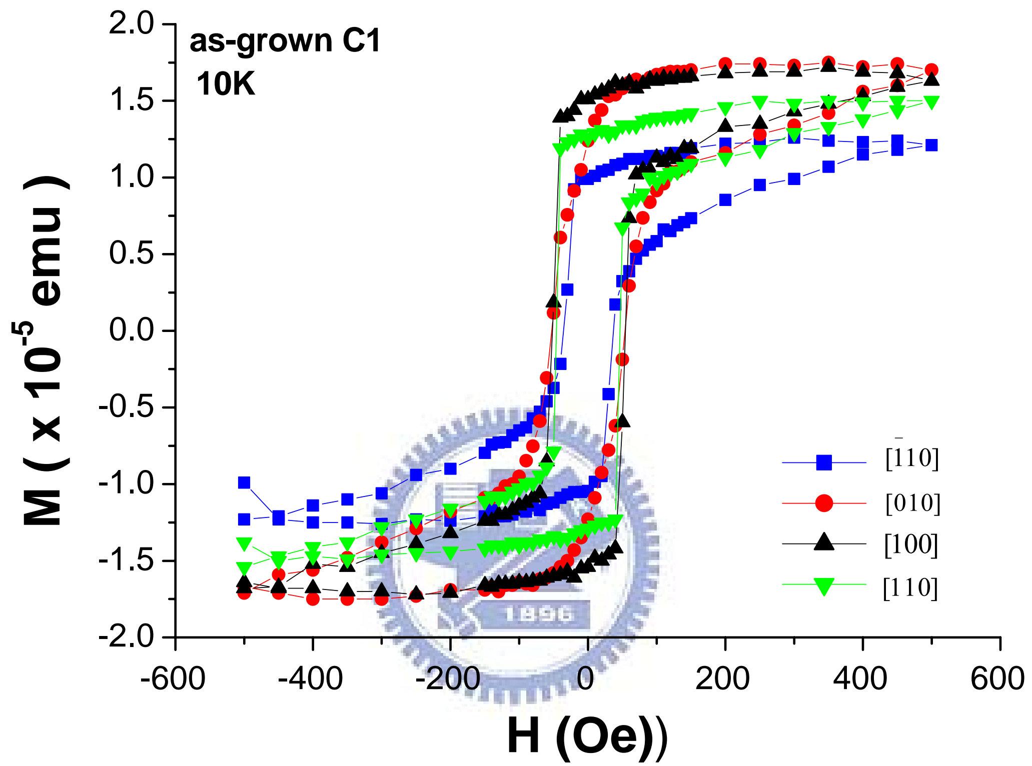

(a)

Figure 4.12(a) M-H curves of as-grown (Ga, Mn)As DMS (Sample C1) measured with in-plane magnetic field applied along [110], [$\bar{1}$10], [100], [010] directions, respectively, at 10K

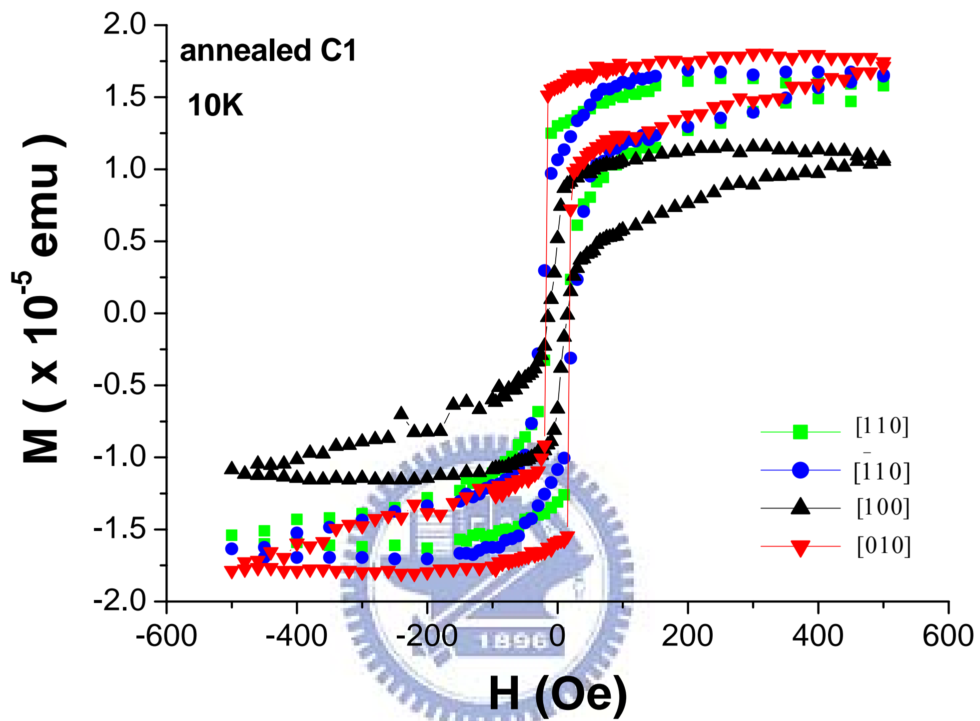

(b)

Figure 4.12(b) M-H curves of post-annealed sample C1 measured with in-plane magnetic field applied along [110], [$\bar{1}$10], [100], [010] directions, respectively, at 10K

4.4 Effects of substrates orientation on the magnetic properties of $Ga_{0.93}Mn_{0.07}As$

The effects of substrate orientation on magnetic properties of $Ga_{0.93}Mn_{0.07}As$ were grown on (001), and (311)A GaAs substrates. The M-T curves of as grown and post-annealed Samples D1 and D2 were measured in small magnetic field (H = 1 Oe) applied in-plane directions. The diamagnetic contribution from the substrate has been subtracted. Figure 4.13(a) shows M-T curves of as-grown and post-annealed Samples D1, with $Ga_{0.93}Mn_{0.07}As$ epi-layer on (001) oriented substrate, measured with a small in-plane magnetic field of 1 Oe applied. Figure 4.13(b) shows M-T curves of as-grown and post-annealed Samples D2, with $Ga_{0.93}Mn_{0.07}As$ epi-layer on (311)A oriented substrate, measured with a small in-plane magnetic field of 1 Oe applied.

Annealed samples showed T_c value of 160K if (001) oriented and 140K if (311)A oriented. It is apparent that in post-annealed samples, T_c is dependent on the orientation of substrates. Compared with the as-grown and post-annealed samples increments in T_c dependent on the orientation of substrates are exhibited. The increment of T_c value of $Ga_{0.93}Mn_{0.07}As$ was 80K if (001) oriented and 60K if (311)A oriented.

All samples showed a ferromagnetic state at 10 K as confirmed by the M-H curves. Figure 4.14(a) shows M-H curves of $Ga_{0.93}Mn_{0.07}As$ epi-layer on (001) oriented substrate Sample D1, measured with in-plane magnetic field applied along [110], $[\bar{1}10]$] directions at 10K. Figure 4.14(b) shows M-H curves of $Ga_{0.93}Mn_{0.07}As$ epi-layer on (311)A oriented substrate Sample D2, measured with in-plane magnetic field applied along $[01\bar{1}]$, $[\bar{2}33]$ directions at 10K. The M-H curves indicates a typical ferromagnetic hysteresis behavior and easy axis near [110] direction if (001) oriented and easy axis was clearly in $[01\bar{1}]$ direction if (311)A oriented. The coercive fields of $Ga_{0.93}Mn_{0.07}As$ epilayers were 20 Os if (001) oriented, and 75 Os if (311)A oriented.

Figure 4.15 shows the DXRD rocking curve of (004) as-grown and post-annealed Sample D3 exhibiting three distinct peaks for GaAs substrate, LT-GaAs buffer layer and $Ga_{0.93}Mn_{0.07}As$ epi-layer, respectively. The rocking curves of Sample D3 layers clearly reveal an expansion of the lattice constant along the growth direction, indicating that samples are tetragonal and coherently strained to the GaAs substrate. When growing at a temperature of about 230℃, LT-GaAs buffer layer and LT-(Ga, Mn)As epi-layers are non-stoichiometric containing As_{Ga}, Mn_{Ga} and Mn_I defects, resulting in an expansion of the lattice and a high concentration of As_{Ga} and Mn_I defects with a donor-like character. The $Ga_{0.93}Mn_{0.07}As$ epi-layers peaks are 696 and 636 arcsec for post-annealed and as-grown Sample D3. Annealing decreases the lattice expansion of $Ga_{0.93}Mn_{0.07}As$ epi-layers by about 60 arcsec. But the peak separation of LT-GaAs buffer layers for post-annealed and as-grown Sample D3 shows no obvious difference. It reveals that annealing effect removes not the As_{Ga} defects, but the Mn_I defects. A large proportion of donor-like Mn_I defects of $Ga_{0.93}Mn_{0.07}As$ epi-layers are removed by annealing. The model proposed [Blinowski-03-121204], Mn_I may form antiferromagnetic coupling pairs with the nearest substitutional Mn_{Ga}, which would also suppress the total ferromagnetic exchange interaction and further reduces T_c. Therefore, the Mn_I defects diffusion during growth and low temperature annealing play a key role in determining the magnetic properties of (Ga, Mn)As epilayers.

In the previous reports [Lee-05-6399], the effect of substrate orientation on arsenic precipitation in low-temperature-grown GaAs, had proved that As_{Ga} defects on (311)A were higher than (001) substrates. Similarly in $Ga_{0.93}Mn_{0.07}As$ epilayers, As_{Ga} defects were higher on (311)A than on (001) oriented. As_{Ga} defects cannot be completely removed during low temperature annealing. Disparity of the hole concentration of the $Ga_{0.93}Mn_{0.07}As$ epilayers are compensated by the donor-like As antisite (As_{Ga}) defects, resulting in higher ΔT_c of $Ga_{0.93}Mn_{0.07}As$ epilayers on (001) oriented than on (311)A oriented.

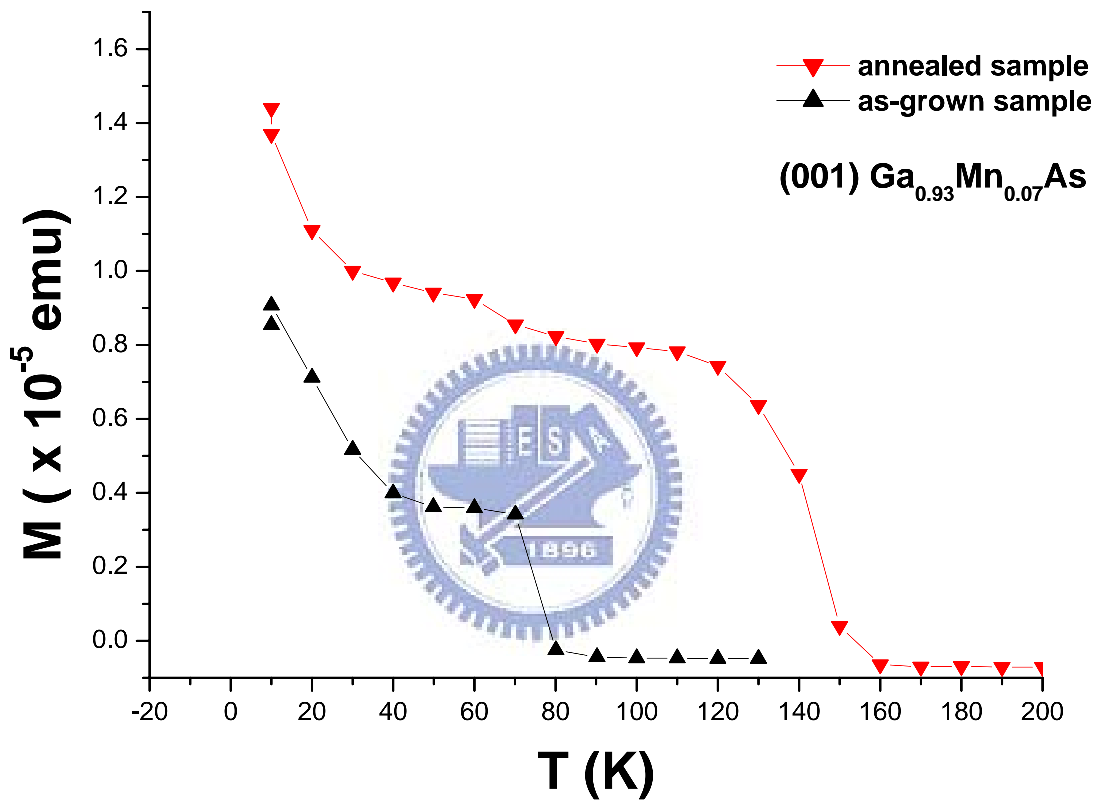

(a)

Figure 4.13(a) M-T curves of as-grown and post-annealed (Ga, Mn)As DMS (Samples D1), with $Ga_{0.93}Mn_{0.07}As$ epi-layer on (001) oriented substrate, measured under 1 Oe in-plane magnetic field

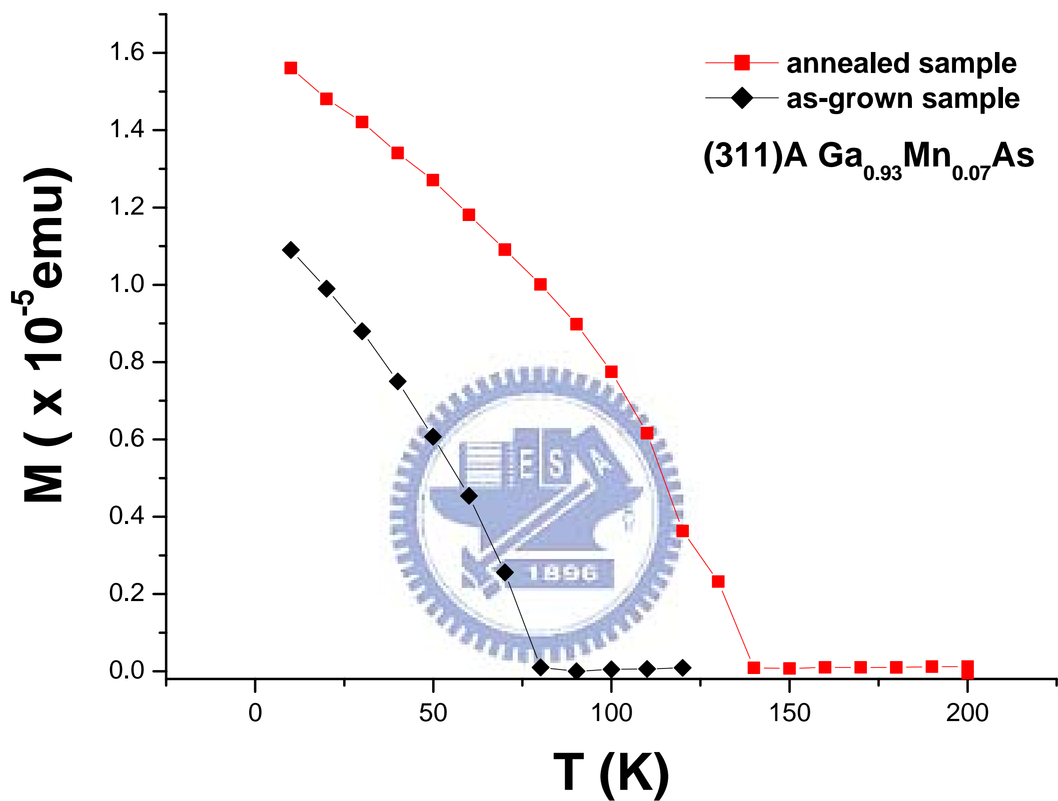

(b)

Figure 4.13(b) M-T curves of as-grown and post-annealed (Ga, Mn)As DMS (Samples D2), with $Ga_{0.93}Mn_{0.07}As$ epi-layer on (311)A oriented substrate, measured under 1 Oe in-plane magnetic field

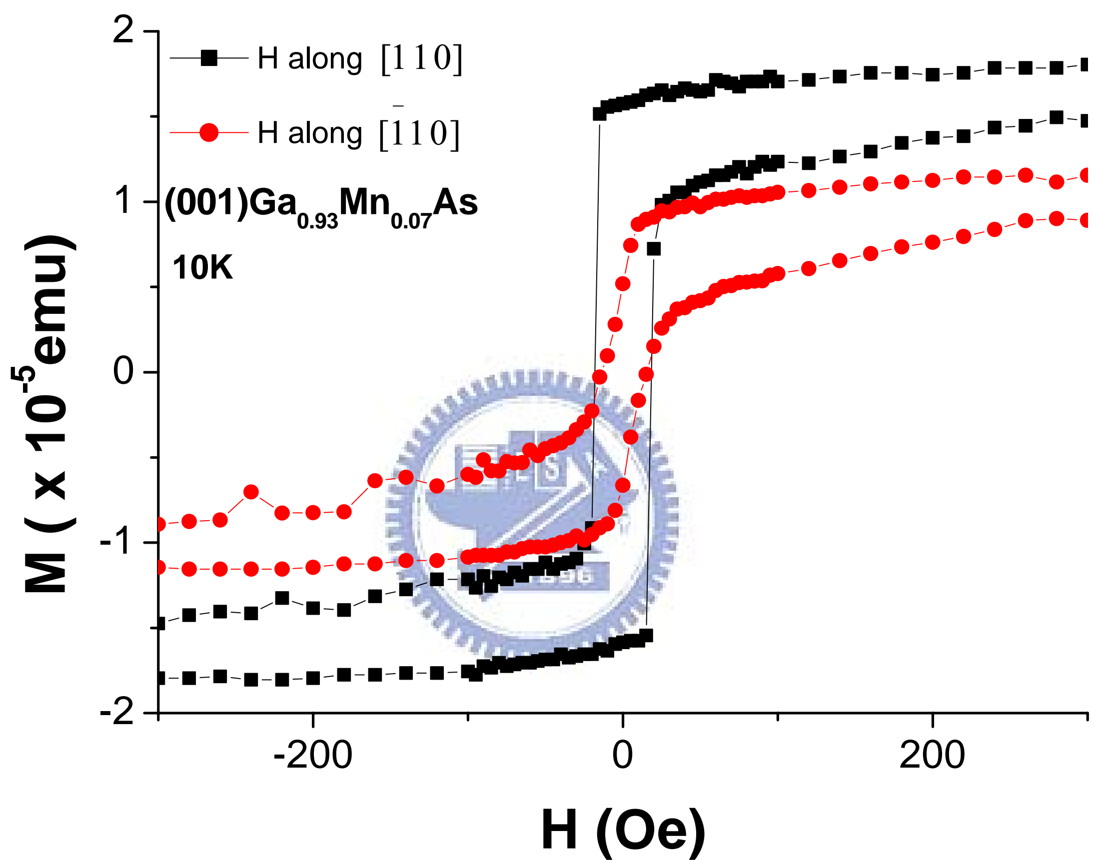

(a)

Figure 4.14(a) M-H curves of $Ga_{0.93}Mn_{0.07}As$ epi-layer on GaAs(001) oriented substrate (Sample D1), measured with in-plane magnetic field applied along [110], [$\bar{1}$10]] directions at 10K

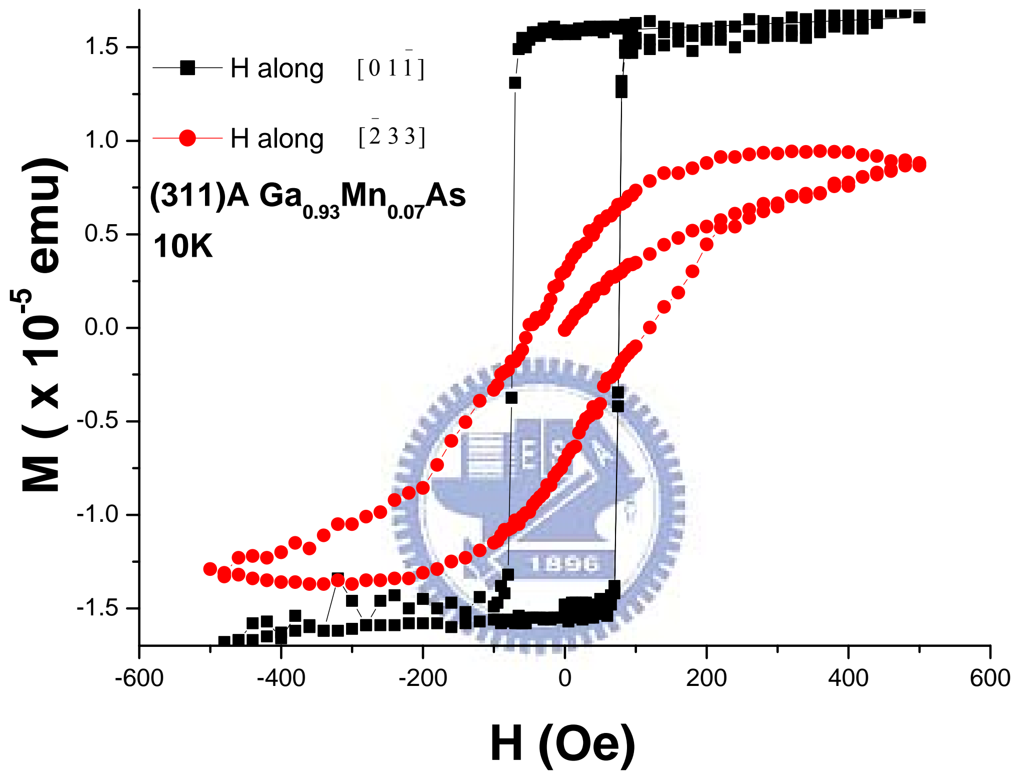

(b)

Figure 4.14(b) M-H curves of $Ga_{0.93}Mn_{0.07}As$ epi-layer on GaAs(311)A oriented substrate (Sample D2), measured with in-plane magnetic field applied along $[01\bar{1}]$, $[\bar{2}33]$ directions at 10K

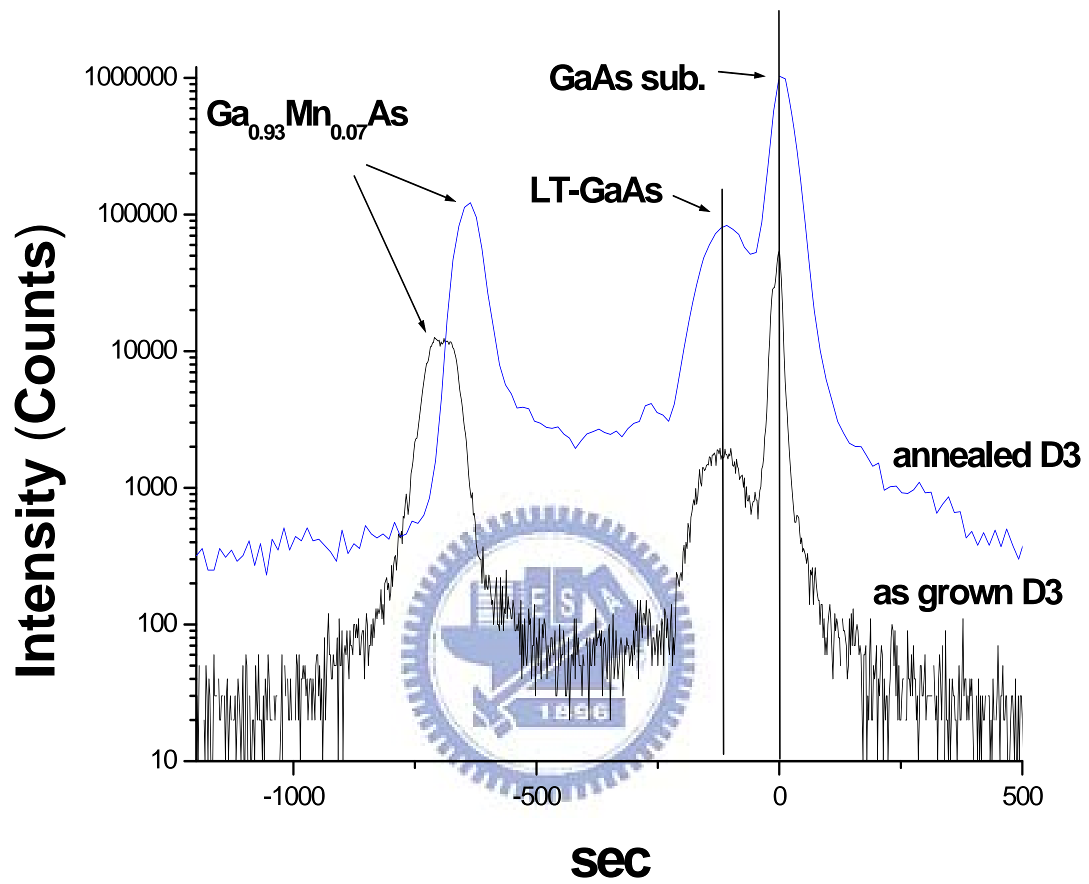

Figure 4.15 The DXRD rocking curves of as-grown and post-annealed (Ga, Mn)As DMS (Sample D3)

4.5 **Property of $(In_{0.52}Al_{0.48})_{1-x}Mn_xAs$ / $In_{0.52}Al_{0.48}As$ / InP layer structure**

A series of diluted magnetic semiconductors, $(In_{0.52}Al_{0.48})_{1-x}Mn_xAs$ ($0 < x \leq 0.11$), was grown on InP substrate by low-temperature molecular beam epitaxy. The cross-sectional image projected along [110] zone of Sample E4 is shown in Figure 4.16(a) is the bright field TEM image of the interfacial region between $(In_{0.52}Al_{0.48})_{0.92}Mn_{0.08}As$ epilayer and $In_{0.52}Al_{0.48}As$ buffer layer and (b) is the lattice image with $(In_{0.52}Al_{0.48})_{0.92}Mn_{0.08}As$ epilayer on the top and $In_{0.52}Al_{0.48}As$ buffer layer at the bottom. Both RHEED patterns and TEM measurements confirmed that the epitaxial $(In_{0.52}Al_{0.48})_{1-x}Mn_xAs$ active layer has a zinc-blend structure. Figure 4.17 shows the DXRD rocking curves of (004) for Sample E2, E4, and E5 with x = 0.05, 0.08, and 0.11, respectively. Obvious peak separation due to the incorporation Mn atoms was observed. The lattice expansion is about 0.20, 0.29, and 0.50 % for Samples E2, E4, and E5, respectively, increasing with the increase in Mn content.

All samples of magnetization were measured with the $[\bar{1}10]$ direction in-plane magnetic field. The total magnetization of $(In_{0.52}Al_{0.48})_{1-x}Mn_xAs$/InP samples includes two components, i.e., the magnetization of $(In_{0.52}Al_{0.48})_{1-x}Mn_xAs$ epilayer and InP substrate. Therefore, in order to obtain the “net” magnetization of the active layer, the magnetization of the “bare” InP substrate with same size must be separately measured and carefully subtracted from the total magnetization. Inset of Fig. 4.18 shows the magnetization as a function of applied field of $(In_{0.52}Al_{0.48})_{0.95}Mn_{0.05}As$/InP and corresponding “bare” InP substrate with same size. We can find that the *M-H* curve of InP substrate shows almost a linear relationship, which suggests that the semi-insulating InP substrate exhibits diamagnetic behavior, similar to that of semi-insulating GaAs substrate. Compared with that of the InP substrate, *M-H* curve of $(In_{0.52}Al_{0.48})_{0.95}Mn_{0.05}As$/InP shows a similar linear relationship with a smaller absolute slope. Figure 4.18 shows the “net” magnetization as a function of applied field of $(In_{0.52}Al_{0.48})_{0.95}Mn_{0.05}As$ epilayer at 5K after carefully subtracting the diamagnetic signal of InP substrate. There is a good coincidence between the linear fit and experimental data.

Therefore, The Sample E2 [$(In_{0.52}Al_{0.48})_{0.95}Mn_{0.05}As$] is belived to possess the paramagnetic-like behavior at 5K. It should be noted that similar phenomenon was also observed in Sample E1 with x = 0.03.

Samples with $x \geq 0.06$ showed a ferromagnetic state at 5 K as confirmed by the *M-H* curves. For example, the *M-H* curves of Sample E4 and E5 are shown in Fig. 4.19 Obviously, both epilayers exhibit typical ferromagnetic state. In addition, the coercivity of $(In_{0.52}Al_{0.48})_{1-x}Mn_xAs$ is very low (< 15 G). We also measured the field cooling *M-T* curves of the epilayers with the $[\bar{1}10]$ direction in-plane applied magnetic field (*H* = 100 Oe). Fig. 4.20 selectively shows the *M-T* curves samples E4 (x = 0.08) and E5 (x = 0.11) epilayer and the corresponding Curie temperatures are 20, and 25K, respectively.

The reason for $(In_{0.52}Al_{0.48})_{1-x}Mn_xAs$ to exhibit paramagnetic-like behavior for $x \leq 0.05$ and ferromagnetic behavior for $x \geq 0.06$ can be simply analyzed as follows. A similar paramagnetic-like phenomenon observed in $Al_{0.96}Mn_{0.04}As$ [Liu-02-967]. The electrical transport measurements indicate deep acceptor level of Mn inside AlAs, resulting in lacking of free carriers and semi-insulating and hence paramagnetic [Liu-02-967]. In light of this viewpoint, that Mn atoms in $(In_{0.52}Al_{0.48})_{1-x}Mn_xAs$ could acts as deep level acceptors depreciating the free holes and hence paramagnetic. While $x \geq 0.06$, the increased Mn atoms tend to form "shallow" level acceptors and provide free holes and thus leading to ferromagnetic exchange interaction. Further electrical and magnetic transport measurements must be done to provide deeper insight to this phenomenon and prove the assumption.

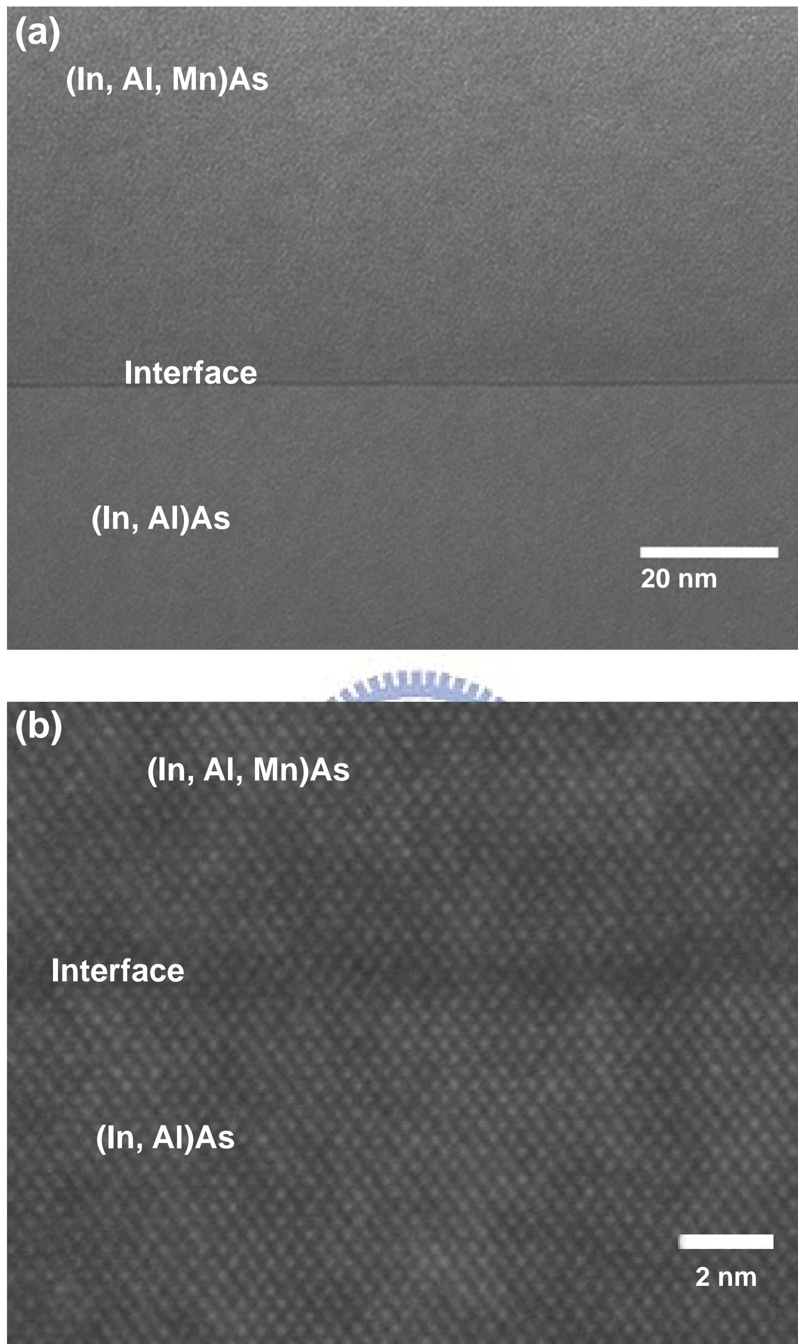

Figure 4.16 The interfacial micrographs between (In, Al, Mn)As and InAlAs (Sample E4): (a) bright field TEM image and (b) lattice image

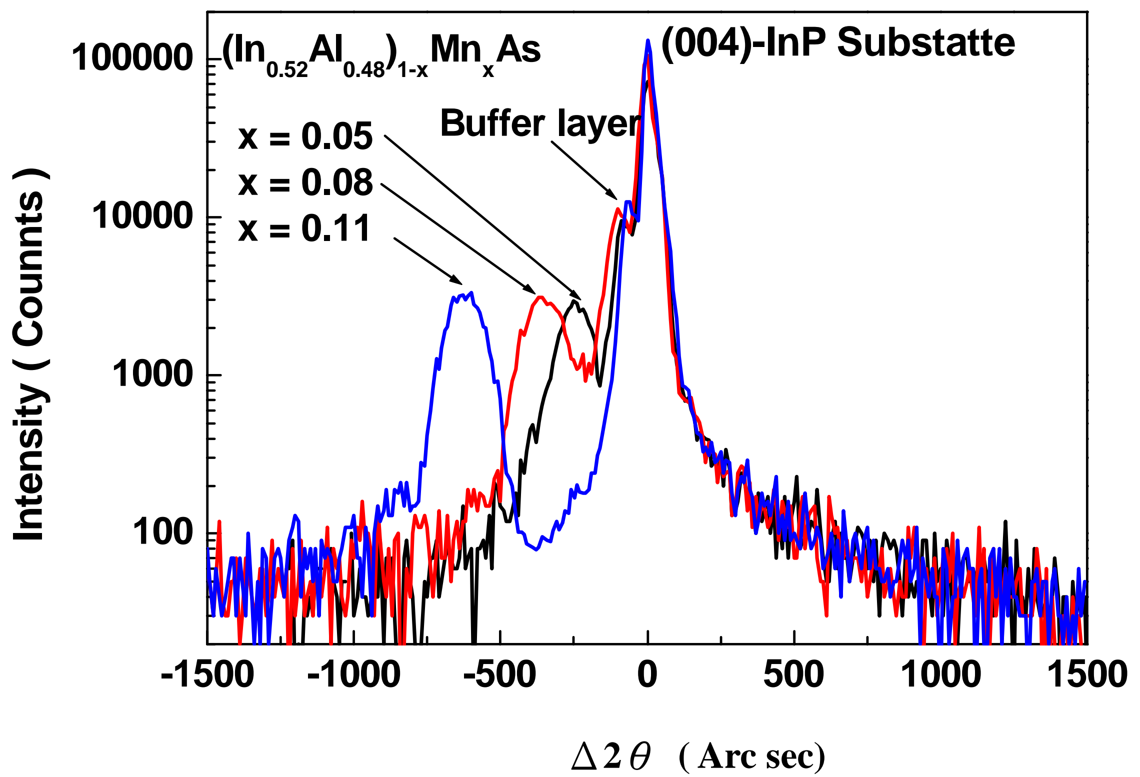

Figure 4.17 The DXRD rocking curves of (004) for (In, Al, Mn)As on InP (Sample E2, E4, and E5)

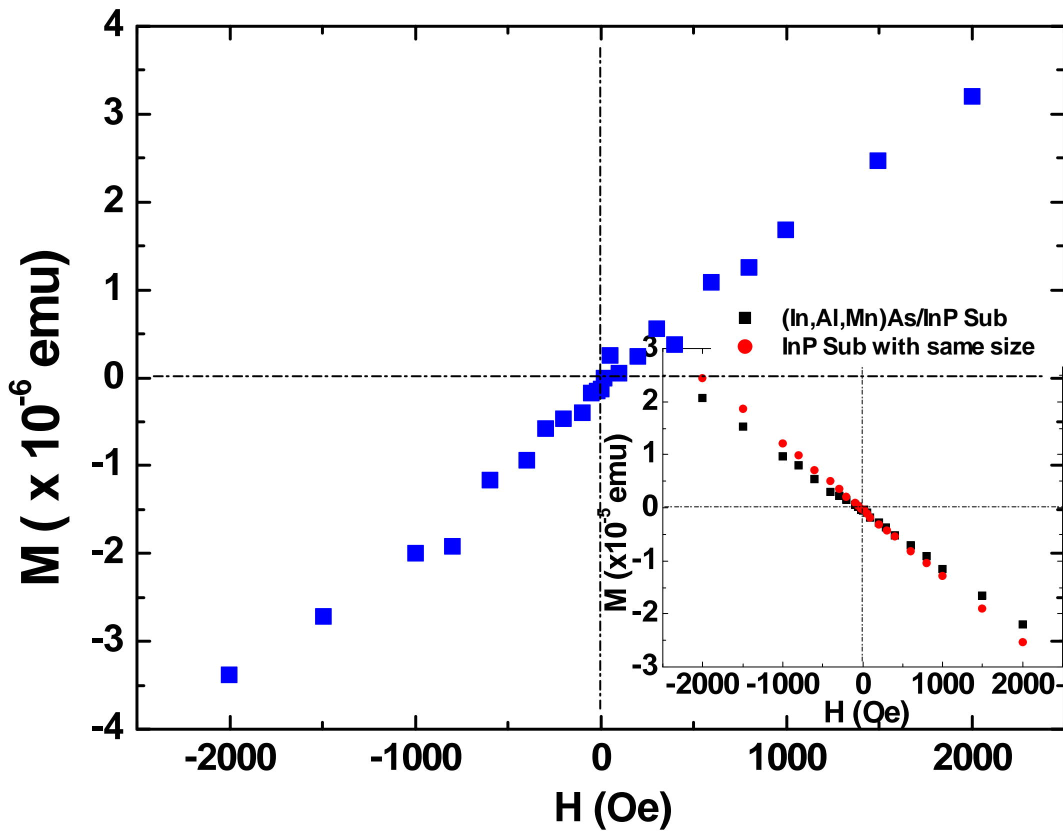

Figure 4.18 The M-H curves for $(In_{0.52}Al_{0.48})_{0.95}Mn_{0.05}As$ epilayer on InP (Sample E2), measured with in-plane magnetic field at 5K. Closed circles stand for "net" magnetization after subtracting the magnetization of InP substrate and solid line is results of linear fit of the experimental data. Inset shows the applied field dependence of magnetization at 5K for $(In_{0.52}Al_{0.48})_{0.95}Mn_{0.05}As$ epilayer on InP (Sample E2) and "bare" InP substrate with same size

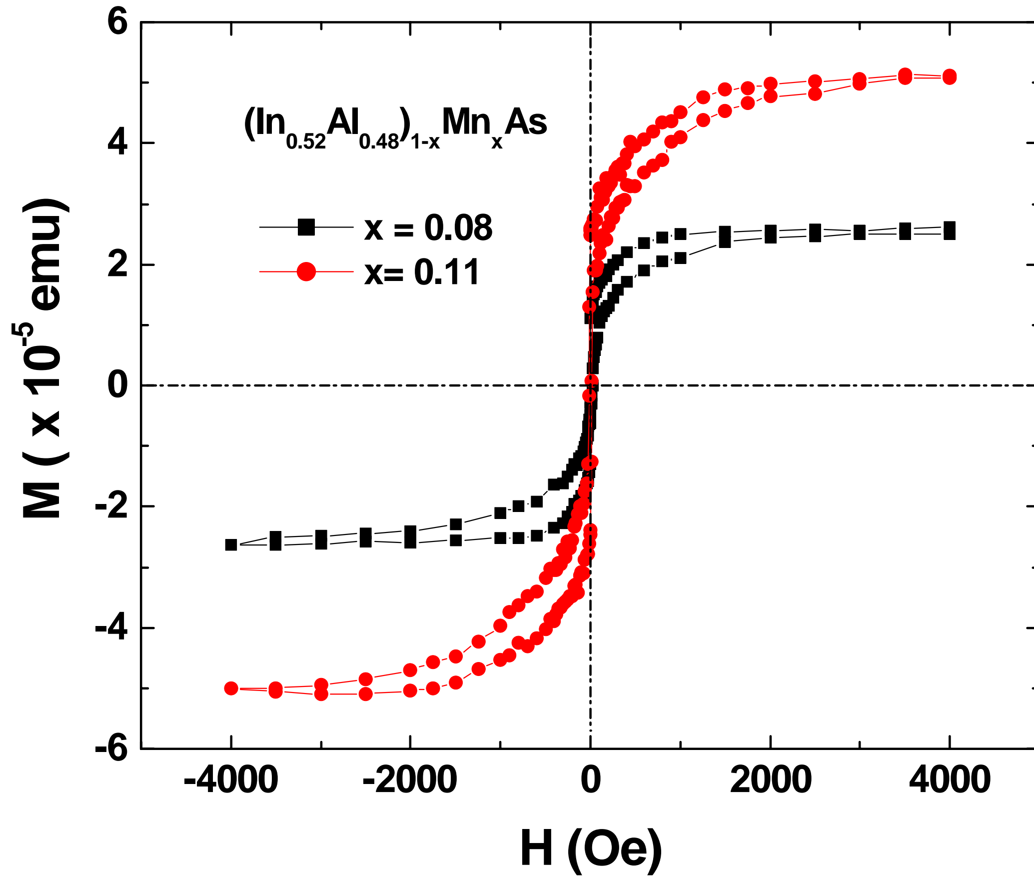

Figure 4.19. M-H curves of as-grown and post-annealed for $(In_{0.52}Al_{0.48})_{0.92}Mn_{0.08}As$ epilayer on InP (Sample E4) and $(In_{0.52}Al_{0.48})_{0.89}Mn_{0.11}As$ epilayer on InP (Sample E5) measured with in-plane magnetic field at 5K

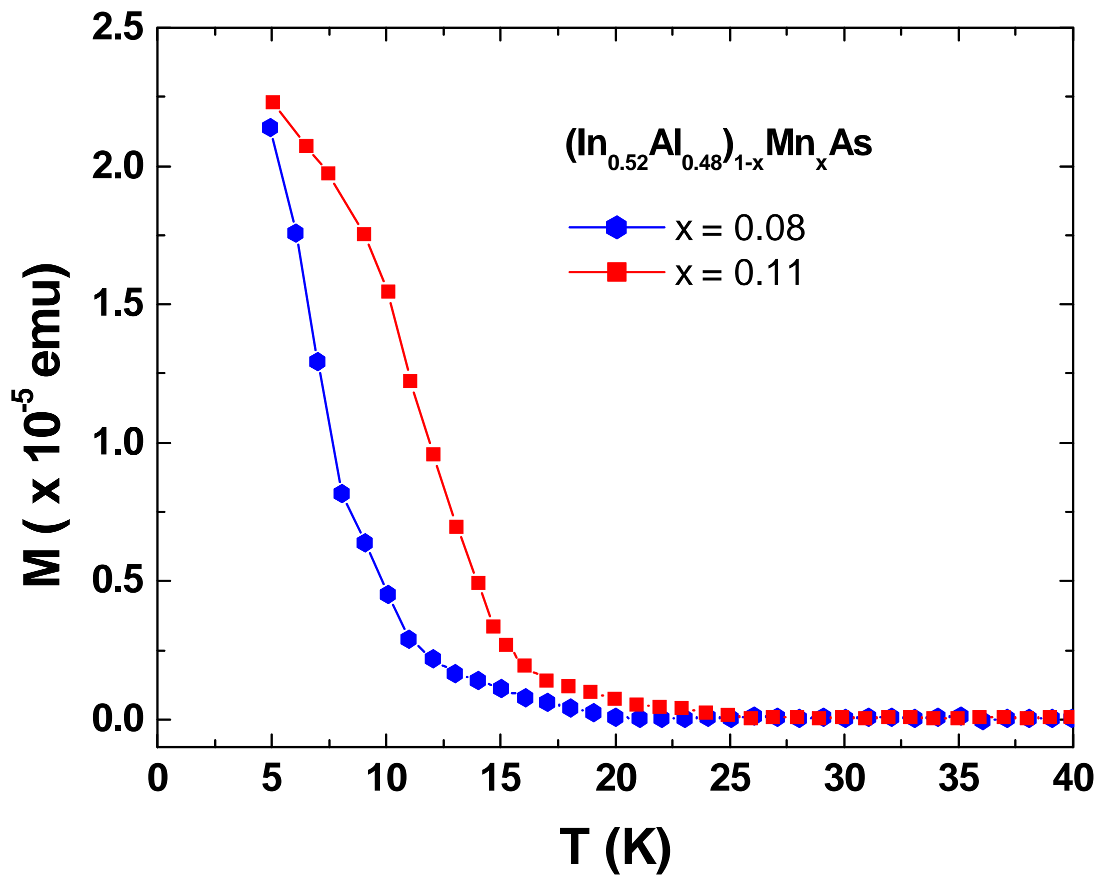

Figure 4.20 M-T curves under 100 Oe in-plane applied magnetic field along with [100] direction for $(In_{0.52}Al_{0.48})_{0.92}Mn_{0.08}As$ epilayer on InP (Sample E4) and $(In_{0.52}Al_{0.48})_{0.89}Mn_{0.11}As$ epilayer on InP (Sample E5)

4.6 Property of $(In_{1-y}Al_y)_{1-x}Mn_xAs$ / $(In_{1-y}Al_y)As$ / InP layer structure

A series of quaternary diluted magnetic semiconductors, $(In_{1-y}Al_y)_{1-x}Mn_xAs$, have been successfully grown on InP substrates by low-temperature molecular beam epitaxy. The $(In_{0.52}Al_{0.48})_{1-x}Mn_xAs$ with $x \leq 0.11$ were grown on a nearly lattice-matched $In_{0.52}Al_{0.48}As$ buffer, while the $(In_{1-y}Al_y)_{1-x}Mn_xAs$ with a higher Mn content of $0.11 < x \leq 0.18$ were grown on a graded 3-layer $In_{1-y}Al_yAs$ buffer structure. In order to check the crystalline structure and growth quality of (In, Al, Mn)As epilayers, DXRD rocking curves in the vicinity of InP (004) reflections were collected. Figure 4.21 shows the DXRD rocking curves for Samples G1, G2, and G4. All curves clearly exhibit well-separated diffraction peaks corresponding to the (In, Al)As buffer structures and the (In, Al, Mn)As epilayers, indicating that all samples are tetragonal and coherently full strained to the InP substrate. To resolve the diffraction peaks of Sample G4, a control sample consisting of only the graded buffer structure as used for Sample G4 has been also grown under otherwise the same growth conditions. As a result, the extra peak of each sample was identified to be due to the (004) Bragg reflection of the (In, Al, Mn)As epilayer. The peak separations between the (In, Al, Mn)As epilayers and the InP substrate were found to be -280, -370, and -828 arc sec for Samples G1, G2, and G4, respectively. This indicates that (In, Al, Mn)As epilayers have larger lattices than InP. Moreover, the lattice constant of the (In, Al, Mn)As epilayers increases with increasing Mn content x, which agrees with what have observed for most (In, Ga, Mn)As [Ohya-03-139] and (Ga, Mn)As [Sadowski-04-075206] epilayers with appreciable Mn content. It has been noticed that the relationship between Mn content and lattice constant depends on many factors: the growth conditions, the size of the atoms that were substituted by Mn atoms, etc.

As already mentioned, appreciable Mn-containing III-V alloys have a larger lattice than the supporting substrate, GaAs or InP, and the lattice constant in general increases linearly with increasing Mn content. However, the lattice-mismatch-induced strain associated with the enlarged (III, Mn)As lattice inhibit the growth of (III, Mn)As films beyond a certain

thickness; i.e. the critical thickness. Therefore, the amount of Mn atoms that can be introduced to a III-V host should be lower than its chemical solubility if a high-quality (III, Mn)As film with fair thickness is needed. This problem can be overcome in principle by utilizing a buffer that is nearly lattice-matched to the (III, Mn)As epilayer.

Once the lattice-mismatch-induced compressive strain is greatly reduced, the III-V host can accommodate Mn atoms up to the chemical solubility limit; otherwise second phase or precipitation would form in the (III, Mn)As matrix to minimize the Gibbs free energy. In this study, that a graded buffer structure was employed nearly lattice-matched to the (In, Al, Mn)As films with high Mn content. As can be seen in Figure 4.21, the peak separation between the $(In_{0.61}Al_{0.39})_{0.85}Mn_{0.15}As$ epilayer and the $In_{0.61}Al_{0.39}As$ buffer is only ~70 arc sec, indicating both layers are nearly lattice matched to each other. In contrast, the $(In_{0.61}Al_{0.39})_{0.85}Mn_{0.15}As$ is ~828 arc sec apart from the InP. Without this graded buffer, it was found that only ~10 nm $(In_{0.61}Al_{0.39})_{0.85}Mn_{0.15}As$ could be grown prior to the onset of island growth.

The cross-sectional high-resolution lattice image projected along the [110] zone of Sample G3 is shown in Fig. 4.22 (a), which shows a high-quality interface between the $(In_{0.52}Al_{0.48})_{0.89}Mn_{0.11}As$ epilayer and the $In_{0.52}Al_{0.48}As$ buffer. Moreover, the image shows no trace of Moiré fringes, implying the films are free of structural defects, such as twins and/or precipitates [Huang-03-3005]. The selected area diffraction pattern of the $(In_{0.52}Al_{0.48})_{0.89}Mn_{0.11}As$ layer shown in Fig. 4.22 (b) further shows no extra diffractive spots. Therefore, from Fig. 4.22, it can be concluded that the $(In_{0.52}Al_{0.48})_{0.89}Mn_{0.11}As$ layer is of coherently strained epi-layer with zinc-blende structure. The magnetic field dependence of magnetization (M-H curves) of Samples G1, G2, G3, and G4 at 5 K is shown in Fig. 4.23. Samples were measured with in-plane magnetic field applied along the $[\bar{1}10]$ direction, and the diamagnetic behavior of the InP substrate was carefully subtracted from the measured signals. All curves are not square like, which is a result of the magnetic anisotropy. Obviously, the $[\bar{1}10]$ direction is

not magnetic easy axis. Analogous to a detailed study on this respect has been reported [Welp-04-260], that is investigated the evolution of magnetic anisotropy in a series of $Ga_{1-x}Mn_xAs$ films. Furthermore, it is noticed that the M-H curve of Sample G1 can be perfectly fitted with a straight line, suggesting that the $(In_{0.52}Al_{0.48})_{0.95}Mn_{0.05}As$ exhibits a paramagnetic-like behavior at 5 K. In contrast, all other samples with $x > 0.05$ demonstrate ferromagnetic states at 5 K, as confirmed by their M-H curves.

The temperature dependence of magnetization (M-T curve) for the ferromagnetic samples was measured with a small magnetic field of 100 Oe along the $[\bar{1}10]$ direction. Figure 4.24 shows the M-T curves for Samples G2, G3, G4, and G5, from which the Curie temperature, T_c, of each sample is determined. The values of T_c for Samples G2, G3, G4, and G5 are 20, 25, 30, and 40 K, respectively. The increase of T_c with increasing Mn content is an unambiguously result, as generally expected for III-V DMS materials.

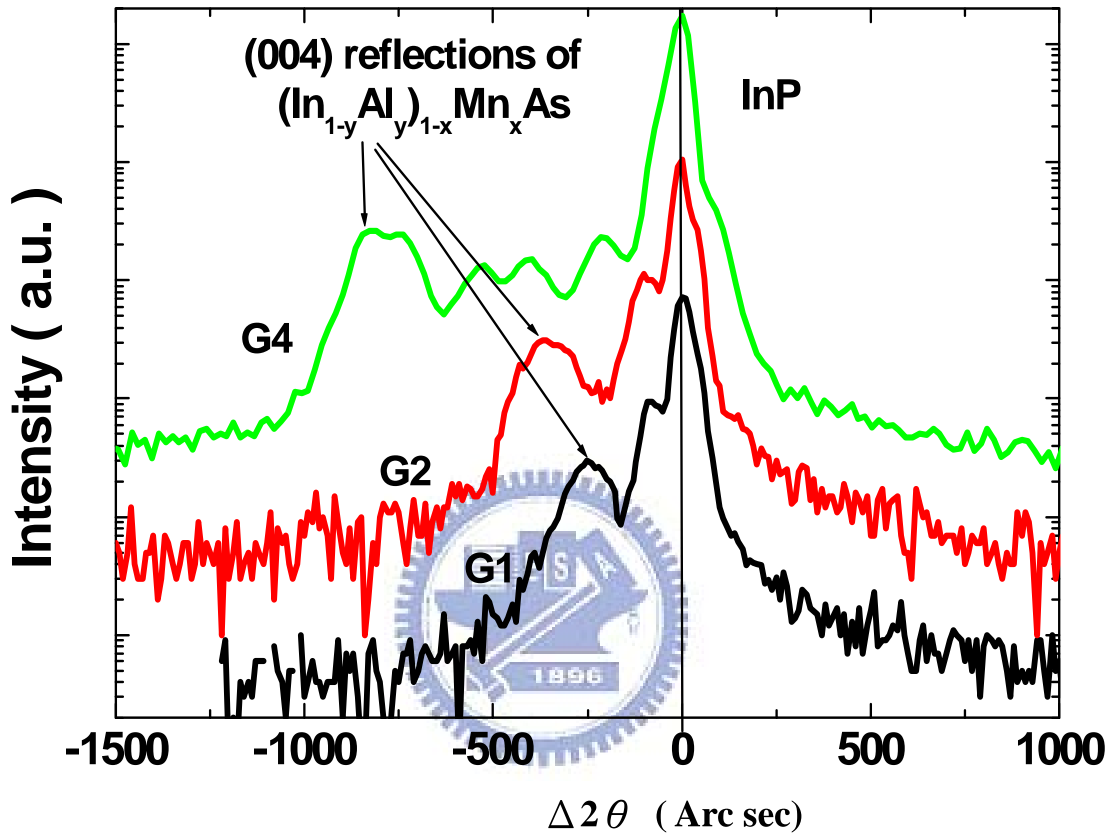

Figure 4.21 The DXRD rocking curves of $(In_{1-y}Al_y)_{1-x}Mn_xAs$ epilayer on InP substrate (Samples G1, G2, and G4)

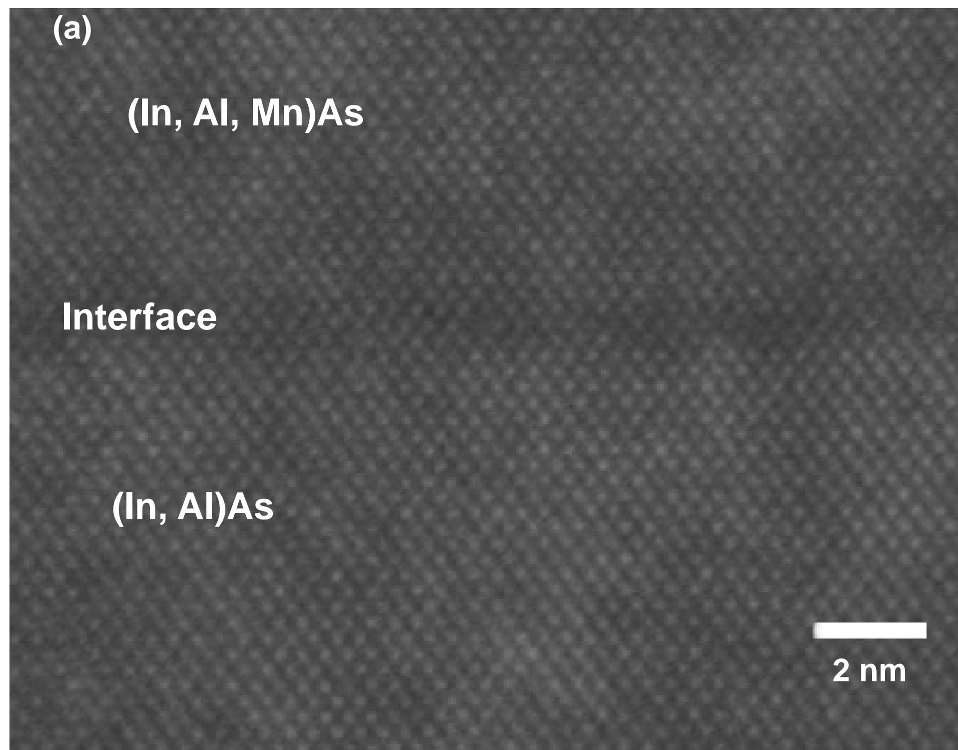

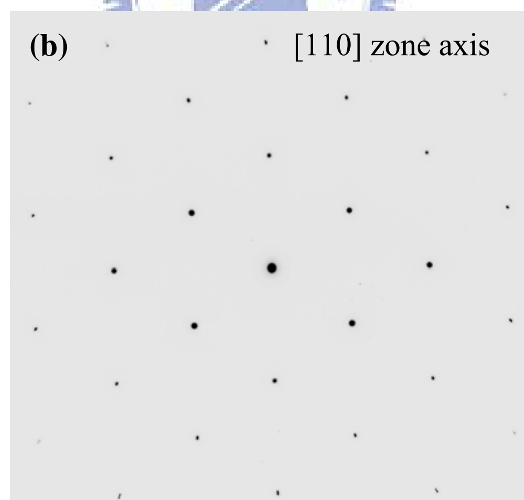

Figure 4.22 (a) High-resolution lattice image of the $In_{0.52}Al_{0.48})_{0.89}Mn_{0.11}As/In_{0.52}Al_{0.48}As$ interface region (Sample G3) and (b) the selected area diffraction pattern of $(In_{0.52}Al_{0.48})_{0.89}Mn_{0.11}As$ layer along [110] zone axis

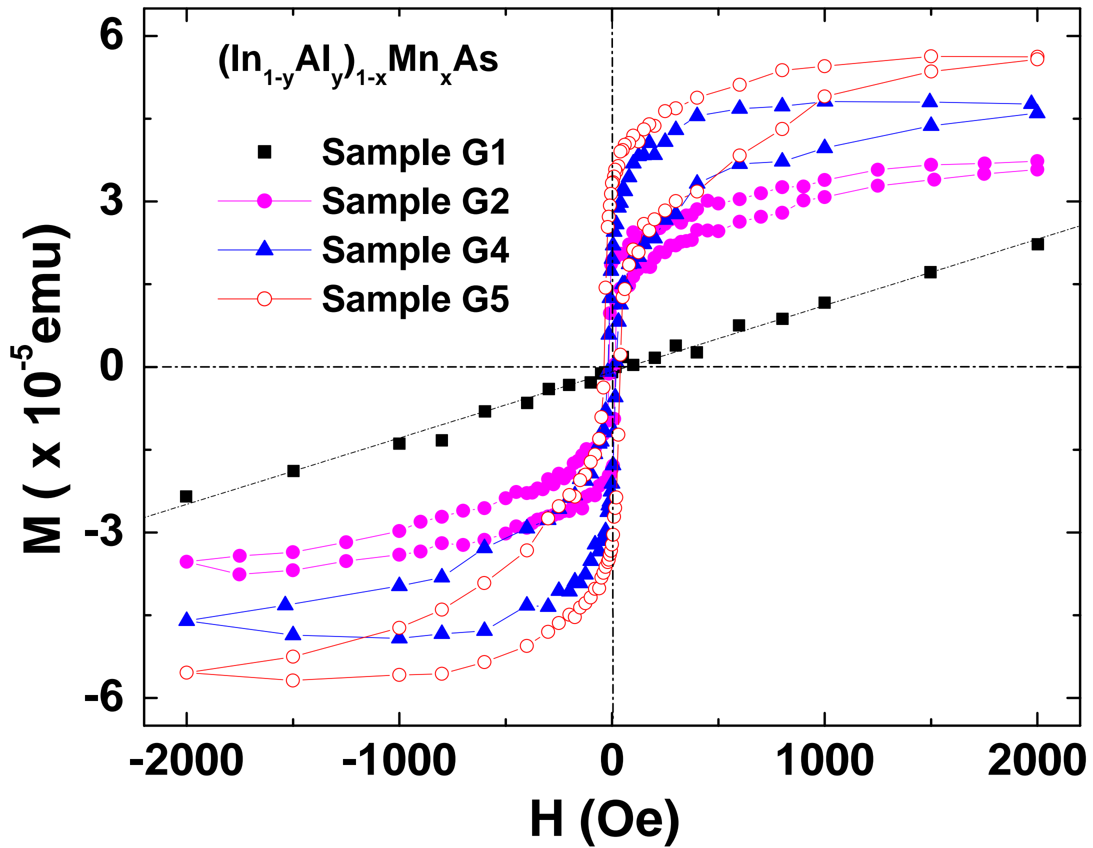

Figure 4.23 M-H curves for $(In_{1-y}Al_y)_{1-x}Mn_xAs$ on InP substrate (Sample G1, G2, G4, and G5) with in-plane magnetic field applied along the $[\bar{1}10]$ direction. The dash dot line is a linear fit of the *M-H* curve for Sample G1

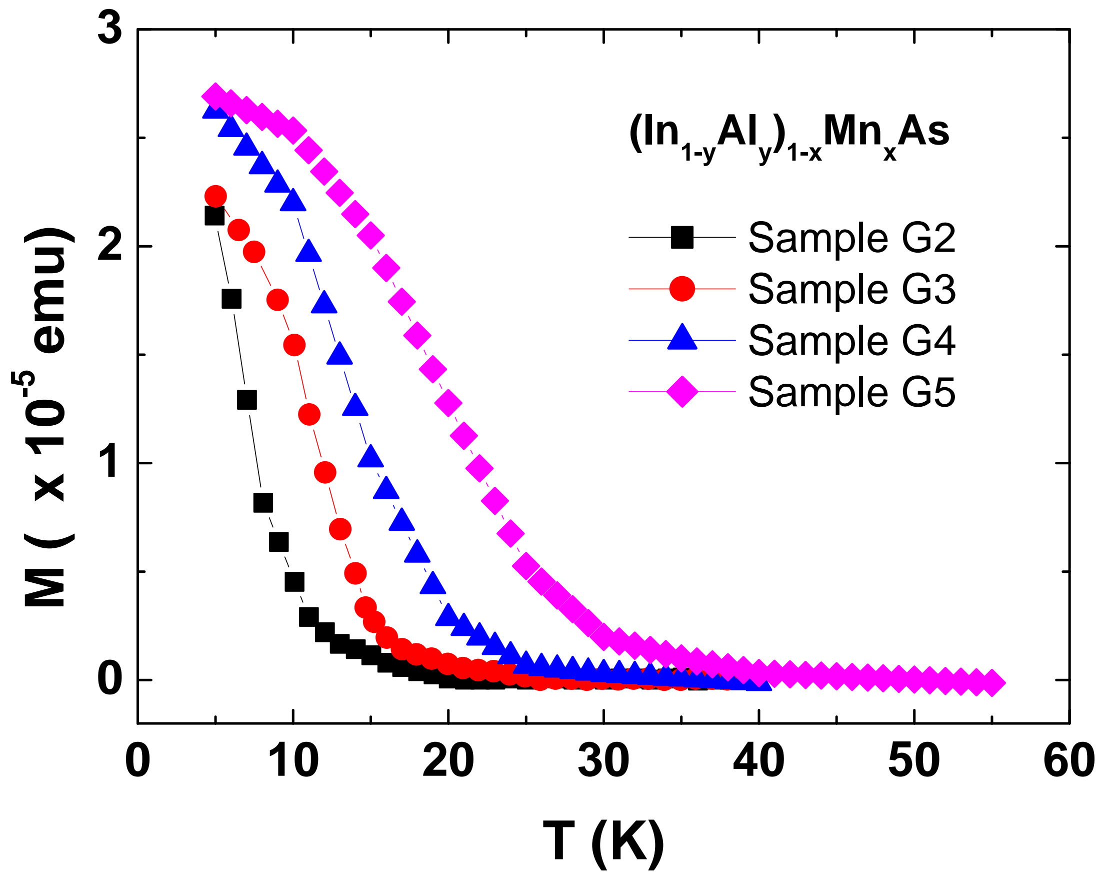

Figure 4.24 M-T curves under 100 Oe in-plane applied magnetic field along with $[\bar{1}10]$ direction for $(In_{1-y}Al_y)_{1-x}Mn_xAs$ on InP substrate (Samples G2, G3, G4, and G5)

CHAPTER 5

CONCLUSIONS

In this work, the experimental results are roughly divided into three subjects, i.e. LT-GaAs, LT-(Ga, Mn)As and LT-(In, Al, Mn)As grown by MBE system. The relationships between strctutre and property were examined. From the experimental results, the following conclusions can be drawn:

(1) The precipitation of arsenic in "superlattice" structures of alternately undoped and [Si] = 3×10^{18} cm^{-3}-doped GaAs grown at 250°C on (100), (311)A, and (311)B GaAs substrates has been studied. It is found that upon postgrowth annealing at 800ºC, As precipitates are nearly all confined in the Si-doped regions, forming two-dimensional clusters arrays located approximately at the center of each Si-doped layer. Nevertheless, different arsenic precipitation was also observed in these LT-GaAs "superlattice" structures: arsenic precipitates in the (311)B substrate are slightly denser and larger than those in the (311)A substrate and both are far denser and larger than those in the (100) substrate. This may be due to a combination effect of the accommodation factors of the crystallographic plane and bonding site difference.

(2) The effect of doping type and concentration on arsenic precipitation in LT-GaAs epi-layers upon post-growth annealing at 600, 700 and 800°C was investigated. The results show that the arsenic precipitation is dependent on doping type and doping concentration. Arsenic depletion was observed in all Be-doped regions. However, a "dual" arsenic precipitation phenomenon was observed in Si-doped regions: arsenic precipitation accumulation was observed in [Si] = 2 x 10^{18} cm^{-3} doped layer for all annealing temperatures, while arsenic precipitation depletion was observed in [Si] = 2 x 10^{16} and 2 x 10^{17} cm^{-3} doped layers. The "dual" arsenic precipitation phenomenon in Si-doped layers can be attributed to

the different depletion depths caused by various doping concentrations.

(3) Effects of thickness and post-annealing on magnetic properties of $Ga_{0.93}Mn_{0.07}As$ epilayers, have been studied. The T_c of as-grown samples were from 60 K ~ 95 K, which were dependent on the thickness of the $Ga_{0.93}Mn_{0.07}As$. Post-annealing at 250 ^{o}C for 1.5 hrs, increases the T_c to 70 K ~ 160 K. Both T_c and ΔT_c of $Ga_{0.93}Mn_{0.07}As$ decreases with increasing epilayer thickness. The DXRD explains the above result by attributing to the Mn interstitial defects and their insufficient out diffusion process during growth and annealing. The easy axis of as-grown and annealed Sample C1 can be rotated from [100] direction to [010] direction by low-temperature annealing.

(4) The magnetic properties of $Ga_{0.93}Mn_{0.07}As$ on (001) and (311)A oriented samples have been examined. The T_c of $Ga_{0.93}Mn_{0.07}As$ on both (001) and (311)A oriented as-grown samples were 80K. Post-annealing at 250 ^{o}C for 1.5 hrs, the T_C values of $Ga_{0.93}Mn_{0.07}As$ samples increase to 160 K if (001) oriented, or 140 K if (311)A oriented, and the ΔT_c of $Ga_{0.93}Mn_{0.07}As$ of as-grown and post-annealed samples were 80 K if (001) oriented and 60 K if (311)A oriented. The DXRD results explain the above observation due to the high density of As_{Ga} defects cannot be removed during low temperature annealing, and caused disparity of the holes concentration of $Ga_{0.93}Mn_{0.07}As$ compensated by the As_{Ga} defects.

(5) A series of quaternary diluted magnetic semiconductors, $(In_{1-y}Al_y)_{1-x}Mn_xAs$, have been grown on InP substrates by low-temperature molecular beam epitaxy. The $(In_{0.52}Al_{0.48})_{1-x}Mn_xAs$ with $x \leq 0.11$ were grown on a nearly lattice-matched $In_{0.52}Al_{0.48}As$ buffer, while the $(In_{1-y}Al_y)_{1-x}Mn_xAs$ with a higher Mn content of $0.11 < x \leq 0.18$ were grown on a graded 3-layer $In_{1-y}Al_yAs$ buffer structure. The results of TEM and DXRD reveal that all $(In_{1-y}Al_y)_{1-x}Mn_xAs$ epilayers are single crystal with zinc-blende structure, and the lattice constant increases with increasing the Mn content. The magnetic measurements show that the $(In_{1-y}Al_y)_{1-x}Mn_xAs$ semiconductors exhibit a paramagnetic-like state for $x \leq 0.05$ while a

ferromagnetic state for $x > 0.05$, and the Curie temperature of ferromagnetic $(In_{1-y}Al_y)_{1-x}Mn_xAs$ increases with increasing Mn content. This work provides important information for the study of InP-based spintronic devices with heterostructures.

CHAPTER 6

FURTURE WORK

(1) Further study on the effect of substrate orientations on property of (Ga, Mn)As

(Ga, Mn)As epilayers grown on (001) oriented and (311)A oriented GaAs substrates have been reported by this thesis. The magnetic properties of (Ga, Mn)As are strongly influenced by the substrate orientation. Heterostructures, quantum dots and ultrathin epilayers on non-(001) orientated GaAs substrates is worthy of further systematic study.

(2) The magnetic anisotropy properties of (Ga, Mn)As

The magnetic anisotropy properties of (Ga, Mn)As epilayers are dependent on strain, thickness, substrates orientation and measuring temperature and shape. Further systematic study on magnetic anisotropy is important owing to its strong influence on the application of spintronic devices.

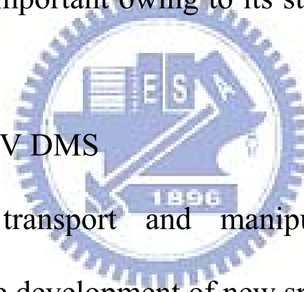

(3) The transport properties of III-V DMS

Fundamental studies on the transport and manipulation of polarized carriers in semiconductors are essential to the development of new spintronics devices.

REFERENCES

A

1. Akiba, N., F. Matsukura, A. Shen, Y. Ohno, H. Ohno, A. Oiwa, S. Katsumoto and Y. Iye, Appl. Phys. Lett. 73 (1998) 2122, " Interlayer exchange in (Ga,Mn)As/ (Al,Ga)As/ (Ga,Mn)As semiconducting ferromagnet/nonmagnet/ferromagnet trilayer structures".
2. Ando, K. T. Hayahi, M. Tanaka, and A. Twardowski, J. Appl. Phys. 83 (1998) 6548, " Magneto-optic effect of the ferromagnetic diluted magnetic semiconductor $Ga_{1-x}Mn_xAs$".
3. Andrews, A. M. et al., Appl. Phys. Lett. 77 (2000) 3740, " Development of cross-hatch morphology during growth of lattice mismatched layers".

B

4. Bert, N. A., A. I. VeÏnger, M. D. Vilisova, S. I. Goloshchapov, I. V. Ivonin, S. V. Kozyrev, A. E. Kunitsyn, L. G. Lavrent'eva, D. I. Lubyshev, V.V. PreobrazhenskiÏ, B. R. Semyagin, V. V. Tret'yakov, V. V. Chaldyshev, and M. P. Yakubenya, Phys. Solid State 35 (1993) 1289, " Gallium arsenide grown by molecular beam epitaxy at low temperatures: crystal structure, properties, superconductivity".
5. Blinowski, J., and P. Kacman, Phys. Rev. B 67 (2003) 121204, "Spin interactions of interstitial Mn ions in ferromagnetic GaMnAs".
6. Braden, J. G. et al., Phys. Rev. Lett. 91 (2003) 056602, " Direct Measurement of the Spin Polarization of the Magnetic Semiconductor (Ga,Mn)As".

C

7. Chandra, A., C. E. C. Wood, D. W. Woodard, and L. F. Eastman, Solid-State Electron. 22 (1979) 645, "Surface and interface depletion corrections to free carrier-density determinations by hall measurements".

8. Chang, L. L., and A. Koma, Appl. Phys. Lett. 29 (1976) 138, " Interdiffusion between GaAs and AlAs".

9. Chang, M. N., J.-W. Pan, J.-I. Chyi, K. C. Hsieh, and T.-E. Nee, Appl. Phys. Lett. 72 (1998) 587, "Effect of column III vacancy on arsenic precipitation in low-temperature grown III–V arsenides".

10. Chang, M. N., K. C. Hsieh, T. E. Nee, and J.-I. Chyi, J. Appl. Phys. 86 (1999) 2442, "Effects of point defect distribution on arsenic precipitation in low-temperature grown III–V arsenides"

11. Cheng, T. M., C. Y. Chang and J. H. Huang, Appl. Phys. Lett. 66 (1995) 55, "Substrate orientation dependence of low-temperature GaAs grown by molecular beam epitaxy".

12. Cheng, T. M., C. Y. Chang, and J. H. Huang, Jpn. J. Appl. Phys. 34 (1995) 1185, " Control of As Precipitation in Low-Temperature GaAs by Electronic and Isoelectronic Delta Doping".

13. Chiba, D., N. Akiba, F. Matsukura, Y. Ohno and H. Ohno, Appl. Phys. Lett. 77 (2000) 1873, " Magnetoresistance effect and interlayer coupling of (Ga, Mn)As trilayer structures".

14. Chiba, D., K. Takamura, F. Matsukura, and H. Ohno, Appl. Phys. Lett. 82 (2003) 3020, " Effect of low-temperature annealing on (Ga,Mn)As trilayer structures".

15 Cho, A. Y., Thin Solid Films 100, (1983) 291, "Growth of III-V semiconductors by molecular beam epitaxy and their properties".

D

16. Dietl, T., H. Ohno, F. Matsukura, J. Cibert, and D. Ferrand, Science 287 (2000) 1019, "Zener Model Description of Ferromagnetism in Zinc-Blende Magnetic Semiconductors".

E

17. Edmonds, K. W., K. Y. Wang, R. P. Campion, A. C. Neumann, N. R. S. Farley, B. L. Gallagher, and C. T. Foxon, Appl. Phys. Lett. 81 (2002) 4991, “High-Curie-temperature $Ga_{1-x}Mn_xAs$ obtained by resistance-monitored annealing”.

18. Edmonds, K. W., P. Boguslawski, K.Y. Wang, R. P. Campion, S. N. Novikov, N. R. S. Farley *et al.*, Phys. Rev. Lett. 92 (2004) 037201, **“**Mn Interstitial Diffusion in (Ga,Mn)As”.

19. Erwin, S. C. and A. G. Petukhov, Phys. Rev. Lett. 89 (2002) 227201, “Self-Compensation in Manganese-Doped Ferromagnetic Semiconductors”.

F

20. Flatt´e, M. E. and G. Vignale, Appl. Phys. Lett. 78, (2000) 1273, “Unipolar spin diodes and transistors”.

21. Fiederling, R., M. Kelm, G. Reuscher, W. Ossau, G. Scmidt, A. Waag and L. W. Molenkamp, Nature 402 (1999) 787, “Injection and detection of a spin-polarized current in a light-emitting diode”.

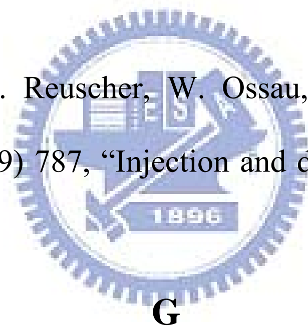

G

22. Gupta,S., M. Y. Frankel, J. A. Valdmanis, J. F. Whitaker, G. A. Mourou, F. W. Smith and A. R. Calawa, Appl. Phys. Lett. 59 (1991) 3276, “Subpicosecond carrier llifetime in GaAs grown by molecular beam epitaxy at low temperatures”.

H

23. Hanbicki, A. T. et al., Appl. Phys. Lett. 80 (2002) 1240, “Efficient electrical spin injection from a magnetic metal/tunnel barrier contact into a semiconductor”.

24. Haneda, S., M. Yamamura, Y. Takatani, K. Hara, S. Harigae and H. Munekata, Jpn. J. Appl. Phys. 39 (2000) L9, “Preparation and Characterization of Fe-Based III-V Diluted Magnetic Semiconductor (Ga, Fe)As “.

25. Harris, J. J., B. A. Joyce, and P.J. Dobson, Surf. Sci. 103, (1980) L90, “Oscillations in the Surface Structure of Sn-doped GaAs During Growth by MBE”.

26. Hayashi, T., M. Tanaka, T. Nishinaga, and H. Shimada, J. Appl. Phys. 81 (1997) 4865, “Magnetic and magnetotransport properties of new III-V diluted magnetic semiconductors: GaMnAs”.

27. Hayashi, T., Y. Hashimoto, S. Katsumoto, and Y. Iye, Appl. Phys.Lett. 78 (2001) 1691, “Effect of low-temperature annealing on transport and magnetism of diluted magnetic semiconductor (Ga, Mn)As“.

28. Higo, Y., H. Shimizu and M. Tanaka, Physica E 10 (2001) 292, “Large tunneling magnetoresistance (70%) in GaMnAs/AlAs/GaMnAs single-barrier ferromagnetic semiconductor tunnel junctions”.

29. Hirsch, J. E., Phys. Rev. Lett. 83 (1999) 1834, “Spin Hall Effect“.

30. Hsieh, K. C., K. Y. Hsieh, Y. L. Hwang, T. Zhang and R. M. Kolbas, Appl. Phys. Lett. 68 (1996) 1790, “Strain-induced phase separation in annealed low-temperature grown $Al_{0.3}Ga_{0.7}As$”.

31. Huang, J. H., L. Z. Hsieh, X. J. Guo, and Y. O. Su, Appl. Phys. Lett. 82 (2003) 305, “Dual accumulation and depletion behaviors of the arsenic precipitation in low-temperature-grown Be delta-doped GaAs”.

J

32. Jungwirth, T., Jürgen König, Jairo Sinova, J. Ku□era, and A. H. MacDonald, Phys. Rev. B. 66 (2002) 012402, “Curie temperature trends in (III,Mn)V ferromagnetic semiconductors”.

K

33. Kaminska, M. Z., Liliental-Weber, E. R. Weber, T. George and J. B. Kortright, Appl. Phys. Lett. 54 (1989) 1881, “Structural properties of As-rich GaAs grown by molecular beam epitaxy at low temperatures”.

34. Kawakami, R. K., Y. Kato, M. Hanson, I. Malajovich, J. M. Stephens, E. Johnston-Halperin, G. Salis, A. C. Gossard and D. D. Awshalom, Science 294 (2001) 131, “Ferromagnetic Imprinting of Nuclear Spins in Semiconductors”.

35. Ku, K. C., S. J. Potashnik, R. F. Wang, M. J. Seong, E. Johnston-Halperin, R. C. Meyers *et al*., Appl. Phys. Lett. 82 (2003) 2302, “Highly enhanced Curie temperature in low-temperature annealed [Ga,Mn]As epilayers”.

L

36. Lavrent’eva, L. G., M. D. Vilisova, V. V. Preobrazhenskii and V.V. Chaldyshev, Crystallog. Rep. 47 (2002) S118, “Low-Temperature Molecular Beam Epitaxy of GaAs: Influence of Crystallization Conditions on Structure and Properties of Layers”.

37. Lee, W. N., Y. F. Chen, J. H. Huang, X. J. Guo and C. T. Kuo, Jpn. J. Appl. Phys., 44 (2005) 6399, “Effect of Substrate Orientation on Arsenic Precipitation in Low-Temperature-Grown GaAs”.

38. Liliental-Weber, Z., W. Swider, K. M. Yu, J. Kortright, F. W. Smith and A. R. Calawa, Appl. Phys. Lett. 58 (1991) 2153, “Breakdown of crystallinity in low-temperature-grown GaAs layers”.

39. Liu, X., A. Prasad, J. Nishio, E. R. Weber, Z. Liliental-Weber, and W. Walukiewicz, Appl. Phys. Lett. 67 (1995) 279, “Native point defects in low-temperature-grown GaAs”.

40. Liu, Z. Y., J. De Boecka, V.V. Moshchalkovb, and G. Borghsa, J. Magn MagnMater, 242–245 (2002) 967, “Growth and characterization of $Al_{1-X}Mn_{X}as$ ($X \leq 4\%$) magnetic semiconductor: thin film and superlattices”.

41. Look, D. C., and D. C. Walters, Phys. Rev. B 42 (1990) 3578, “Anomalous Hall-effect results in low-temperature molecular-beam-epitaxial GaAs: Hopping in a dense *EL*2-like band”.

42. Look, D. C., D. C. Walters, M. Mier, C. E. Stutz, and S. K. Brierley, Appl. Phys. Lett. 60 (1992) 2900, “Native donors and acceptors in molecular-beam epitaxial GaAs grown at 200 °C”.

43. Loukakos, P. A. C., Kalpouzos, I. E. Perakis, Z. Hatzopoulos, M. Logaki and C. Fotakis, Appl. Phys. Lett. 79 (2001) 2883, “Ultrafast electron trapping times in low-temperature-grown gallium arsenide: The effect of the arsenic precipitate spacing and size”.

M

44. Man, Yu Kin, M. Kaminska and Z. Liliental-Weber, J. Appl. Phys. 72 (1992) 2850, “Characterization of GaAs layers grown by low temperature molecular beam epitaxy using ion beam techniques”.

45. Mathieu, R., B. S. Sørensen, J. Sadowski, U. Södervall, J. Kanski, P. Svedlindh *et al.*, Phys. Rev. B 68 (2003)184421, “Magnetization of ultrathin (Ga,Mn)As layers”.

46. Matsukura, F., H. Ohno, T. Dietl; III-V Ferromagnetic Semi-conductors, in: Handbook of Magnetic Materials, vol. 14, ed. K.H.J. Buschow (Elsevier, Amsterdam, 2002) pp. 1-38, “III-V Ferromagnetic Semiconductors”.

47. Melloch, M. R., N. Otsuka, J. M. Woodall, A. C. Warren and J. L. Freeouf, Appl. Phys. Lett. 57 (1990) 1531, “Formation of Arsenic precipitates in GaAs buffer layers grown bbby molecular beam epitaxy at low substrates temperatures”.

48. Melloch, M. R., N. Otsuka, K. Mahalingam, C. L. Chang, J. M Woodall, G. D. Pettit, P. D. Kirchner, F. Cardone, A. C. Warren, and D. D. Nolte, J.Appl. Phys. 72 (1992) 3509, “Arsenic cluster dynamics in doped GaAs”.

49. Melloch, M. R. N., Otsuka, K. Mahalingam, P. D. Kirchner, J. M. Woodall, and A. C .Warren, Appl. Phys. Lett. 61 (1992) 177, "Formation of two-dimenslmal arsenic-precipitate arrays in GaAs".

50. Missous, M., and S. O'Hagan, J. Appl. Phys. 75 (1994) 3396, "Nonstoichiometry and dopants related phenomena in low temperature GaAs grown by molecular beam epitaxy".

51. Missous, M., and S. O'Hagan, J. Cryst. Growth 175-176 (1997) 197, "Low temperature (LT) and stoichiometric low temperature (SLT) MBE GaAs and related compounds: improved structural, electrical and optical properties".

52. Moodera, J. S. L. R. Kinder, T. M. Wong, and R. Meservey, Phys. Rev. Lett. 74(1995) 3273, "Large Magnetoresistance at Room Temperature in Ferromagnetic Thin Film Tunnel Junctions".

53. Munekata, H., H. Ohno, S. von Molnár, A. Segmüller, L. L. Chang, and L. Esaki, Phys. Rev. Lett. 63 (1989) 1849, "Diluted Magnetic III-V Semiconductors".

N

54. Nazmul, Ahsan M., S. Sugahara, and M. Tanaka, Phys. Rev. B 67, (2003) 241308, "Ferromagnetism and high Curie temperature in semiconductor heterostructures with Mn δ-doped GaAs and *p*-type selective doping".

55. Nolte, D. D., Melloch, J. M.Woodall and S. J. Ralph: Appl. Phys. Lett. 62 (1993) 1356, "Enhanced electro-optic properties of low-temperature-growth GaAs and AlGaAs".

O

56. Ogawa, T., M. Shirai, N. Suzuki and I. Kitagawa, J. Magn. Magn. Mater. 196 (1999) 428, "First-principles calculations of electronic structures of diluted magnetic semiconductors (Ga,Mn)As" .

57. O'Hagan, S., and M. Missous, J. Appl. Phys. 82 (1997) 2400, "The effect of substrate

orientation on the properties of low temperature molecular beam epitaxial GaAs".

58. O'Hagan, S. P., M. Missous, A. Mottram, and A. C. Wright, J. Appl. Phys.79 (1996) 8384, "Interaction of dopants with a host GaAs lattice: The case of lowtemperature grown molecular beam epitaxial GaAs(Si)".

59. Ohno, H., A. Shen, F. Matsukura, A. Oiwa, A. Endo, S. Katsumoto, and Y. Iye, Appl. Phys. Lett. 69, (1996) 363, "(Ga,Mn)As: A new diluted magnetic semiconductor based on GaAs".

60. Ohno, H., F. Matsukura, A. Shen, Y. Sugawara, A. Oiwa, A. Endo, S. Katsumoto and Y. Iye, 1996, in: M. Scheffler and R. Zimmermann (Eds.), Proceedings of the 23rd International Conference on Physics of Semiconductors, World Scientific, Singapore, pp. 405-408.]

61. Ohno, H., H. Munekata, T. Penney, S. von Molnár, and L. L. Chang, Phys. Rev. Lett. 68, (1992) 2664, "Magnetotransport properties of *p*-type (In,Mn)As diluted magnetic III-V semiconductors".

62. Ohno, H., N. Akiba, F. Matsukura, A. Shen, K. Ohtani and Y. Ohno, Appl. Phys. Lett. 73 (1998) 363, "Spontaneous splitting of ferromagnetic (Ga, Mn)As valence band observed by resonant tunneling spectroscopy".

63. Ohno, H., Solid State Commun. 117 (2001) 179, "A ferromagnetic III–V semiconductor: (Ga,Mn)As".

64. Ohno, H., Science 281, (1998) 951, "Making Nonmagnetic Semiconductors Ferromagnetic".

65. Ohno, Y., D. K. Young, B. Beschoten, F. Matsukura, H. Ohno and D. D. Awschalom, *Nature* 402 (1999) 790, "Electrical spin injection in a ferromagnetic semiconductor heterostructure".

66. Ohya, S., H. Kobayashi, and M. Tanaka, Appl. Phys. Lett. 83 (2003) 2175, "Magnetic properties of heavily Mn-doped quaternary alloy ferromagnetic semiconductor (InGaMn)As

grown on InP".

67. Ohya, S., H. Yamaguchi, and M. Tanaka, J. Supercond. 16 (2003) 139, "Properties of Quaternary Alloy Magnetic Semiconductor (InGaMn)As Grown on InP".

68. Omiya, T. F., Matsukura, A. Shen, Y. Ohno, H. Ohno, Physica E 10 (2001) 206, "Large tunneling magnetoresistance (70%) in GaMnAs/AlAs/GaMnAs single-barrier ferromagnetic semiconductor tunnel junctions".

P

69. Park, J. B., K. H. Kim, K. J. Lee, D. J. Kim, H. J. Kim and Y. E. Ihm, J. Crystal Growth 273 (2005) 396, "Temperature dependence of the growth morphology in molecular beam epitaxy grown MnAs".

70. Park, J.-H., E. Vescovo, H.-J. Kim, C. Kwon, R. Ramesh, and T. Venkatesan, Phys. Rev. Lett. 81, (1998) 1953, "Magnetic Properties at Surface Boundary of a Half-Metallic Ferromagnet $La_{0.7}Sr_{0.3}MnO_3$".

71. Potashnik, S. J., K. C. Ku, S. H. Chun, J. J. Berry, N. Samarth, and P. Schiffer, Appl. Phys. Lett. 79 (2001) 1495, "Effects of annealing time on defect-controlled ferromagnetism in $Ga_{1-x}Mn_xAs$".

72. Prinz, G. A., Science 282 (1998) 1660, "Magnetoelectronics".

73. Price, G. L., Phys. Rev. Lett. 66 (1991) 469, "Critical-thickness and growth-mode transitions in highly strained $In_xGa_{1-x}As$ films".

R

74. Reinwald, M., U. Wurstbauer, M. Doppe, W. Kipferl, K. Wagenhuber, H.-P. Tranitz, D. Weiss, W. Wegscheider, J. Cryst. Growth 278 (2005) 690, "Growth of (Ga,Mn)As on GaAs(0 0 1) and (31 1)A in a high-mobility MBE system".

S

75. Sadowski, J., J.Z. Domagala, J. Bak-Misiuk, S. Kolesnik, K. Swiatek, J. Kanski, and L. Ilver, Thin Solid Films 367 (2000) 165, "Structural properties of MBE grown GaMnAs layers".

76. Sadowski, J., P. Mathieu, P. Svedlindh, J. Z. Domagala, J. Bak-Misiuk, K. Swiatek, M. Karlsteen, J. Kanski, L. Ilver, H. Åsklund and U. Södervall, Appl. Phys. Lett. 78 (2001) 3271, "Structural and magnetic properties of GaMnAs layers with high Mn-content grown by migration-enhanced epitaxy on GaAs(100) substrates".

77. Sadowski, J., and J. Z. Domagala, Phys. Rev. B 69 (2004) 075206, "Influence of defects on the lattice constant of GaMnAs".

78. Sanvito, S. and N. A. Hill, Appl. Phys. Lett. 78 (2001) 3493, "Influence of the local As antisite distribution on ferromagnetism in (Ga, Mn)As".

79. Sanvito,S. P. Ordej´on, and N. A. Hill, Phys. Rev. B. 63 (2001) 165206, "First-principles study of the origin and nature of ferromagnetism in $Ga_{1-x}Mn_xAs$".

80. Schliemann, J., J. König, H. H. Lin and A. H. MacDonald, Appl. Phys. Lett. 78 (2001) 1550, "Limits on the Curie temperature of (III,Mn)V ferromagnetic semiconductors".

81. Schilfgaarde, M. van and O. N. Mryasov, Phys. Rev. B. 63 (2001) 233205, "Anomalous exchange interactions in III-V dilute magnetic semiconductors".

82. Schmidt, G. et al., Phys. Rev. Lett. 87 (2001) 227203, "Large Magnetoresistance Effect Due to Spin Injection into a Nonmagnetic Semiconductor".

83. Schott, G. M., W. Faschinger, and L. W. Molenkamp, Appl. Phys. Lett. 79 (2001) 1807, "Lattice constant variation and complex formation in zincblende gallium manganese arsenide".

84. Shen, A., F. Matsukura, S. P. Guo, Y. Sugawara, H. Ohno, M. Tani, H.Abe and H. C. Liu, J. Cryst. Growth 201/202 (1999) 679, "Low-temperature molecular beam epitaxial growth of GaAs and (Ga,Mn)As".

85. Shimizu, H. T., Hayashi, T. Nishinaga, and M. Tanaka, Appl. Phys. Lett. 74 (1999) 398, "Magnetic and transport properties of III–V based magnetic semiconductor (GaMn)As: Growth condition dependence".

86. Slupinski, T., H. Munekata, and A. Oiwa, Appl. Phys. Lett. 80 (2002) 1592, "Ferromagnetic semiconductor (In,Ga,Mn)As with Curie temperature above 100 K".

87. Smorchkova, I. P. N. Samarth, J. M. Kikkawa, and D. D. Awschalom, Phys. Rev.Lett. 78 (1997) 3571, "Spin Transport and Localization in a Magnetic Two-Dimensional Electron Gas".

88. Smorchkova, I. P. N. Samarth, J. M. Kikkawa, and D. D. Awschalom, Phys. Rev.B. 58 (1998) R4238, "Giant magnetoresistance and quantum phase transitions in strongly localized magnetic two-dimensional electron gases".

89. Sørensen, B. S., P. E. Lindelof, J. Sadowski, R. Mathieu, P. Svedlindh, Appl. Phys. Lett. 82 (2003) 2287, "Effect of annealing on carrier density and Curie temperature in epitaxial (Ga,Mn)As thin films".

90. Sugahara, S. and M. Tanaka, Appl. Phys. Lett. 80 (2002) 1969, "Tunneling magnetoresistance in fully epitaxial MnAs/AlAs/MnAs ferromagnetic tunnel junctions grown on vicinal GaAs(111)B substrates".

91. Swaminathan, V. and A. T. Macrander, "Materials Aspects of GaAs and InP Based Structures", Prentice Hall (1991)

T

92. Tanaka, M. and Y. Higo, Phys. Rev. Lett. 87 (2002) 026602, "Large Tunneling Magnetoresistance in GaMnAs /AlAs /GaMnAs Ferromagnetic Semiconductor Tunnel Junctions".

93. Tsui, D. C., H. L. Stormer, and A. C. Gossard, Phys. Rev. Lett. 48 (1982) 1559, "Two-Dimensional Magnetotransport in the Extreme Quantum Limit".

V

94. Van Esch, A., L. van Bockstal, J. de Boeck, G. Verbanck, A. S. van Steenbergen, P. J.Wellmann, B. Grietens, R. Bogaerts, F. Herlach, and G. Borghs, Phys. Rev. B 56 (1997) 13103, "Interplay between the magnetic and transport properties in the III-V diluted magnetic semiconductor $Ga_{1-x}Mn_xAs$".

95. Van Schlifgaarde, M. and O. N. Mryasov, Phys. Rev. B 63 (2001) 233205, "Anomalous exchange interactions in III-V dilute magnetic semiconductors".

96. Vurgaftman, I. And J. R. Meyer, Phys. Rev. B 64 (2001) 245207, "Curie-temperature enhancement in ferromagnetic semiconductor superlattices".

W

97. Wang, K. Y., K. W. Edmonds, L. X. Zhao, M. Sawicki, R. P. Campion, B. L. Gallagher, and C. T. Foxon, Phys. Rev. B 72 (2005) 115207, "(Ga,Mn)As grown on (311) GaAs substrates: Modified Mn incorporation and magnetic anisotropies".

98. Wang, W. I., E. E. Mendez, T. S. Kuan and L. Esaki, Appl. Phys. Lett. 47 (1985) 826, "Crystal orientation dependence of silicon doping in molecular beam epitaxial AlGaAs/GaAs heterostructures".

99. Wang, Z. M., V. R. Yazdanpanah, J. L. Shultz and G. J. Salamo, Appl. Phys. Lett. 81 (2002) 2965, "GaAs (311) templates for molecular beam epitaxy growth: surface morphologies and reconstruction".

100. Warren, A. C., J. M. Woodall, J. L. Freeouf, D. Grischkowsky, D. T. Mclnturff, M. R. Melloch and N. Otsuka, Appl. Phys. Lett. 57 (1990) 1331, "Arsenic precipitates and the semi-Insulating properties of GaAs buffer layers grown by low-temperature molecular beam epitaxy" .

101. Welp, U., V. K. Vlasko-Vlasov, A. Menzel, H. D. You, X. Liu, J. K. Furdyna and T. Wojtowicz, Appl. Phys. Lett. 85 (2004) 260, "Uniaxial in-plane magnetic anisotropy of $Ga_{1-x}Mn_xAs$".

102. Welp, U., V. K. Vlasko-Vlasov, X. Liu, J. K. Furdyna, T. Wojtowicz, Phys. Rev. Lett. 90 (2003) 167206, “Magnetic Domain Structure and Magnetic Anisotropy in $Ga_{1-x}Mn_xAs$”.

103. Wolf , S., Science 294 (2001) 1488, “Spintronics: A Spin-Based Electronics Vision for the Future”.

Y

104. Yano,R., Y. Hirayama, S. Miyashita, N. Uesugi, S. Uehara and J. Gebauer, J. Appl. Phys. 94 (2003) 3966, “Arsenic pressure dependence of carrier lifetime and annealing dynamics for low-temperature grown GaAs studied by pump–probe spectroscopy”.

105. Ye, J., Y. B. Kim, A. J. Millis, B. I. Shraiman, P. Majumdar and Z. Tešanović, 1999, Phys. Rev. Lett. 83, 3737, “Berry Phase Theory of the Anomalous Hall Effect: Application to Colossal Magnetoresistance Manganites”.

106. Yin, L. W., Y. Hwang, J. H. Lee, R. M. Kolbas, R. J. Trew and U. K.Mishra, IEEE Electron Device Lett. 11 (1990) 561, “Improved breakdown voltage in GaAs MESFETs utilizing surface layers of GaAs grown at a low temperature by MBE”.

107. Yu, K. M., W. Walukiewicz, T. Wojtowicz, I. Kuryliszyn, X. Liu, Y. Sasaki, and J. K. Furdyna, Phys. Rev. B. 65 (2002) 201303(R), “Effect of the location of Mn sites in ferromagnetic $Ga_{1-x}Mn_xAs$ on its Curie temperature”.

Vita

Wei-Ni Lee

李薇妮

新竹市南雅街187巷
97之1號5樓
電話：03-5333252
F5, No. 97-1, Lane 187,
Nan-Ya St. Hsinchu 300,
Taiwan, Republic of China
E-mail: wnlee@mx.nthu.edu.tw

Summary of Formal Education:

Doctoral (Ph. D.)	Department of Materials Science and Engineering, National Chiao Tung University, R.O.C. (1997~2006)
Bachelors Degree	Department of Physics, Chung Yuan Christian University, R.O.C. (1977~1981)

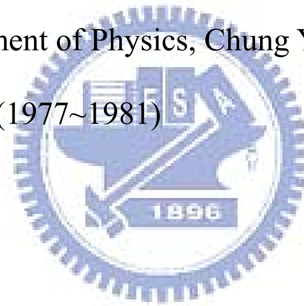

Skills:

Epitaxial growth: MBE growth of semiconductor crystals in the following system:

Low-temperature III-V compounds on GaAs substrates

Low-temperature III-V DMS compounds on GaAs and InP substrates

MBE growth of III-V compounds on non-(001)-oriented GaAs substrates

MBE growth of III-V DMS compounds on non-(001)-oriented GaAs substrates

List of my Publications

(1) W. N. Lee, Y. F. Chen, J. H. Huang, X. J. Guo and C. T. Kuo, “Effect of Substrate Orientation on Arsenic Precipitation in Low-Temperature-Grown GaAs”, Jpn. J. Appl. Phys. Vol. 44, No. 9A, 2005, pp. 6399 – 6402.

(2) W. N. Lee, Y. F. Chen, J. H. Huang, X. J. Guo and C. T. Kuo, “Effects of doping type and concentration on precipitation of nanometer arsenic clusters in low-temperature-grown GaAs”, J. Vac. Sci. Technol. B 23, No.6, Nov/Dec 2005.

(3) W. N. Lee, Y. F. Chen, J. H. Huang, X. J. Guo, C. T. Kuo, T. S. Chin and H. C. Ku, “$(In_{0.52}Al_{0.48})_{1-x}Mn_xAs$ diluted magnetic semiconductor grown on InP substrates”, J. Phys.: Condens. Matter 18 (2006) L15–L20.

(4) W. N. Lee, Y. F. Chen, J. H. Huang, X. J. Guo, C. T. Kuo, and H. C. Ku, “MBE growth and structural and magnetic properties of $(In_{1-y}Al_y)_{1-x}Mn_xAs$ diluted magnetic semiconductors”, J. Crys. Growth. To be published (2006).

(5) W. N. Lee, Y. F. Chen, J. H. Huang, B.W. Huang, C. T. Kuo and T. S. Chin, “Effects of substrate orientation on the magnetic properties of GaMnAs”, submitted.

(6) W. N. Lee, Y. F. Chen, J. H. Huang, B.W. Huang, C. T. Kuo, T. S. Chin, and C. T. Kuo, "The magnetic anisotropy properties of $Ga_{0.93}Mn_{0.07}As$ by low-temperature annealing”, submitted.